115 p.

GEOPHYSICS CORPORATION OF AMERICA
BEDFORD, MASSACHUSETTS

Title

AN EXPERIMENTALLY DETERMINED MODEL FOR THE PERIODIC CHARACTER OF WINDS FROM 85 TO 135 KM

E. MANRING, J. BEDINGER, H. KNAFLICH, and D. LAYZER Nov. 1963

115 p. refs.

(NASA CONTRACT NO. NASw-712)

PREPARED FOR
NATIONAL AERONAUTICS AND SPACE ADMINISTRATION
WASHINGTON 25, D. C.
NOVEMBER 1963

AN EXPERIMENTALLY DETERMINED MODEL FOR THE PERIODIC CHARACTER OF WINDS FROM 85 TO 135 KM

E. Manring
J. Bedinger
H. Knaflich
D. Layzer

Contract No. NASw-712

GCA Technical Report No. 63-27-N

November 1963

GEOPHYSICS CORPORATION OF AMERICA
Bedford, Massachusetts

Prepared for

NATIONAL AERONAUTICS AND SPACE ADMINISTRATION
Washington 25, D. C.

ABSTRACT

19607

Since 1959, measurements of upper atmospheric winds have been made from Wallops Island, Virginia, utilizing the sodium vapor technique. To date, measurements from 22 different vapor trails have been analyzed. In the region 85 to 135 km, the measurements show a relation which is cyclic with time. The data have been analyzed in terms of cyclic components with periods of 24-hours, 12-hours, and 8-hours. A new picture of the wind structure at these altitudes is proposed.

TABLE OF CONTENTS

SECTION 1

INTRODUCTION

During the past four years, the sodium vapor technique has been used to measure upper atmospheric winds from Wallops Island, Virginia. The method has been completely described elsewhere.[1-4] Briefly, winds are derived from the rate of motion of a trail of sodium vapor ejected from a rocket during twilight. Resonance scattering of sunlight of the D-line emission provides sufficient brightness for the trail to be photographed during twilight. Triangulation techniques are used to determine exact trail position from simultaneous photographs taken at widely separated known locations. The data is reduced by an analog method which allows very precise wind determinations at height intervals as small as desired.

Results from a total of 22 different trails are reported here. About half of these have previously been published.[5,6] The remainder have received only limited distribution in contractual reports.[2,7,8] The altitude range of the data varies for different trails, with the upper limit determined by rocket performance. Three types of rockets have been used: Nike-Cajuns which reach about 140 km, Nike-Apaches which usually attain about 180 km, and Nike-Asps which have reached 220 km. The lower limit of observations is often determined by atmospheric conditions and partial cloud cover.

Below about 80 km, chemical recombination of the atomic sodium is rapid, and the trail is white in color rather than the characteristic orange or red of sodium or lithium vapor. This white trail is more affected by atmospheric attenuation at low elevation angles from distant locations and generally persists for only a short time. Photography of this portion is generally possible from close-in sites, but often there is so much overlapping of the trail in the viewing direction that accurate winds cannot be determined in the observing time available. Thus, although measurements have been made from 50 km to 200 km, the largest number of measurements are in the region 80 to 140 km. All of the data that have so far been obtained are included in Appendix A.

SECTION 2

WIND DATA

2.1 CLASSIFICATION OF WIND PROFILES

Examination of the wind profiles shows that they may be grouped into three general classes determined by the velocity variations at different heights. Examples illustrating this classification are shown in Figure 1. Wind speed and wind direction (direction toward which the wind is blowing) are shown separately as functions of altitude. Photographs of these trails, taken from the launch site, are shown in Figure 2.

Class I. The direction varies rapidly with height, but does not change by more than 90^{o}. Wind speed fluctuations with height are numerous, but usually do not deviate by more than 40 m/sec.

Class II. The primary characteristic of these trails is a single large-shear region which usually occurs between 100 and 110 km. In this region a large directional change, usually 180^{o}, occurs. Above and below this region, the wind speed is small, sometimes near 0. The maximum speed in the shear region is always large and often as great as 150 m/sec.

Class III. The characteristic of these trails is a continuous, spiraling change in direction with height. The wind speed gradually increasing with height until a maximum of 120 to 150 m/sec is reached at about 110 km.

Above this level the speed decreases to about 80 m/sec and then, in most cases, remains relatively constant at greater heights. The direction of rotation of the spiral motion is clockwise, i.e., N-E-S-W, with height.

Of the 22 individual experiments discussed here, 7 belong to Class I; 6 to Class II; and 8 to Class III. No seasonal preference is noted in any group. There are about equal numbers of morning and evening measurements in Class I. Class II has more morning than evening measurements, and Class III has more evening than morning measurements.

2.2 COMPARISON WITH OTHER MEASUREMENTS

Wind measurements by other methods have been made for some regions below 100 km. Several firings of rocket grenades and sodium vapor have been made within a few minutes of each other. Generally, the winds obtained are in good agreement except in regions of large shear. In these regions, the grenade data give a value averaged over the height interval between successive grenades and do not show all the details which the sodium clouds show. Measurements up to about 60 km with small meteorological rockets have been obtained on a routine basis from many locations.[9] Again, general agreement is found with the sodium vapor trail measurements. Most of the reported data above 90 km are from radar observations of ionized meteor trails. Radar observations give valuable information about the periodic wind components and their seasonal variations, but their height resolution is very much less than that of the sodium trail measurements. The radar data complement, rather than overlap, the sodium-trail data.

2.3 DIURNAL AND SEASONAL VARIATIONS

The present data are not well suited to the determination of seasonal variations, for two reasons. The total number of observations is too small for an analysis of seasonal variations; and almost one third of the data were obtained during March and April.

The data are better suited to a study of diurnal variations since about equal numbers of measurements have been made during morning and evening twilight and the local times of sunrise and sunset vary by nearly three hours through the year. However, no positive indications of diurnal effects were found. Such effects have been observed by radar measurements of ionized meteor trails at Jodrell Bank, England,[10] and Adellaide, Australia,[11] but their amplitudes are very small compared with the amplitude of the non-periodic component of the wind. The best opportunity to detect cyclic variations from the present data came as a result of a series of flights in April, 1961. Firings occurred at Wallops Island and Sardinia, Italy[12] during the same period. The firings were planned to occur during sequential twilights from both sites in order to investigate large scale wind effects. The times at which the flights occurred and the time difference in hours is shown in Table 1. The latitude difference between Wallops Island ($37^{o}50'N$, $75^{o}29'W$) and Sardinia ($39^{o}36'$, $9^{o}26'E$) is small.

The wind velocity at any height may be represented on a polar plot by a vector with length proportional to the speed and pointed in the direction to which the wind is blowing. Such plots were made at selected heights for

TABLE 1

TIME OF OBSERVATION FOR THE APRIL 1961 SERIES

Number	Site	Approximate LMT	Approximate EST	Time Difference
5	Wallops	19 April 04.6 hours	19 April 04.6 hours	
				8.9 hours
6	Sardinia	19 April 19.2	19 April 13.5	
				9.4
7	Sardinia	20 April 04.6	19 April 22.9	
				20.3
8	Wallops	20 April 19.2	20 April 19.2	
				9.4
9	Wallops	21 April 04.6	21 April 04.6	

the five consecutive firings in April, 1961. It was found for each height that the ends of these vectors could be joined in sequence by a continuous, smooth curve rotating from north to west. During September 1961 and March 1962, observations during sequential twilights were obtained from Wallops Island with time difference of about 11 hours. Other sequential measurements were also obtained at Sardinia.[13] Vectors from these additional flights were placed on the previously drawn plots and the new vectors were found to terminate on the same curves.

If all sequential measurements could be represented in this manner, the curve must be a closed loop. Continuation of the curve to close the figure was possible at all heights. The resulting figures had the same general character at all heights. Data from other firings which occurred at random intervals, were added to the figures. Final data plots for selected altitudes are shown in Figures 3 through 31. The numbers accompanying each observed point identify the observation by date, time, and place, and are tabulated in Table 2. It should be noted that the altitude difference between most of the figures is only 1.25 km, and that significant variations occur over such intervals. The regions of high shear would not be observed if the height determinations were less precise or if the data were averaged over height intervals much greater than 1 km.

Above about 135 km, the closed loop figures could not be drawn. Either there are not enough points to determine the shape, or such patterns do not exist at these heights. Measurements of winds above 135 km are shown in Appendix A. It is apparent that if such representations exist, they include a large prevailing component directed toward the south.

TABLE 2

No.	Date	Twilight	Range of Height in km
	(1959)		
1	17 August	AM	140-220
2	18 November	PM	94-163
	(1960)		
3	24 May	PM	84-169
4	9 December	AM	90-138
	(1961)		
5	19 April	AM	92-154
6	19 April	PM Sardinia	83-183
7	20 April	AM Sardinia	108-189
8	20 April	PM	81-165
9	21 April	AM	82-162
7S	7 September	PM Sardinia	90-200
8S	8 September	AM Sardinia	100-200
10	16 September	PM	78-146
11	17 September	AM	96-172
	(1962)		
12	1 March	PM	71-126
13	2 March	AM	65-127
14	23 March	PM	59-140
15	27 March	PM	80-118
16	17 April	AM	76-191
17	6 June	PM	56-137
18	7 November	AM	68-152
19	30 November	AM	77-157
20	5 December	PM	83-138
	(1963)		
21	20 February	PM	58-151
22	21 February	PM	83-164
25	20 May	PM Sardinia	94-195
26	21 May	AM Sardinia	98-200
27	21 May	PM Sardinia	84-205
23	23 May	PM	81-205
24	24 May	PM	84-170

Below about 85 km, data are again insufficient to establish such patterns or to determine whether they exist. Numerous measurements[14-16] in this region have been made by other methods and a large scale, general circulation has been established in which the prevailing direction is toward the east in winter and toward the west in summer.[17-19] The measurements made with sodium clouds are not inconsistent with this result, however, the individual measurements show large fluctuations.

SECTION 3

MATHEMATICAL REPRESENTATION OF THE WIND DATE

The form of the data figures suggests thay they could be represented by a combination of cyclic components. The radar meteor data show that components with periods of 24-hours, 12-hours, and 8-hours are present in the region 85 to 105 kms. It is convenient to represent these components as vectors in a complex plane so that the magnitude and phase are easily separated.

3.1 USE OF THE COMPLEX VARIABLE

Let u, and v denote the components of the wind in the north an west directions respectively. Then, a vector, $\overline{W}$, in the complex (u, v) plane may be written

$$\overline{W} = u + iv = W \exp[i \phi]$$

where W represents the wind speed, and ϕ the wind direction, measured counter-clockwise from the direction north. W and ϕ are related to u and v by

$$W = \sqrt{(u^2 + v^2)}; \quad \phi = \tan^{-1} \frac{v}{u}$$

3.2 PREVAILING WINDS

If the wind over a given region has a constant or slowly varying component, this is represented by a complex function

$$\bar{W}_o(z,t) = u_o(z,t) + iv_o(z,t) = W_o(z,t)\ \exp[i\ \phi_o(z,t)]$$

where z denotes the height and t the time.

3.3 CYCLIC COMPONENTS

Setting $2\pi/\omega$ equal to the 24-hour period of the earth's rotation gives

$$\bar{W}_1 = W_1\ \exp[i(\omega t - \delta_1)]$$

for a component with this period.

Similarly, winds with 12- and 8-hour periods are represented respectively by

$$\bar{W}_2 = W_2\ \exp[i(2\omega t - \delta_2)]$$

$$\bar{W}_3 = W_3\ \exp[i(3\omega t - \delta_3)] \quad ,$$

the δ's are phase angles to be discussed later. The resultant wind, neglecting components with periods of less than 8 hours, is then

$$\bar{W} = W_o \exp[-i\delta_o] + W_1 \exp[i(\omega t - \delta_1)] + W_2 \exp[i(2\omega t - \delta_2)] + W_3 \exp[i(3\omega t - \delta_3)]$$

$$= \sum_{j=0}^{3} W_j(t) \exp[i\phi_j(t)]$$

The eight quantities, W_j, $\phi_j (j = 0,1,2,3)$, determine the magnitude and directional character of the wind with time. In general, both W(t), the magnitude of the resultant wind, and $\phi(t)$, its phase, may be complicated functions of time. However, the mathematical representation depends upon only three of the four phase angles ϕ_j since the choice of zero time is arbitrary.

3.4 ANALYSIS OF DATA FIGURES

The observed wind vectors at specific heights were plotted and the resulting curves were analyzed to determine the 12-hour, 8-hour and prevailing components. To accomplish this, a large number of computed model figures were drawn using a wide variety of values for the W's and δ's. Some examples of these model figures are shown in Figures 32 through 36. The observed patterns were then matched to the model figures and values of the W's and δ's were obtained for a specific case by scaling the data figures to best fit the most appropriate model. W_o and δ_o were read directly as a difference between the position of the origin in the model and observed figures. Phase angles δ_1 and δ_2 were also determined by direct comparison of model and data figures. The δ's were considered as a phase lag between components so that the direction of the prevailing component, could be written positive when measured in the generally used

clockwise direction from north. Also, it should be noted that although the phase angles δ_1 and δ_2 are associated with the 24-hour and 12-hour components in this analysis, the relationship is not unique. The models could have been computed using phase differences between any two of the three cyclic components. However, the δ's show the zero-time phase difference between one component and the other two and how they all vary with height. The δ's were determined from the orientation of the figures and by the relative position of points of intersection of the curves. The intersecting points were determined from a group of model figures in which δ_2 was approximately correct. The direction of the points of intersection was plotted for varying values of δ_1. The directions of the intersections on the data figures were then read and corresponding values for δ_1 were taken from a computed plot similar to the one shown in Figure 37. It can be seen that phase determination is good in some regions, but not well defined in others. Magnitude variations also affect the relative position of intersecting points, so phase determination in regions of rapidly changing magnitude is less certain.

In order to determine the magnitude of the cyclic components, the distance to selected points on the model was determined in terms of the direction cosines of the various components. The corresponding distances on the data plots were measured and values for the W's were determined by simultaneous solution of the cosine equations. Measurements were taken where the figures were best defined by data and usually between two points on the curve so that the exact location of the origin was not critical.

The measured values of the W's and δ's are tabulated on each data plot in Figures 3 through 31. The altitude variations are shown in Figures 38 through 42, which were drawn from point to point with no attempt to smooth them. In some instances, more than one computed model might have been used. In such cases, the phase was determined from a model with magnitudes close to the observed and which fit best with those above and below. Small uncertainties in phase have negligible effects on the magnitudes of the cyclic components, although they may introduce errors in determination of small prevailing components since the position of the origin in the computed models is effected by the relative phase and magnitude of the components. The difference in phase between two of the components, $\delta_1 - \delta_2$, is shown as a function of height in Figure 43.

3.5 REMARKS

(1) At each height, the observed wind vectors define a pattern which is accurately reproduced by a theoretical figure composed of prevailing, diurnal, semi-diurnal, and 8-hour components.

(2) The parameters that define the pattern vary smoothly with height as shown in Figures 38 through 42. The magnitudes of all components increase to a maximum between 100 and 110 km, and the phase angles change rapidly in this region. This is also the region where the large shears occur most frequently.

(3) The 8-hour component is dominant at all heights. Sometimes its magnitude is twice that of the semi-diurnal component. The diurnal component is small below about 95 km, but increases above this height. The prevailing component varies from near zero to a maximum of 40 m/sec at 105 km. The direction is generally toward the east except above 120 km where it is toward the west.

(4) The motion of the wind vector at a given height is not accurately periodic; that is, it is not true in general that

$$W(t + 24\text{-hr}) = W(t); \quad \delta(t + 24\text{-hr}) = \delta(t)$$

This fact shows up when time differences of the successive measurements in Table 1 are compared with "predicted" time differences obtained from the corresponding computed model. The time differences for the sequential firings as indicated by the model figures are shown in Table 3. The rate of rotation of the tip of the wind vector fluctuates by as much as a factor of three at specific heights. However, average values for a range of heights at a given time, as well as time averages for a given height, are close to the predicted values. It follows that at a given instant of time, there is no unique pattern for the height variation of W or δ. Thus a large variation of the altitude profiles of the wind is to be expected and is observed.

3.6 DISCUSSION

Previous quantitative information about winds in the height range under consideration comes mainly from the work of Greenhow[10,20] and his co-workers

TABLE 3

TIME INTERVAL IN HOURS OF SEQUENTIAL OBSERVATIONS AS OBTAINED FROM MODEL FIGURES. (Occasionally two time intervals were possible)

Height km	Flight Number						
	5-6	6-7	8-9	25-26	7S-8S	12-13	10-11
85						10	
86.25						11	
88.75						3	
90			10			6	
91.25			3			4	
92.5	3		3			9	
93.75	4		9			9	
95	5		10			9	20
96.25	5		5			10	20
97.5	13		5	1		9	20
98.75	11		20	0		0	6
100	5		8	17	17	8	12
101.25	9		7	7	18	12	8
102.5	12		10	7	19	19	9
103.75	11		3(17)	3	10	18	10
105	5		9	10	13	11	6
106.25	11		11	5	13	8	4
107.5	7	13	4	14	13	8	5
108.75	7	10	10	19	14	14	5(12)
110	8	8	3	19	16	7	13
111.25	8	3	19(3)	17	17	11	16
112.5	6	3	19	9	10	0	15
113.75	7	3	1	10	10	0	10
115	7	3	2	11	11	23	14
116.25	7	4	1	10	10	23	23
120	6	4	0	23	10		10
125	5	3	10	2	10		17
130	5	4(9)	2	9	10		5
135	5	9	0	19	10		19
Actual time interval in hours	8.9	9.4	9.4	8.5	10	11.5	10.4

based on a radio-echo technique devised by Greenhow. This technique enables one to measure the velocities of one or more short sections of a suitably oriented ionization trail, such as are produced in large quantities in the height range 85-100 km by meteors. The accompanying absolute height determinations have an uncertainty of ± 2 km; however, Greenhow extended his technique to permit direct measurements of vertical gradients of horizontal winds (wind-shear). From a very extensive set of observations, Greenhow and his co-workers determined, for every month of the year, the height-averaged amplitudes and phases of the prevailing, diurnal, semi-diurnal, and terdiurnal components of the horizontal wind in the height range 90-94 km. They also determined the vertical gradients of these quantities in the height range 90-100 km. Finally they determined the frequency distribution of the amplitude of the horizontal wind and the frequency distribution of the wind shear in the same height range.

The experimental results obtained by the radio-echo method indicate that the aperiodic component of the horizontal wind is much larger, in the height range under consideration, than the prevailing and periodic components. However, owing to their limited height resolution, they contain little information about the nature of the aperiodic component. This is precisely the kind of information that the data presented here supply. On the other hand, these data supply little information about strictly periodic variations. The two experimental approaches are thus largely complementary.

On the basis of the radar data, the winds in the region 85-105 km have been envisioned as made up of three contributions: a prevailing component,

similar to those that occur at lesser heights; a small tidal or thermally driven component which, like the tidal winds at lesser heights, can be anaylzed into a diurnal, a semi-diurnal and a terdiurnal component; and an aperiodic component, much larger than the other two and characterized by steep vertical gradients, sometimes exceeding 0.1 sec^{-1} (= 100 m sec^{-1} km^{-1}). The radio-echo observations, as well as earlier optical observations of persistent meteor trails[21] showed that the aperiodic winds had a very narrow energy spectrum, Fourier components with a vertical wavelength of less than 1 km being essentially absent. The aperiodic winds could therefore not be described as turbulent in the technical hydrodynamic sense. The wave like forms of persistent meteor trails led Hines[22] to attribute the aperiodic winds to upward-propagating waves combining the properties of sound waves and internal gravity waves generated near the surface of the earth. This interpretation has been widely accepted.

Although the picture just sketched seems to rest on a solid observational basis, it is by no means the only picture that is consistent with the radio-echo data, which afford a very incomplete, statistical description of what is, at least numerically, the major component of the horizontal winds. In addition, Hines's interpretation of the aperiodic winds raises certain theoretical questions that have not yet been adequately answered. For example: How are the travelling waves excited? Hines's hypothesis requires an aperiodic driving mechanism that is considerably more effective than the processes responsible for the periodic winds; presumably[23] the absorption of insolation by water vapor and by ozone. What is the nature of this mechanism?

The data from the sodium trails suggest a strikingly different picture. The resultant wind at any height in the region 80 to 135 km may be represented by a prevailing component and cyclic components with periods of 24 hours, 12 hours, and 8 hours. The magnitudes of cyclic components varies smoothly with height, but there is a "phase anomaly". The lack of correlation between the phase anomaly at different heights gives rise to the variability of the $W(z)$ and $\phi(z)$ profiles.

On the present picture, virtually the entire amplitude of the wind at a given height can be attributed to periodic, thermal driving forces. There is no room in this picture for traveling waves produced by nonperiodic driving forces. The dominance of the 8-hour component should find a quantitative explanation in the resonance characteristics of the atmosphere in this height range. In this connection, we recall that Butler and Small[24] have recently shown that the amplitude of the 24-hour component is greatly reduced, in comparison with the 12-hour component, because of the structure of the atmosphere below 80 km.

The origin of the phase anomaly remains to be explained. We tentatively attribute it to magnetohydrodynamic effects which enhance the effective viscous coupling between adjacent layers. This mechanism is under active consideration.

3.7 ADDITIONAL DATA

During 12 different twilight periods in 1959-1960 measurements were made at Eglin Air Force Base, Florida[25] (latitude 29°N). Since none of the chemical trails covered the entire 80-135 km region at one time, only

parts of the wind picture could be observed. Then during May 1963 and December 1962, measurements were again made, but this time the trails covered the 80-135 km region more completely.[26,27] Pre-publication copies of the reports of these data were obtained and compared with the Wallops Island results. The latter flights at Eglin used sodium vapor trails at twilight and photo-chemical reaction during the night to obtain four successive wind measurements within an 8-hour period. These sequential measurements are very similar to the Wallops data plots but also appear different in both magnitude and phase. The amount of data is too small for detailed comparison and the differences may be due to latitude effects.

During December 1962, three consecutive twilight measurements were made at Ft. Churchill, Canada (latitude 59°N). The amount of data is much too small to detect a pattern of the type developed at Wallops Island, but large differences were found when they were compared to the Wallops data.

Recently, the sodium vapor method has been used at other locations, but most of the data are not yet available.

It is perhaps significant that data from two trails at Wallops Island are not contained in the closed loop figures. The observations of 17 August 1959 are not shown on the plots since the wind speeds were greater than the scale of the graph. Some of the data from 24 May 1960 although plotted, are not contained in the figures. These observations were made during times of very great solar activity and the upper winds were noticeably different from the usually observed structure. These differences may be attributed to disturbances in thermal driving forces.

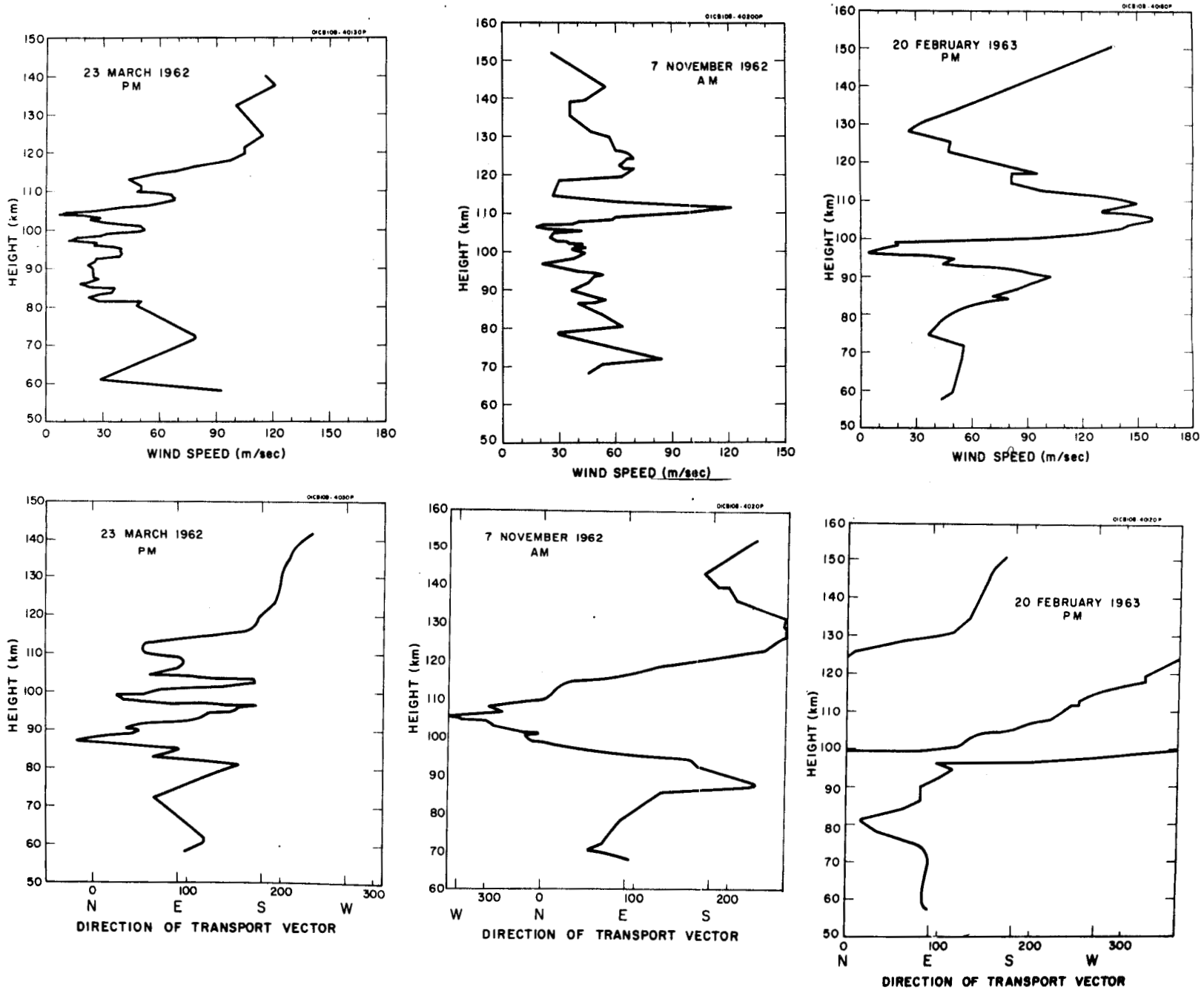

Figure 1. Change of wind speed and direction of transport vector with height for 23 March 1962, 7 November 1962, and 20 February 1963 to illustrate classes I, II, and III respectively.

(a)

(b)

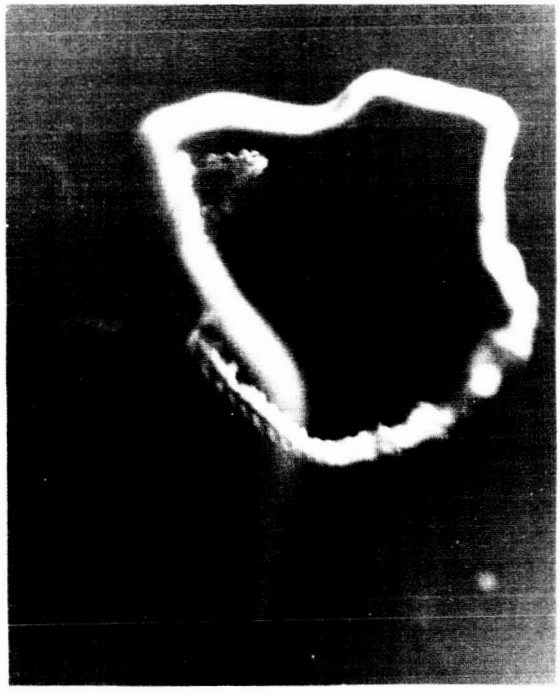

(c)

Figure 2. Photographs of the sodium trail taken 200 sec after launch, from the launch site, on (a) 23 March 1962, (b) 7 November 1962, and (c) 20 February 1963. Note the obvious difference in appearance.

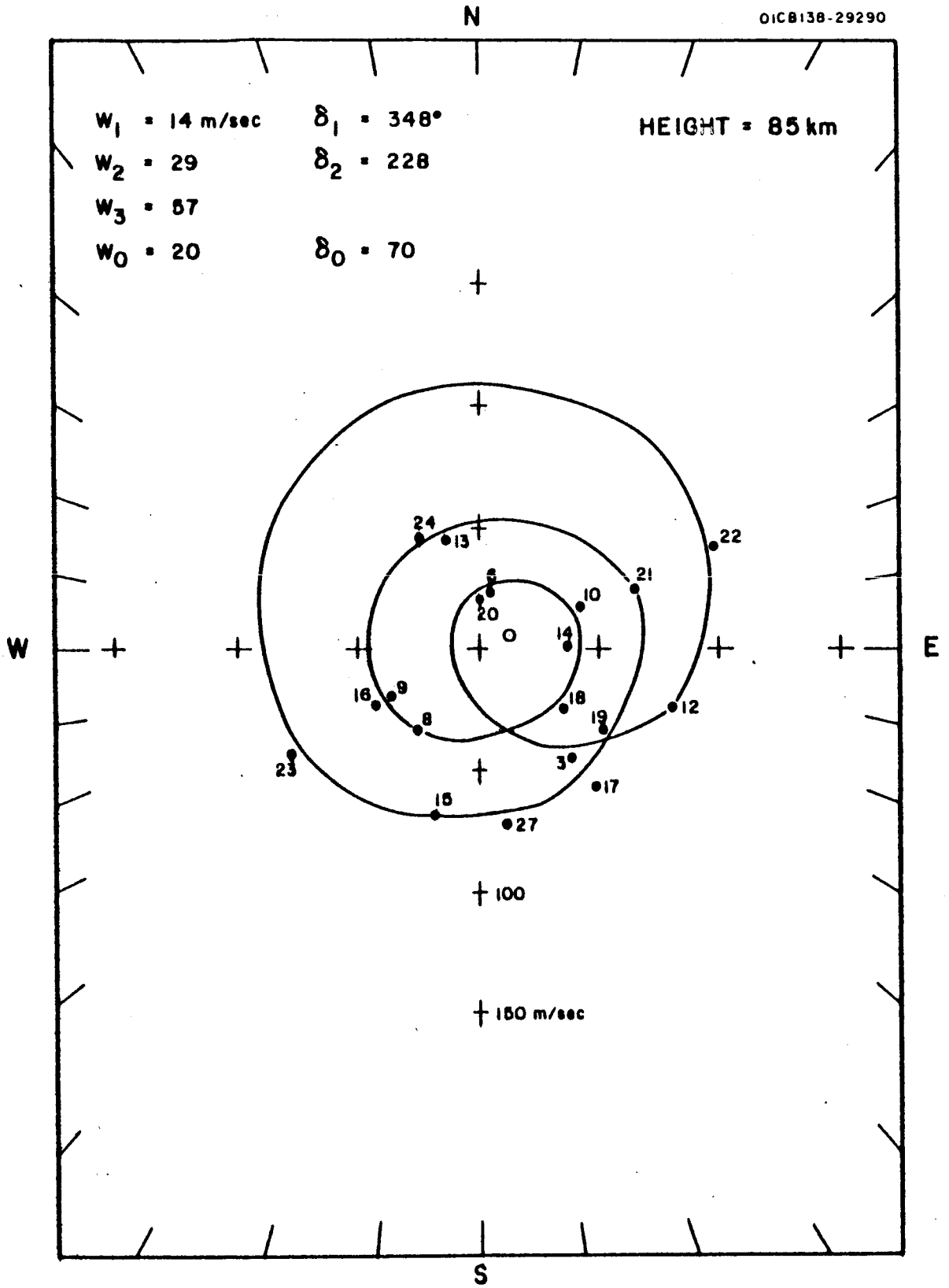

Figure 3. The pattern of wind structure as observed for a height of 85 km. The numbers refer to the dates listed in Table 2. The geometric center of the figure is an open circle. W_1 = 24-hour, W_2 = 12-hour, W_3 = 8-hour, and W_o = prevailing components with accompanying phase angles, δ.

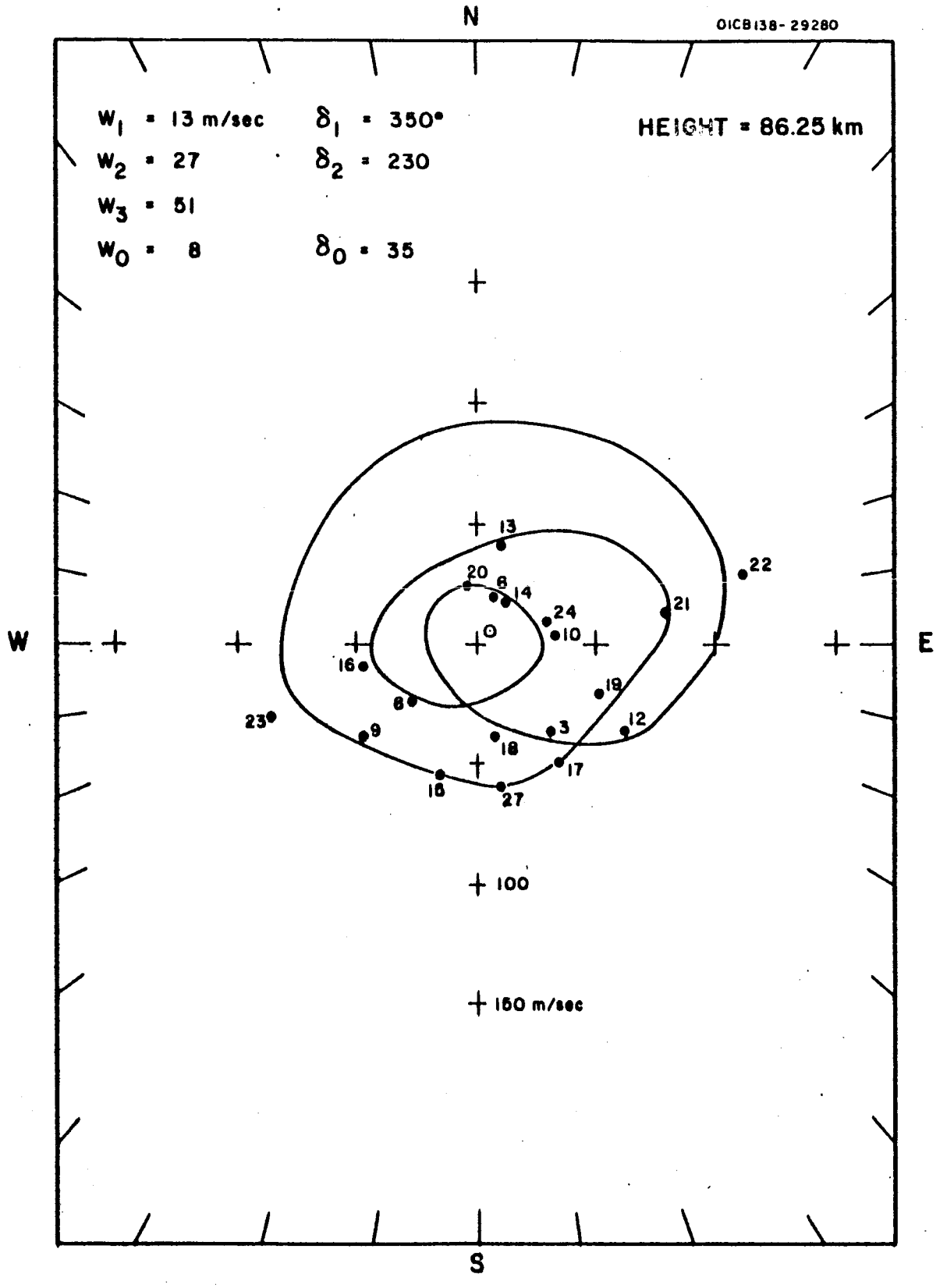

Figure 4. The pattern of wind structure as observed for a height of 86.25 km.

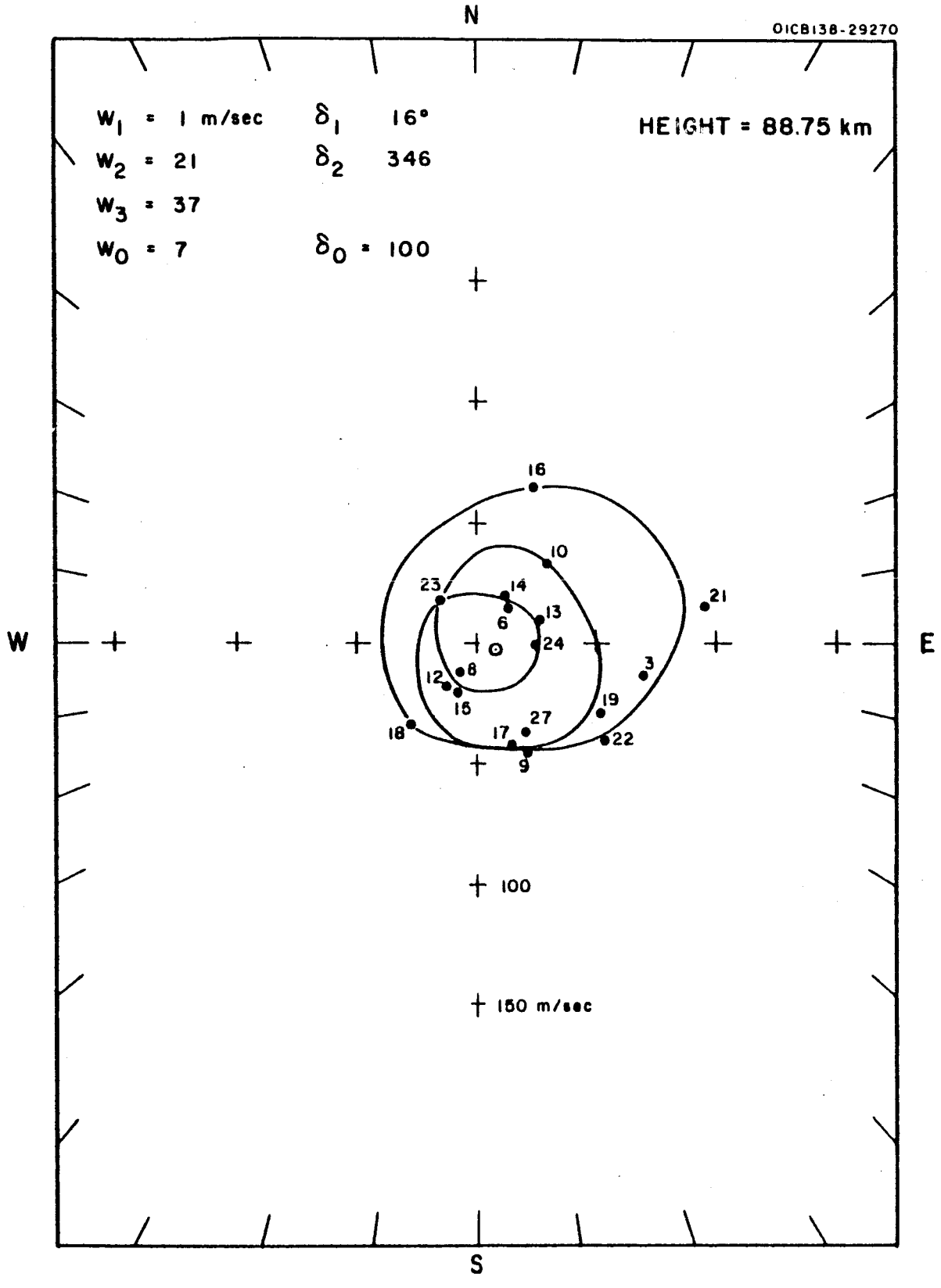

Figure 5. The pattern of wind structure as observed for a height of 88.75 km.

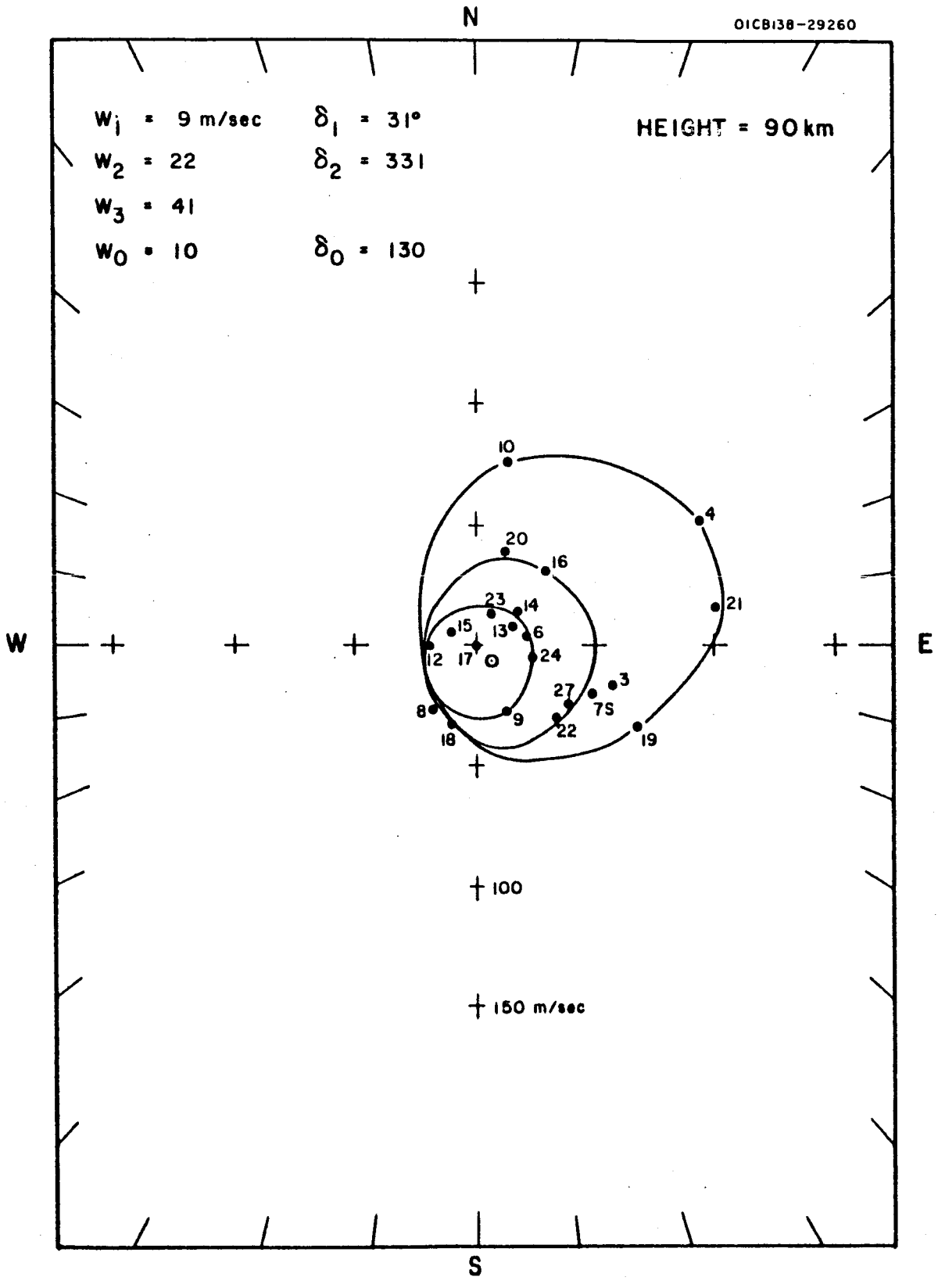

Figure 6. The pattern of wind structure as observed for a height of 90 km.

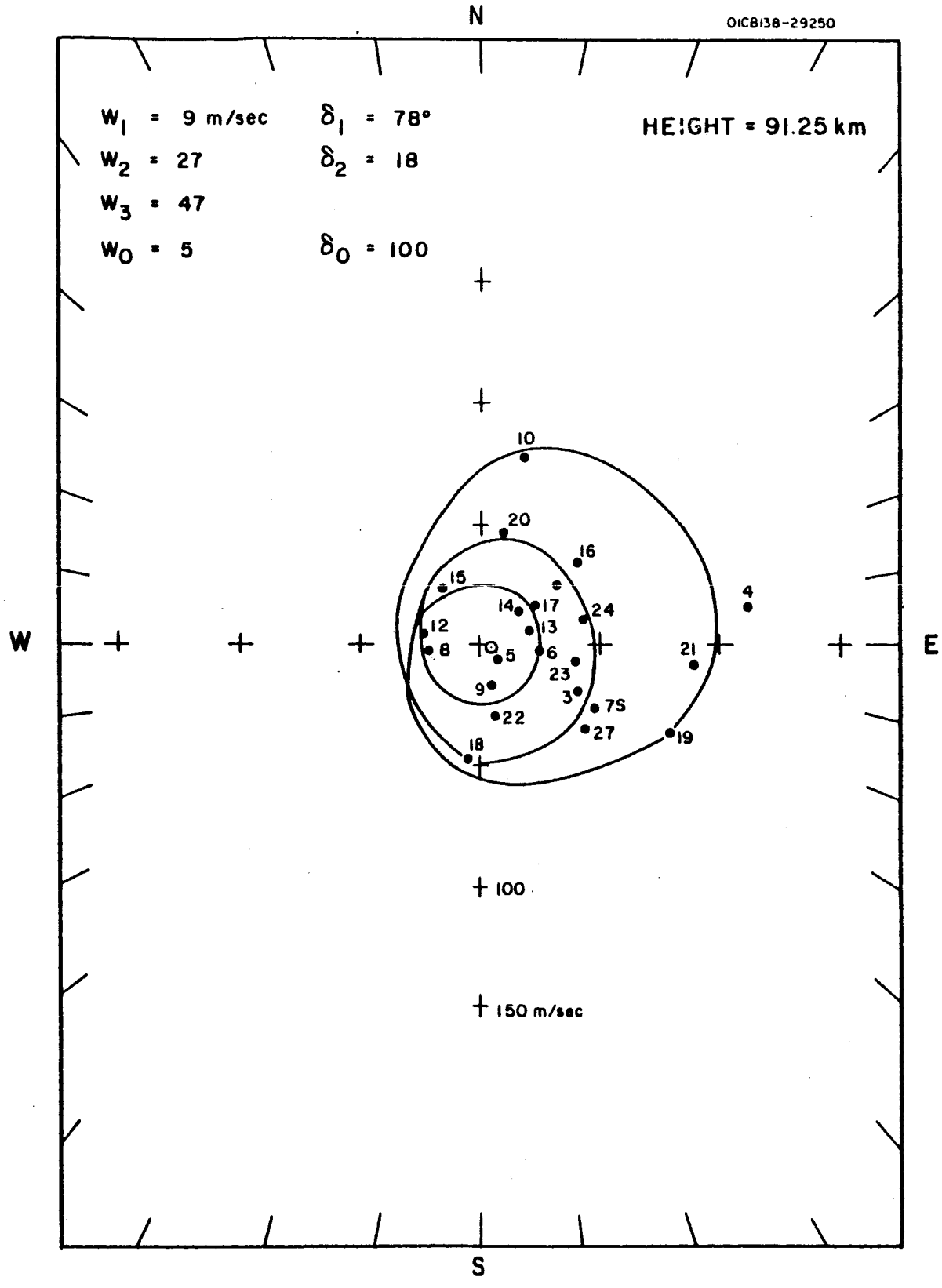

Figure 7. The pattern of wind structure as observed for a height of 91.25 km.

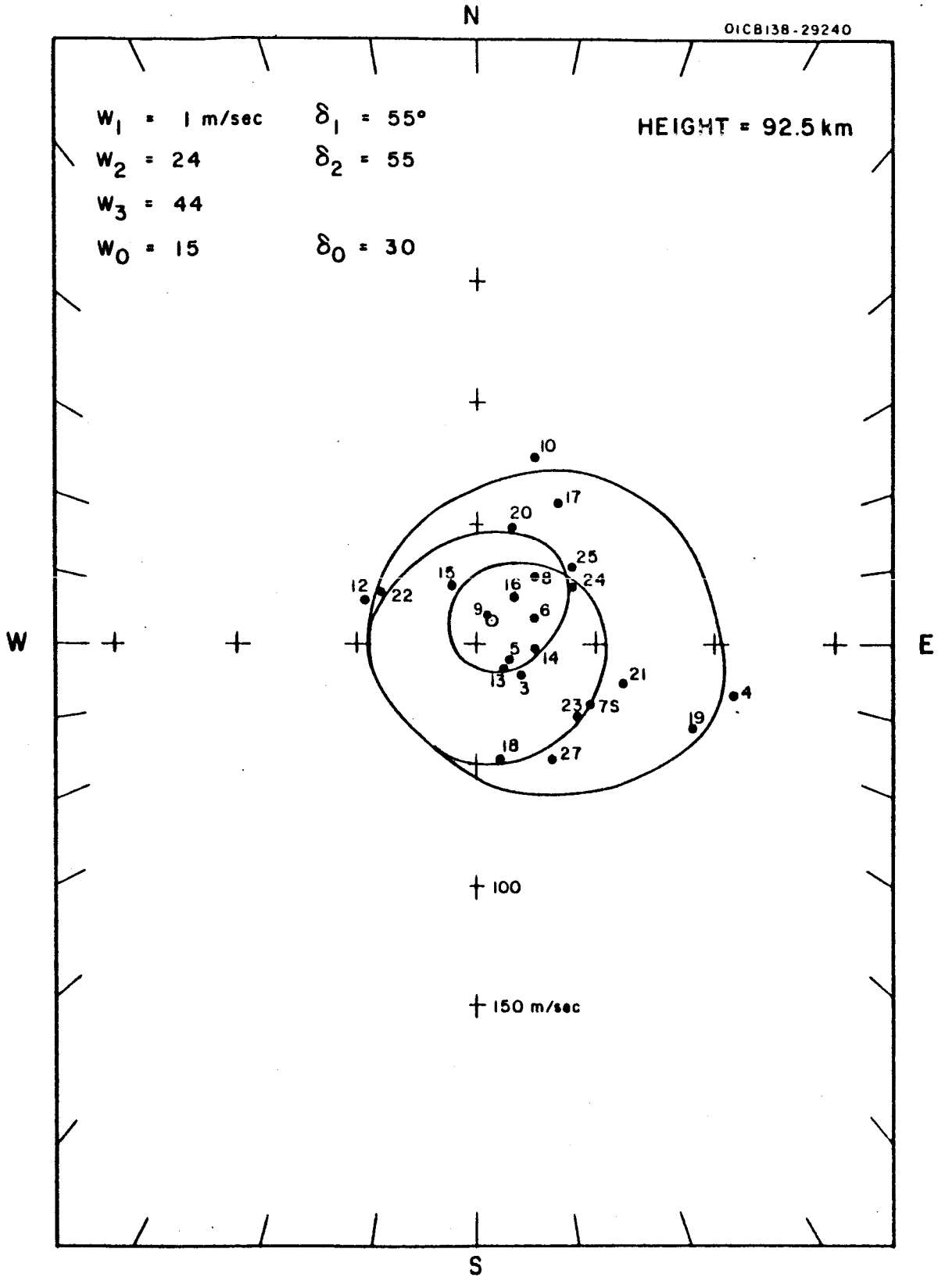

Figure 8. The pattern of wind structure as observed for a height of 92.5 km.

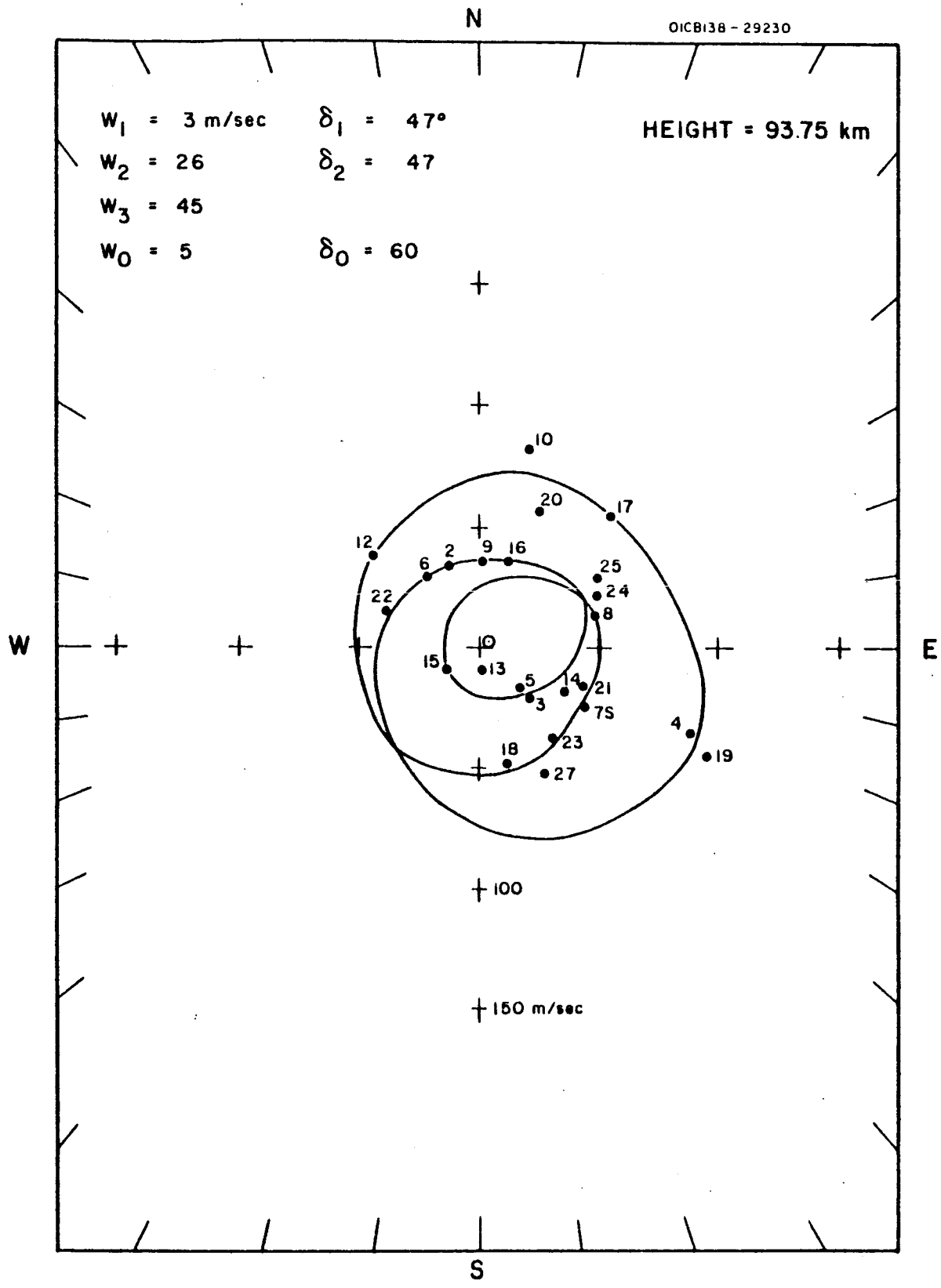

Figure 9. The pattern of wind structure as observed for a height of 93.75 km.

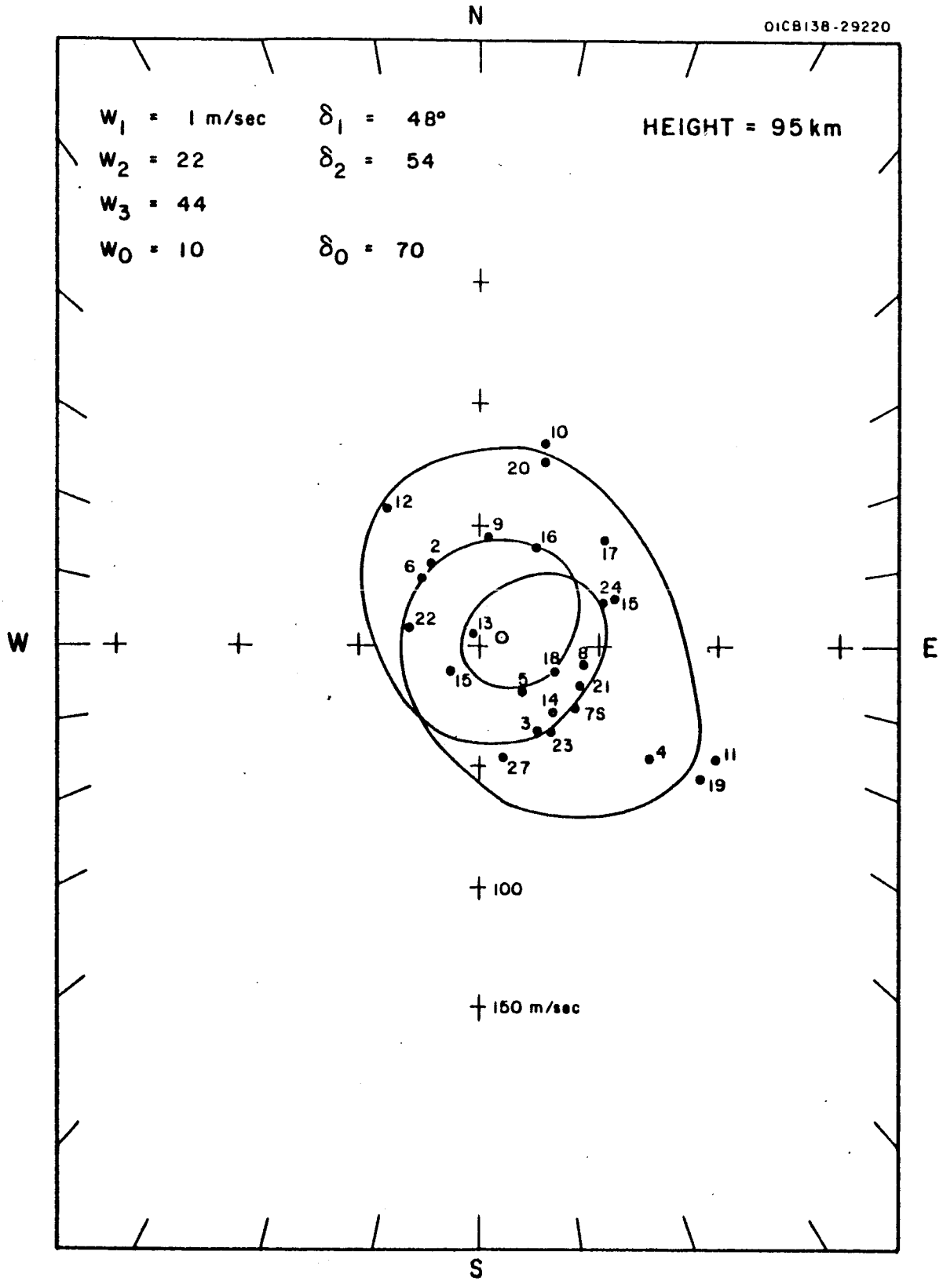

Figure 10. The pattern of wind structure as observed for a height of 95 km.

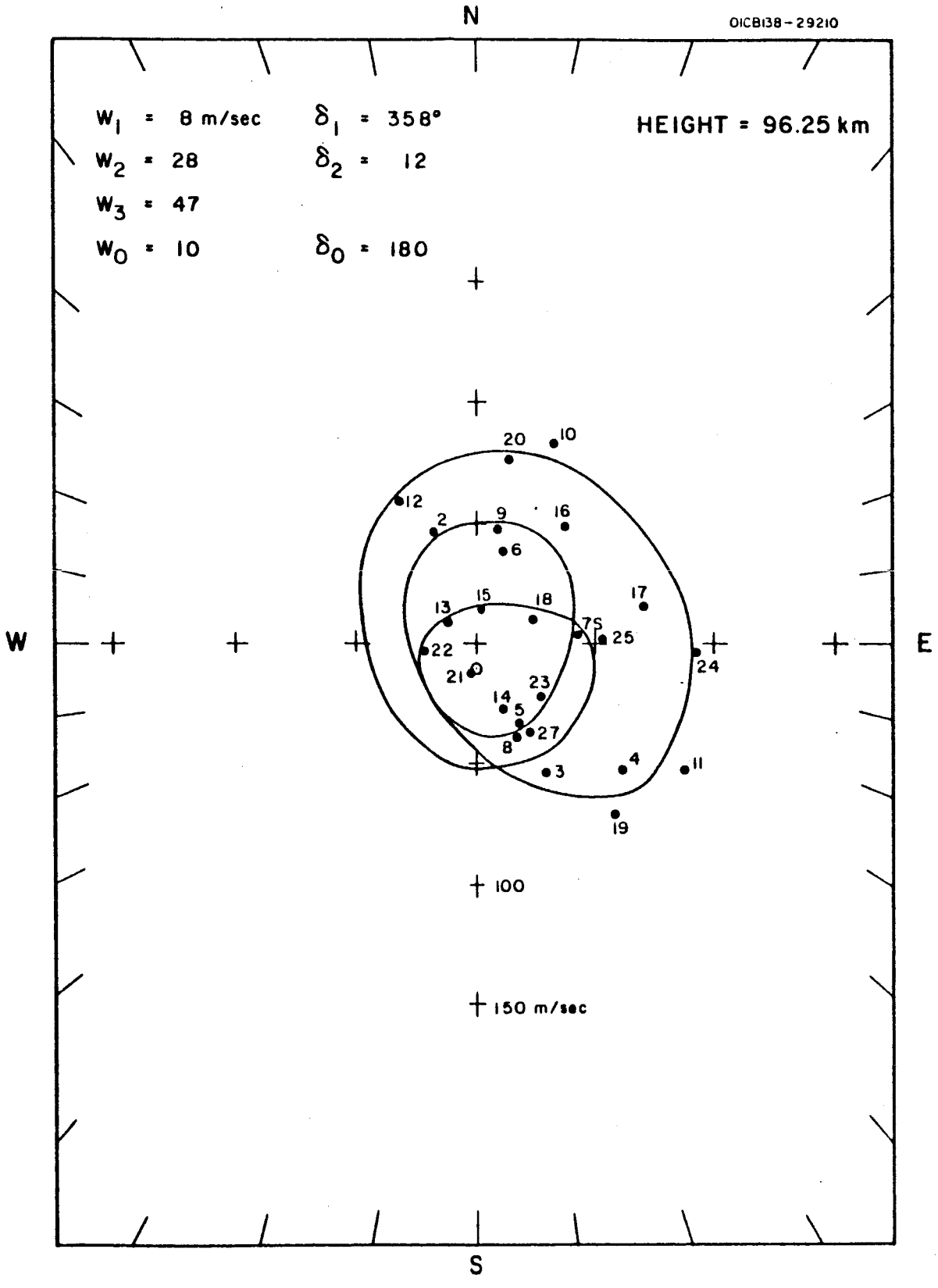

Figure 11. The pattern of wind structure as observed for a height of 96.25 km.

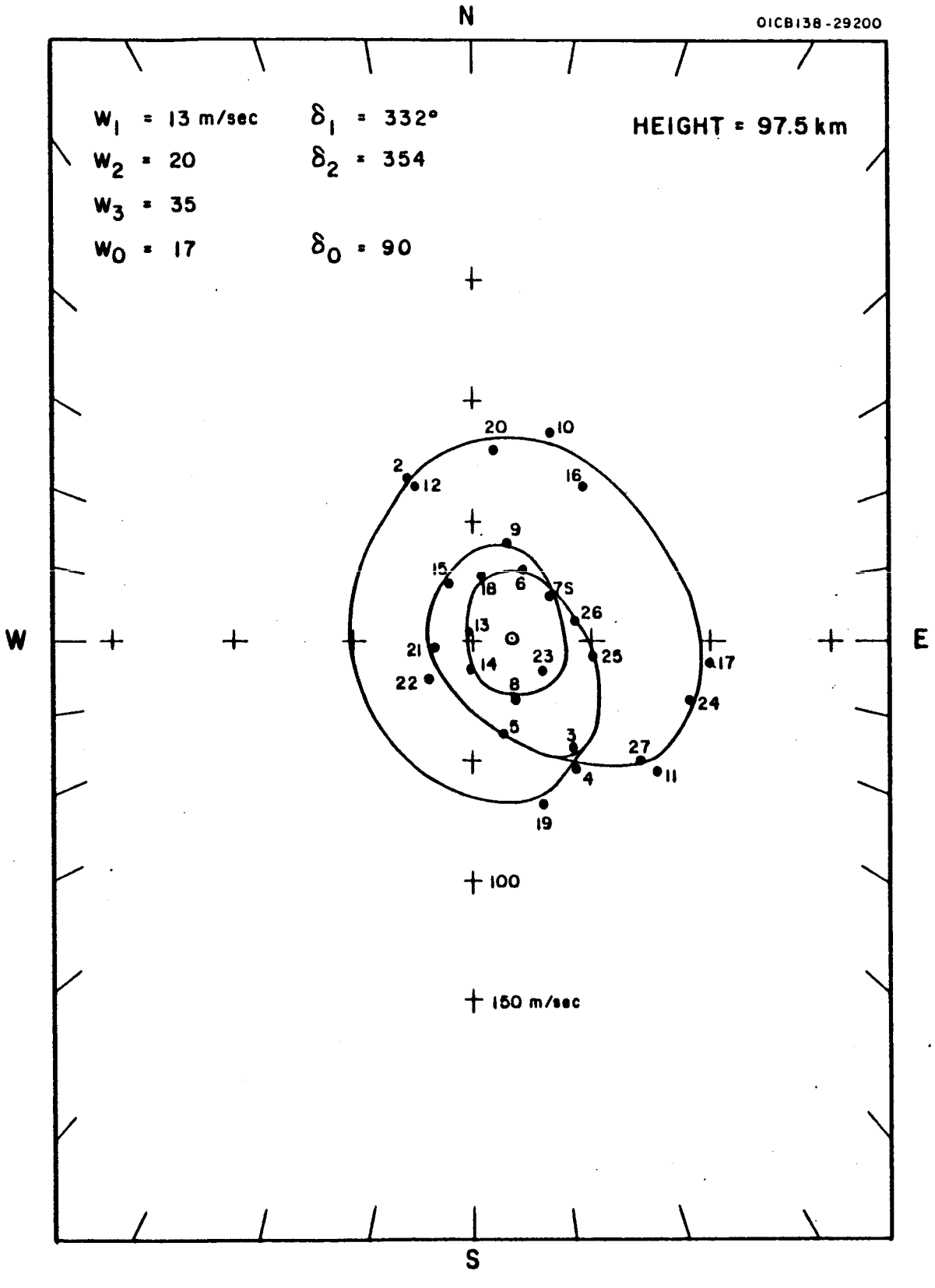

Figure 12. The pattern of wind structure as observed for a height of 97.5 km.

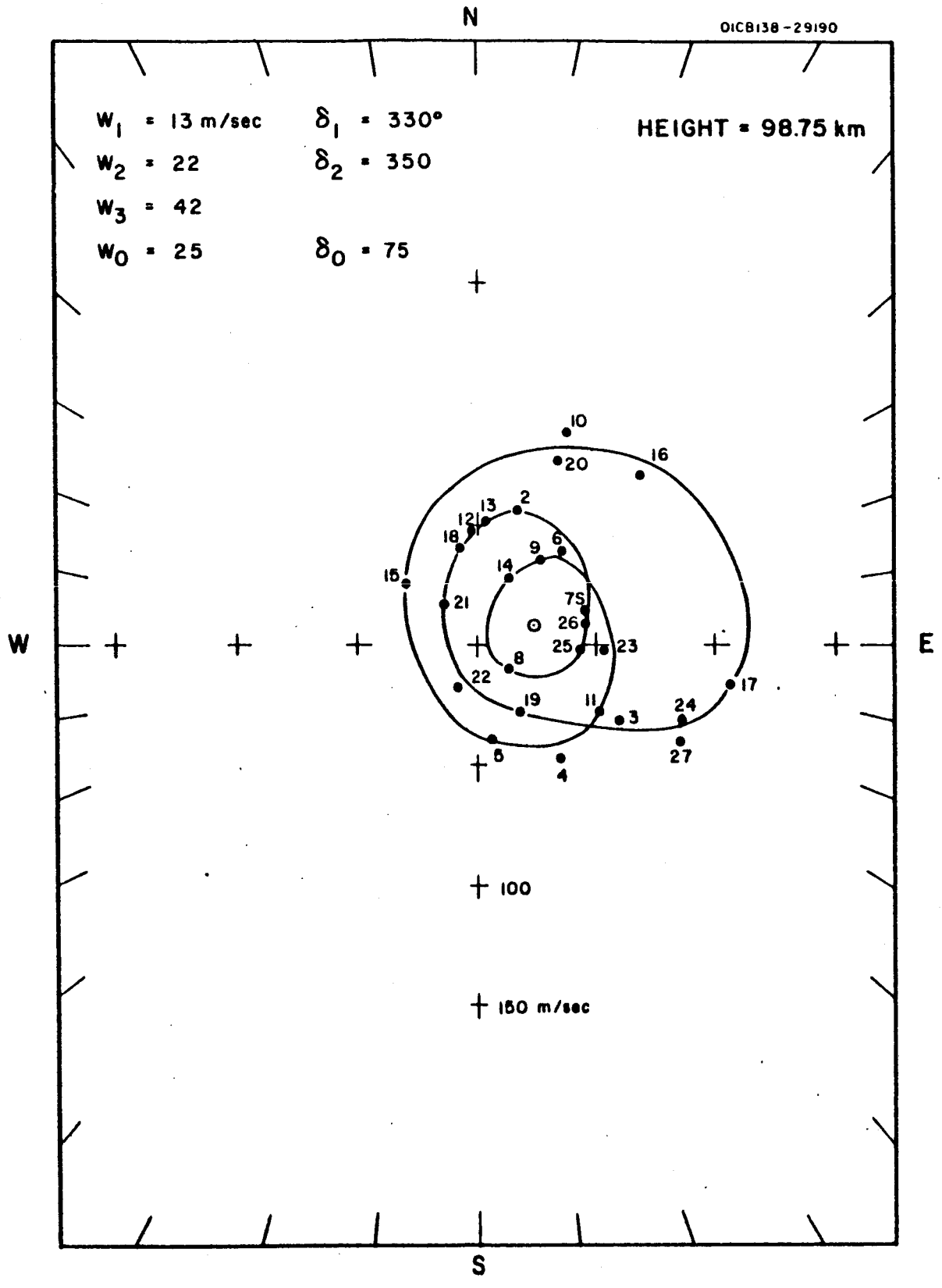

Figure 13. The pattern of wind structure as observed for a height of 98.75 km.

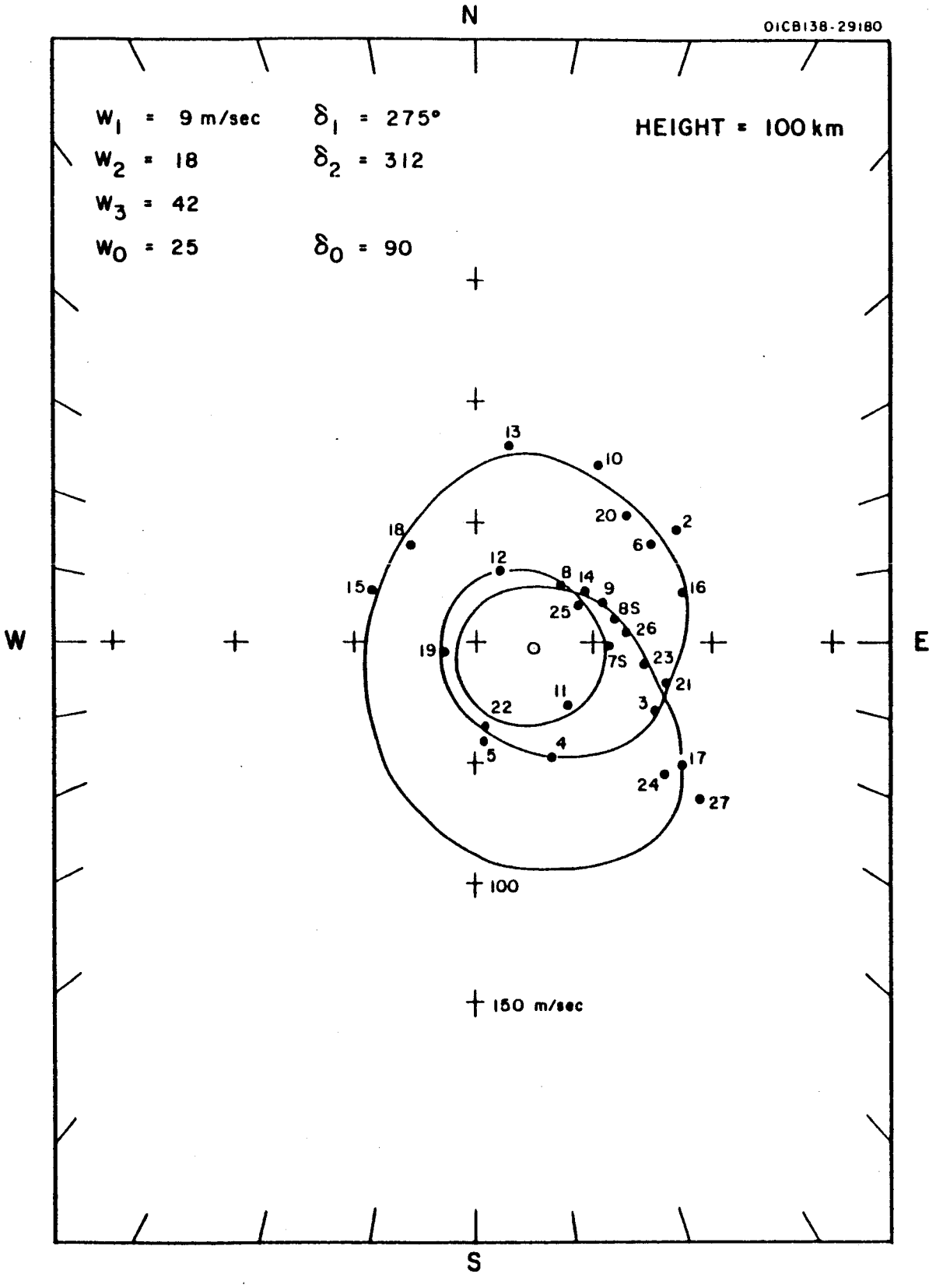

Figure 14. The pattern of wind structure as observed for a height of 100 km.

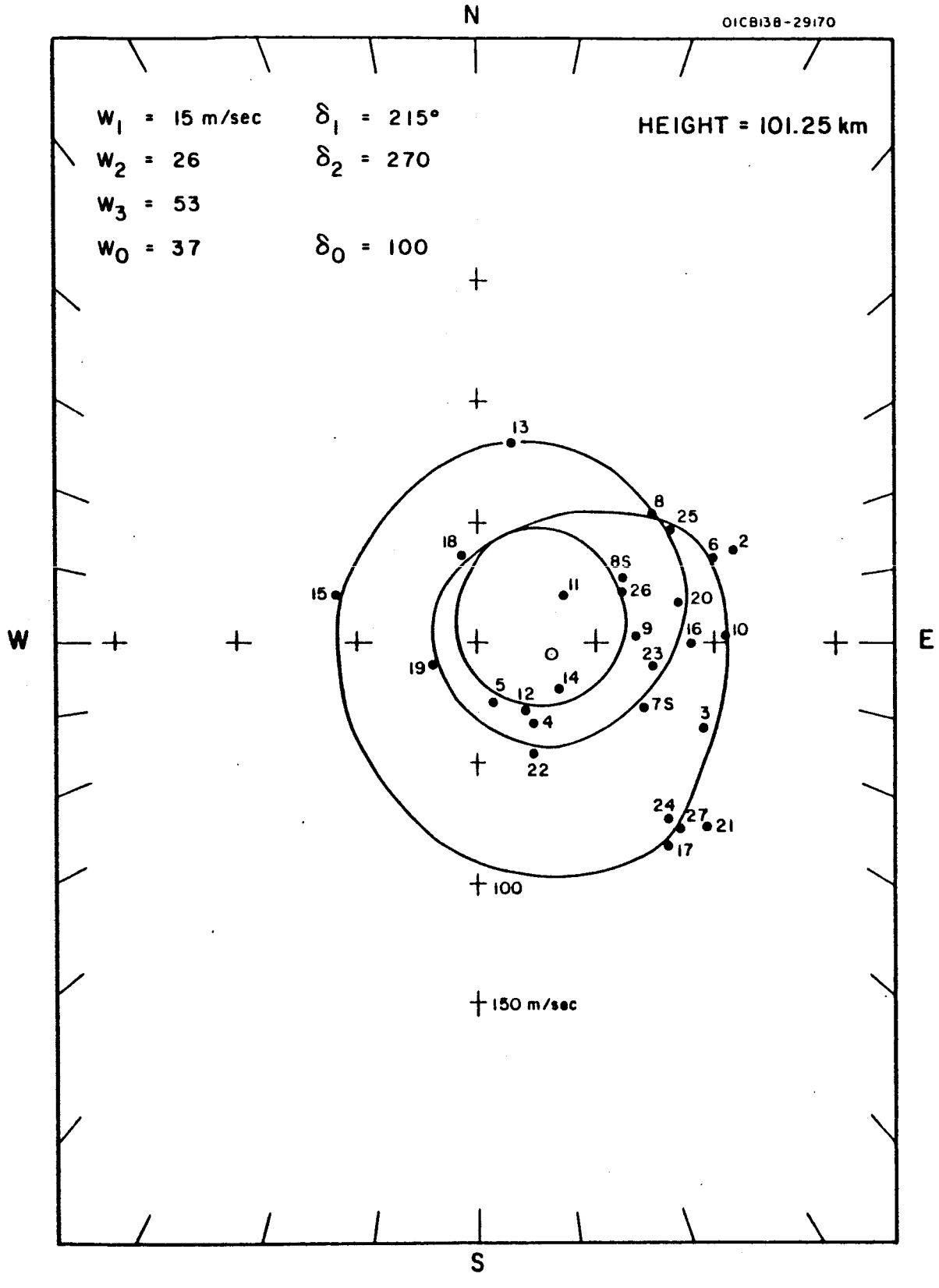

Figure 15. The pattern of wind structure as observed for a height of 101.25 km.

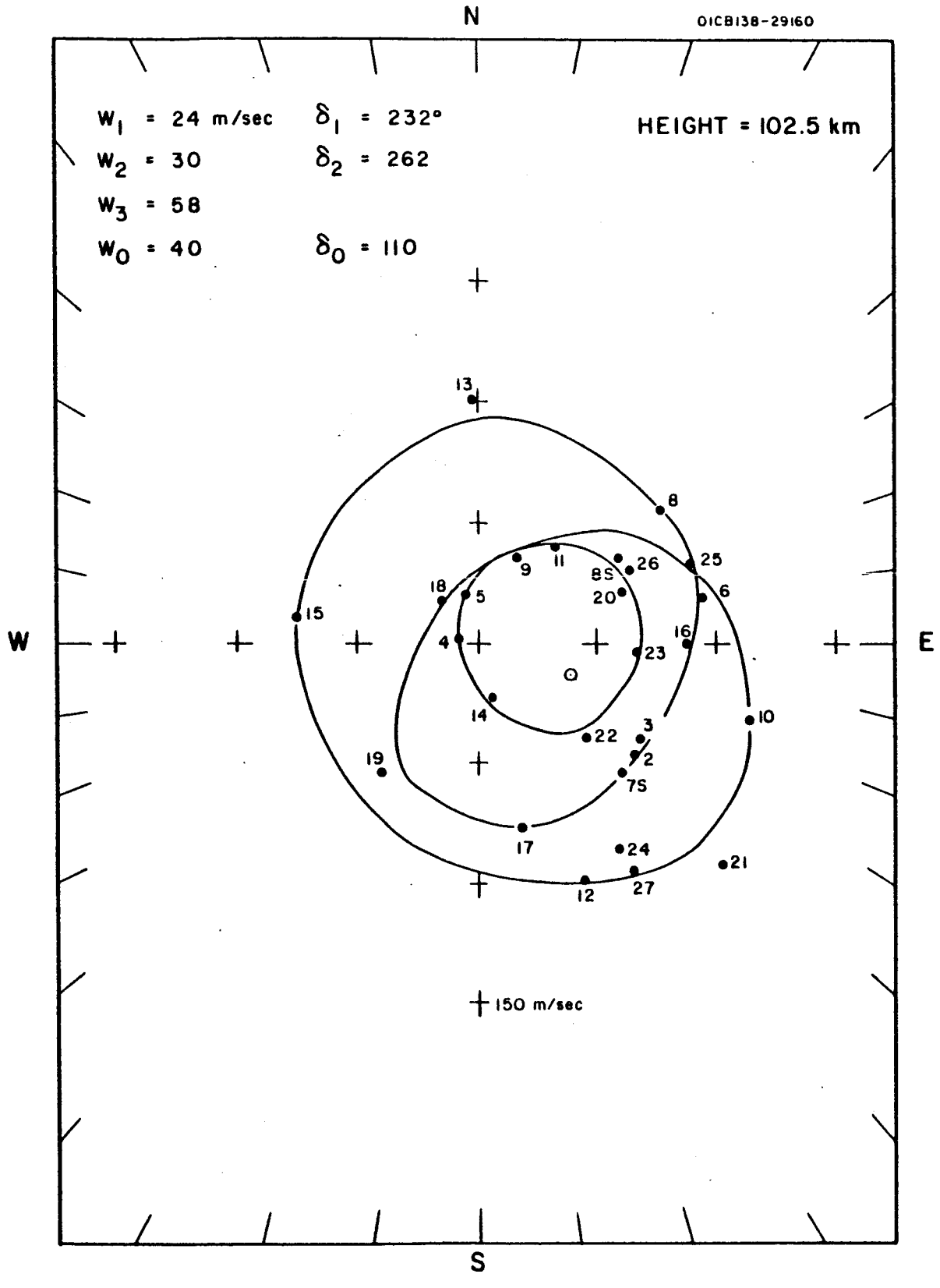

Figure 16. The pattern of wind structure as observed for a height of 102.5 km.

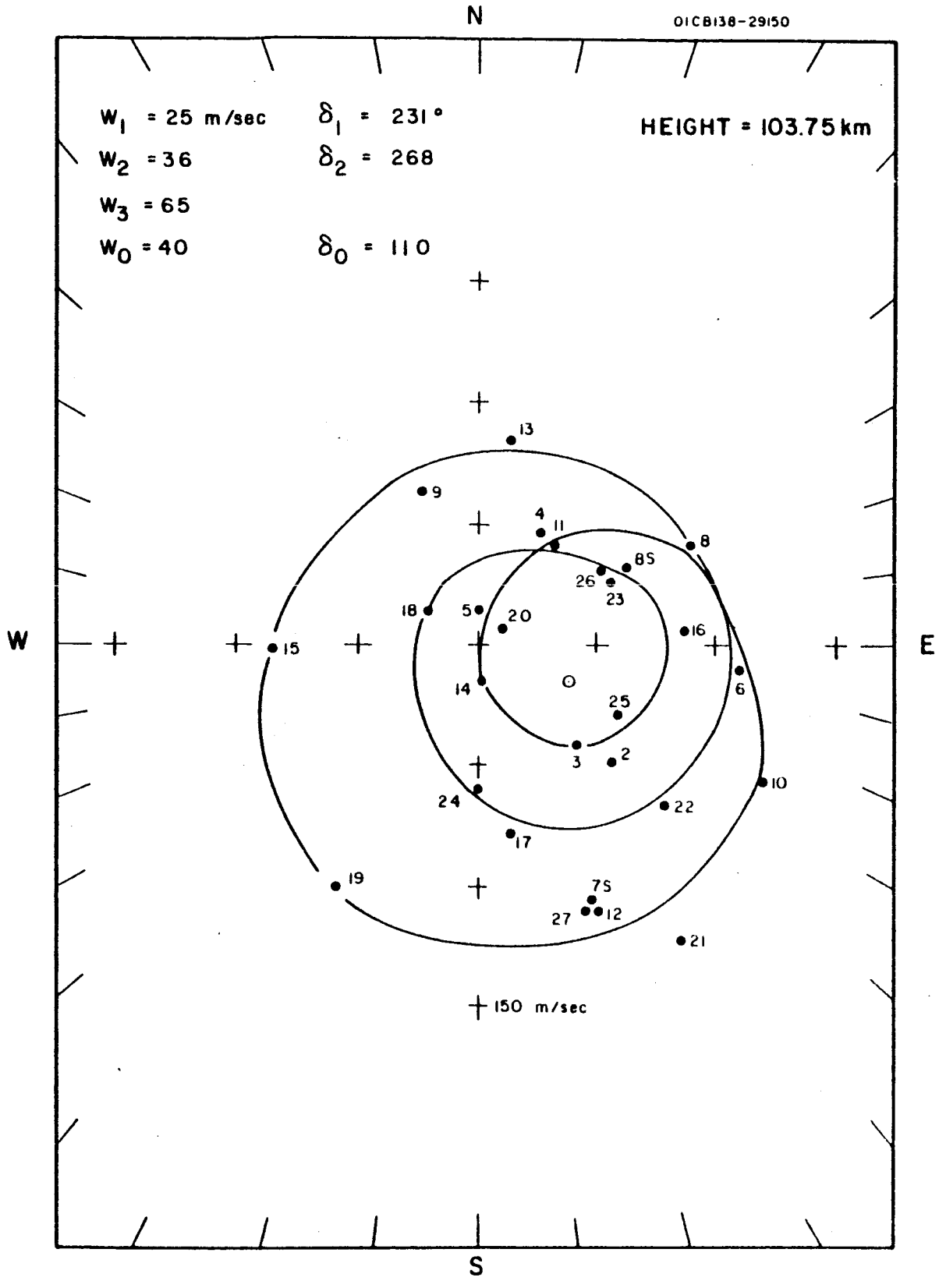

Figure 17. The pattern of wind structure as observed for a height of 103.75 km.

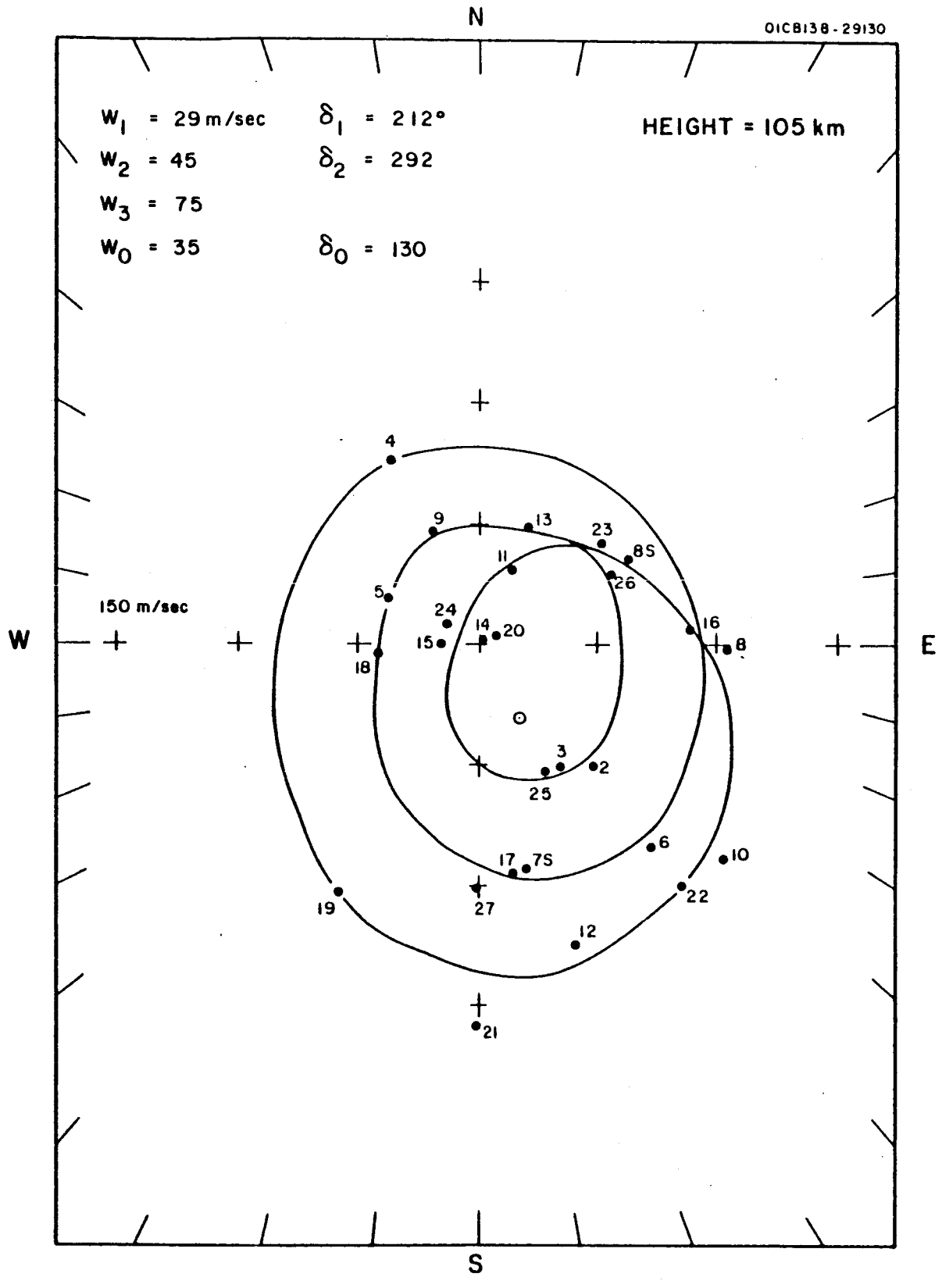

Figure 18. The pattern of wind structure as observed for a height of 105 km.

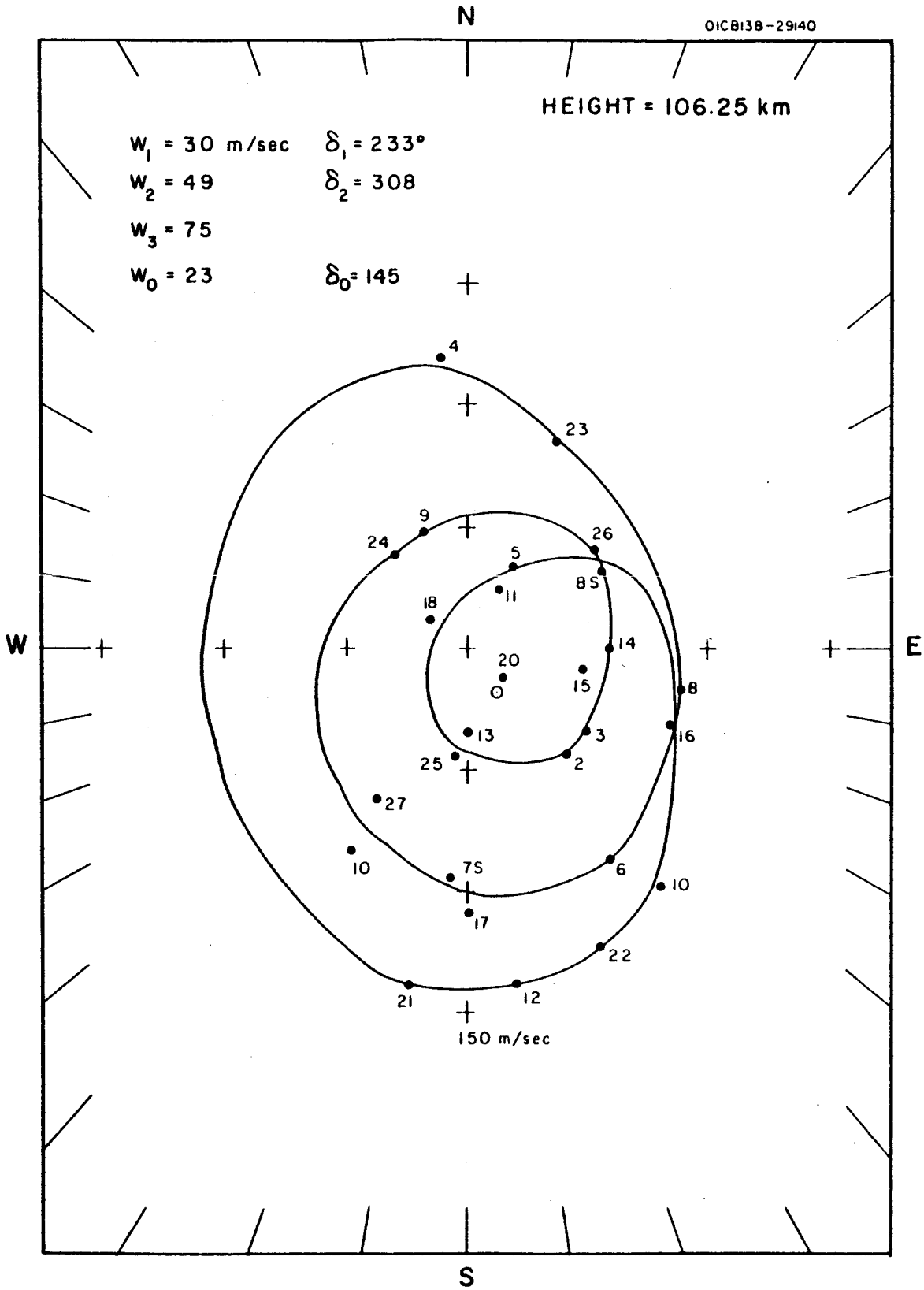

Figure 19. The pattern of wind structure as observed for a height of 106.25 km.

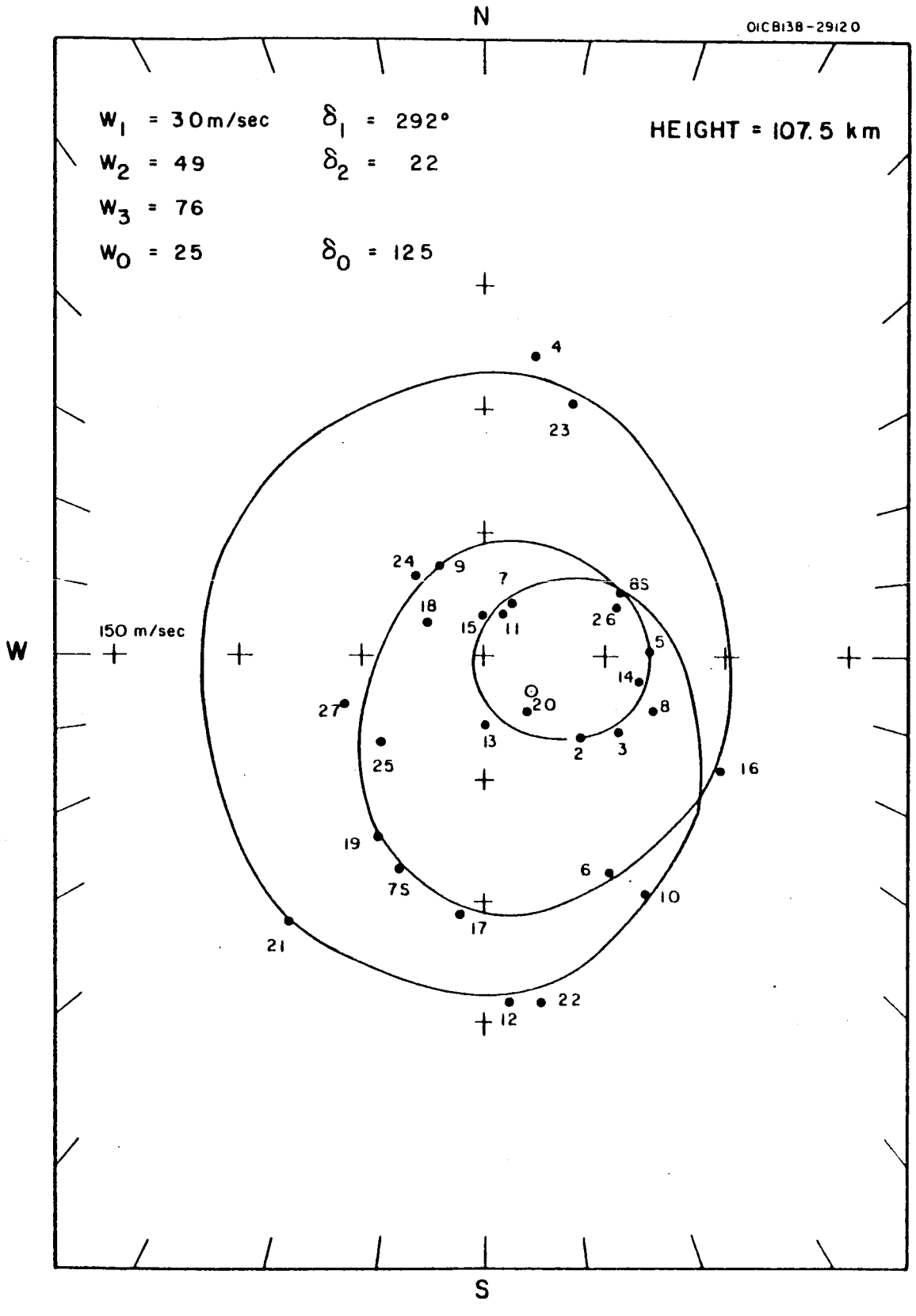

Figure 20. The pattern of wind structure as observed for a height of 107.5 km.

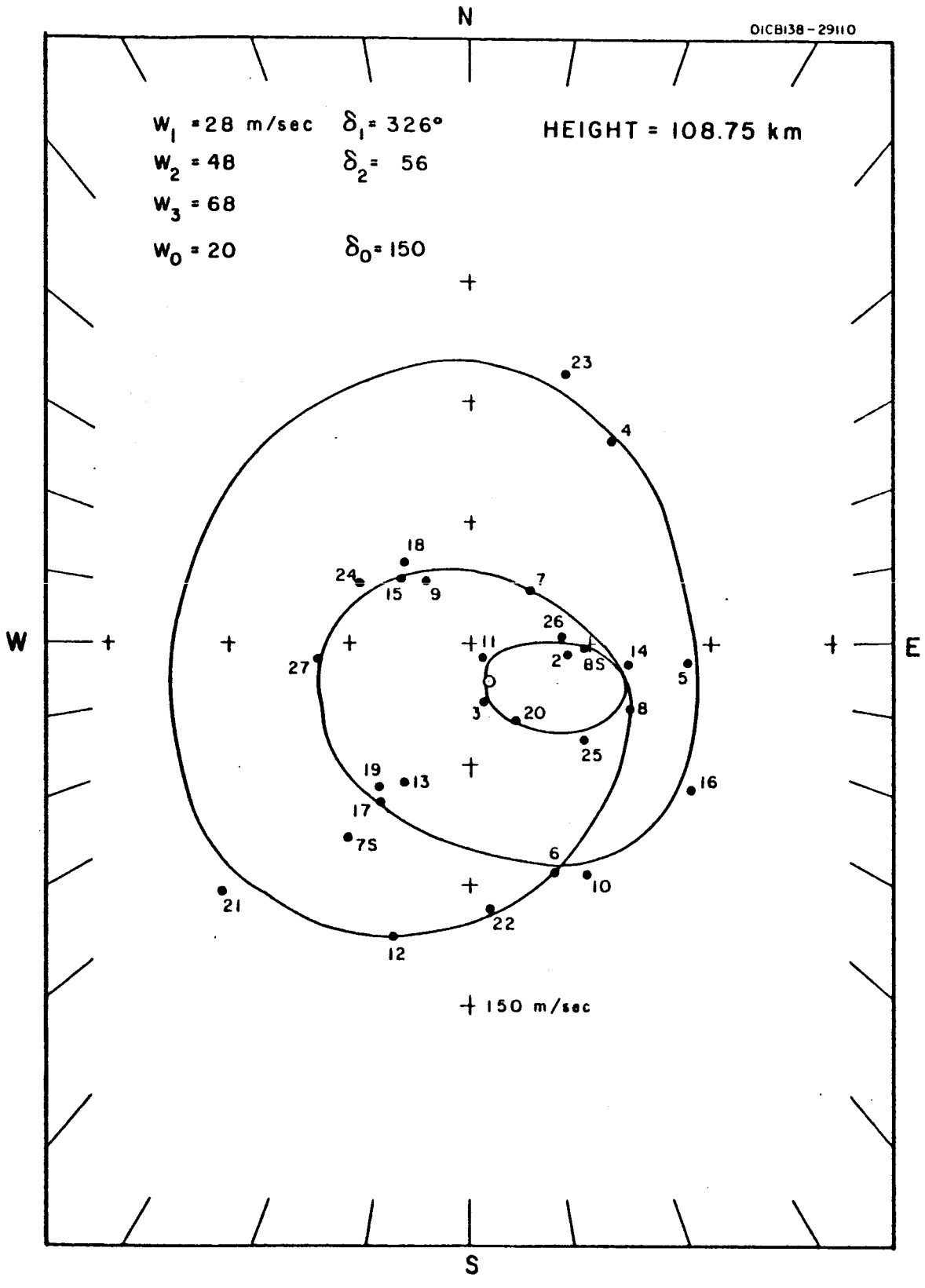

Figure 21. The pattern of wind structure as observed for a height of 108.75 km.

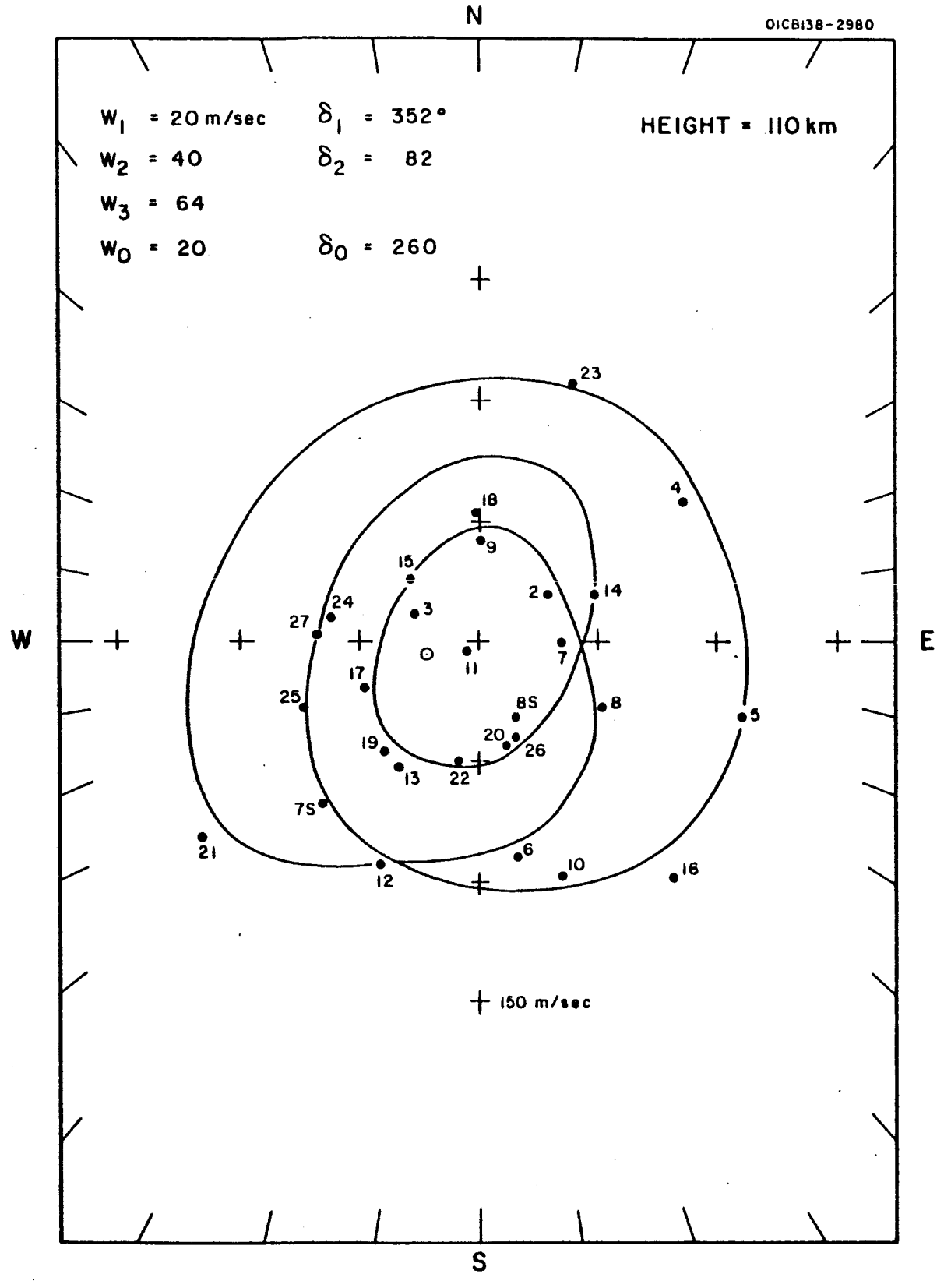

Figure 22. The pattern of wind structure as observed for a height of 110 km.

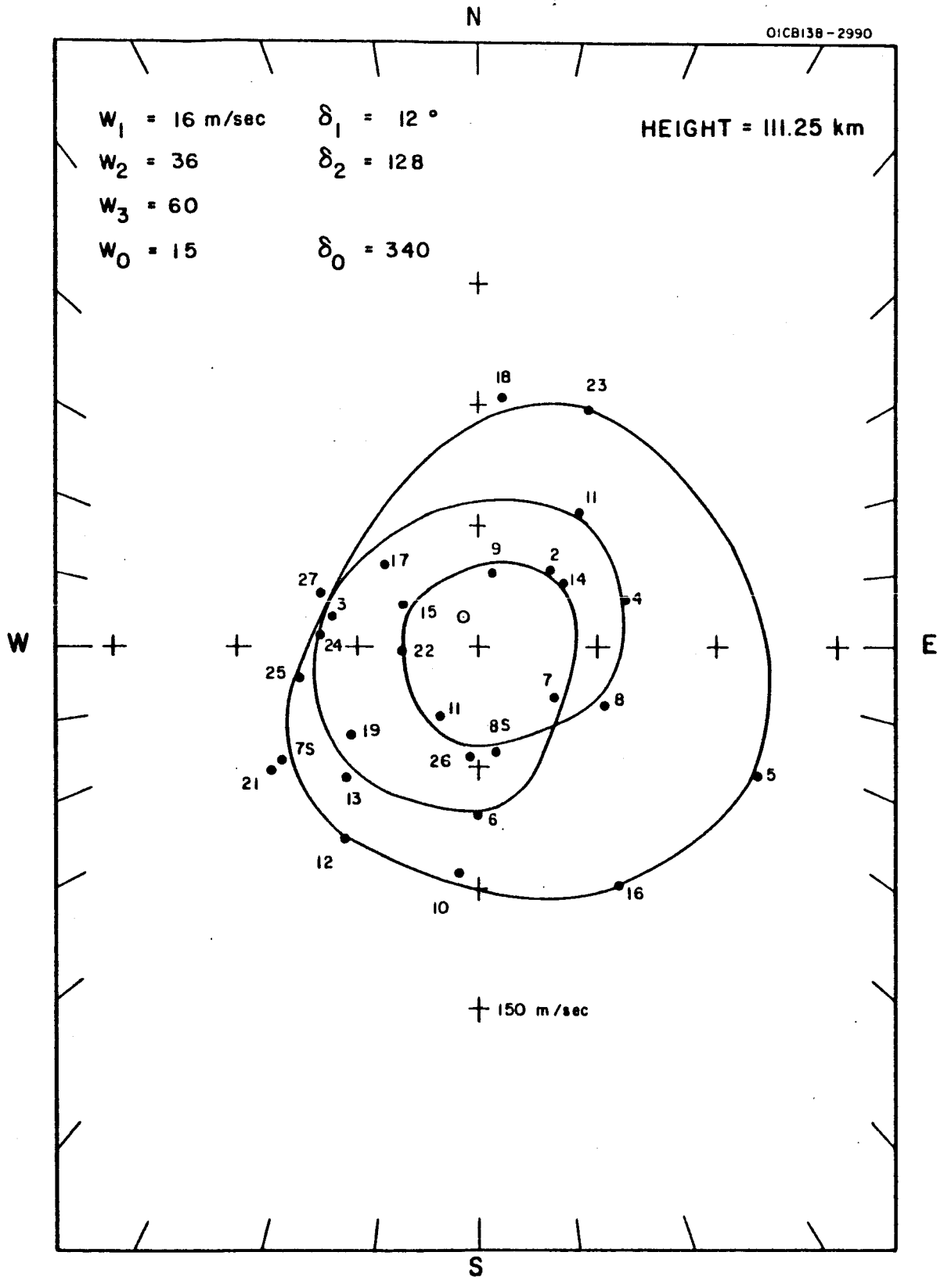

Figure 23. The pattern of wind structure as observed for a height of 111.25 km.

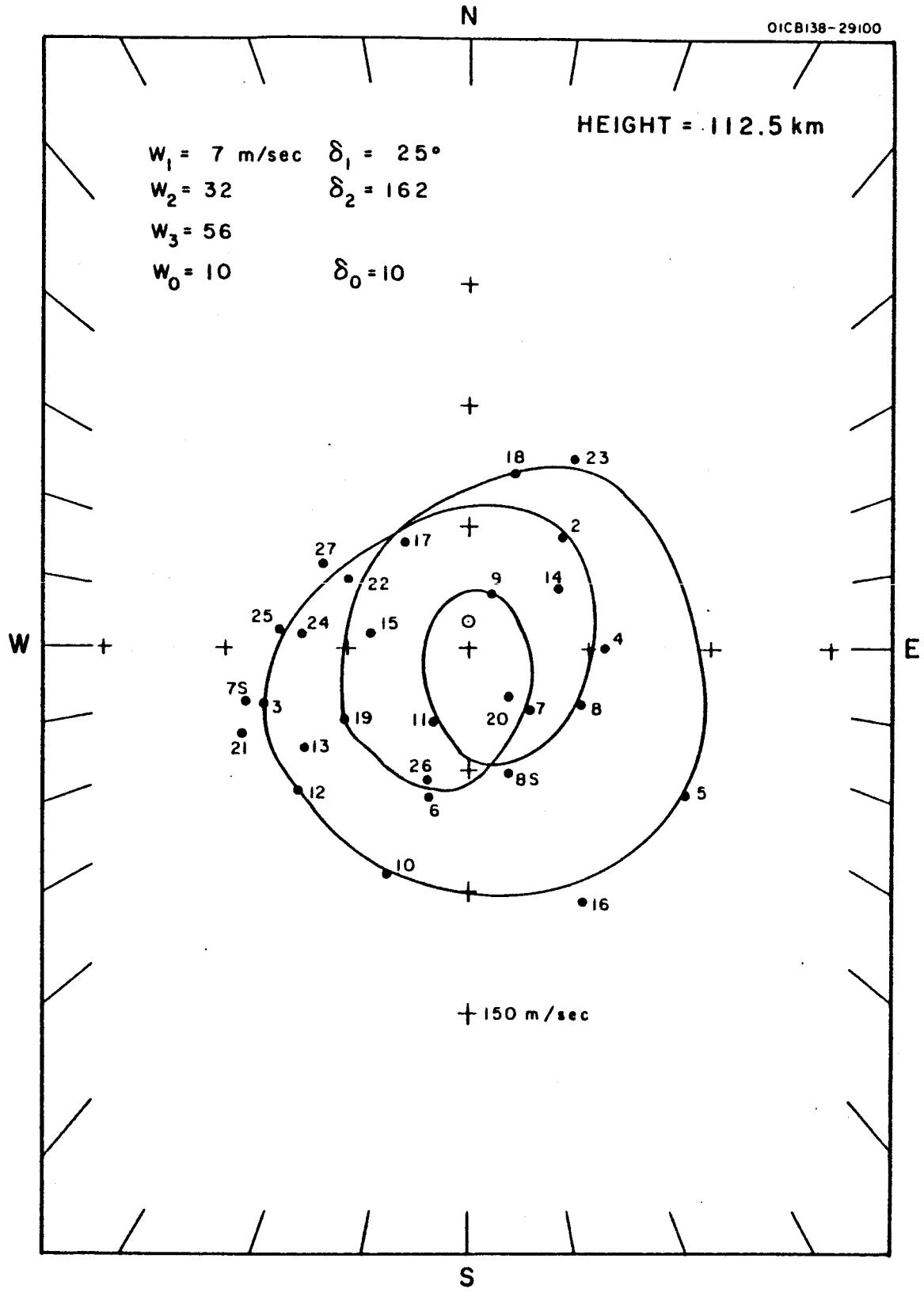

Figure 24. The pattern of wind structure as observed for a height of 112.5 km.

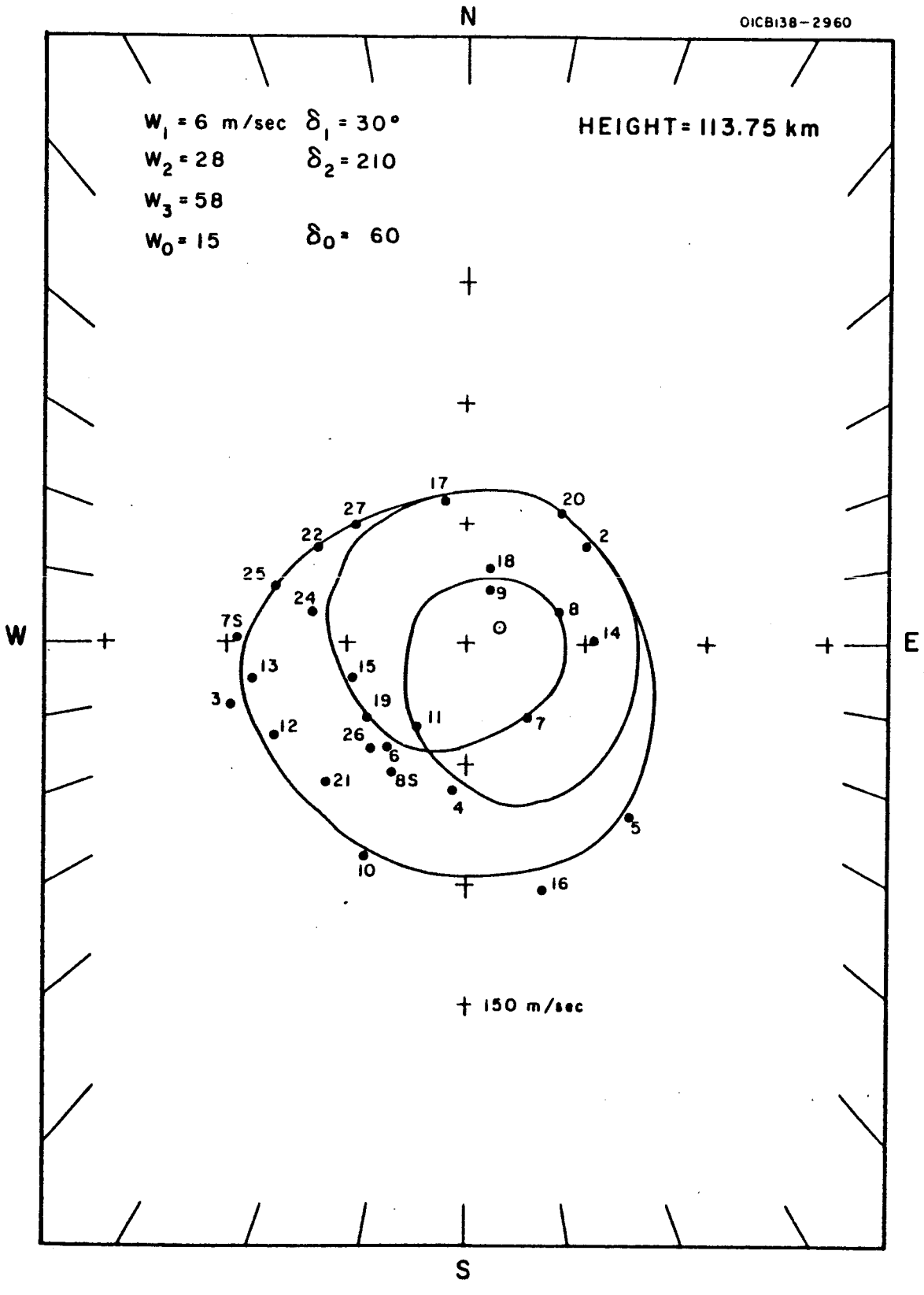

Figure 25. The pattern of wind structure as observed for a height of 113.75 km.

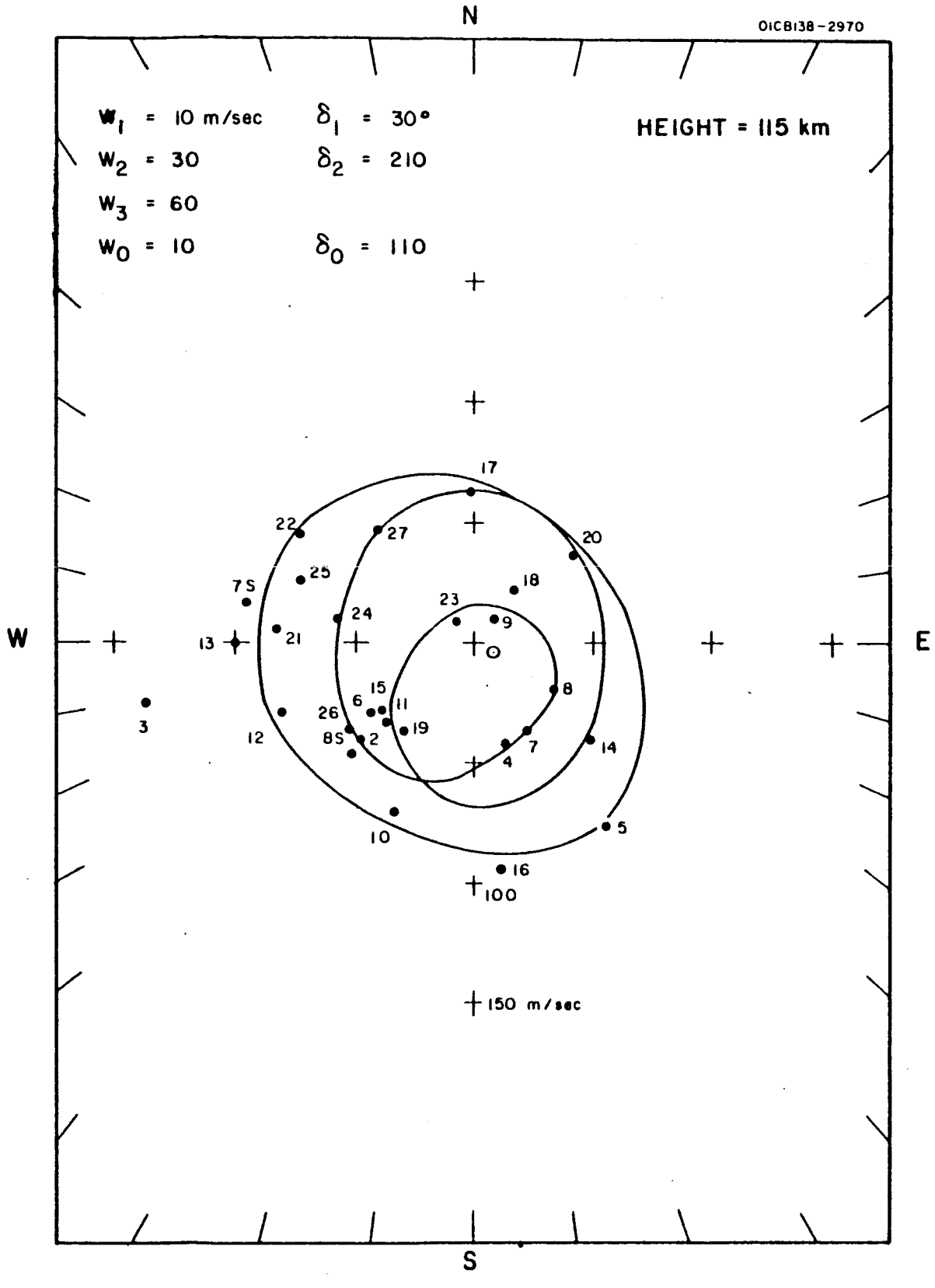

Figure 26. The pattern of wind structure as observed for a height of 115 km.

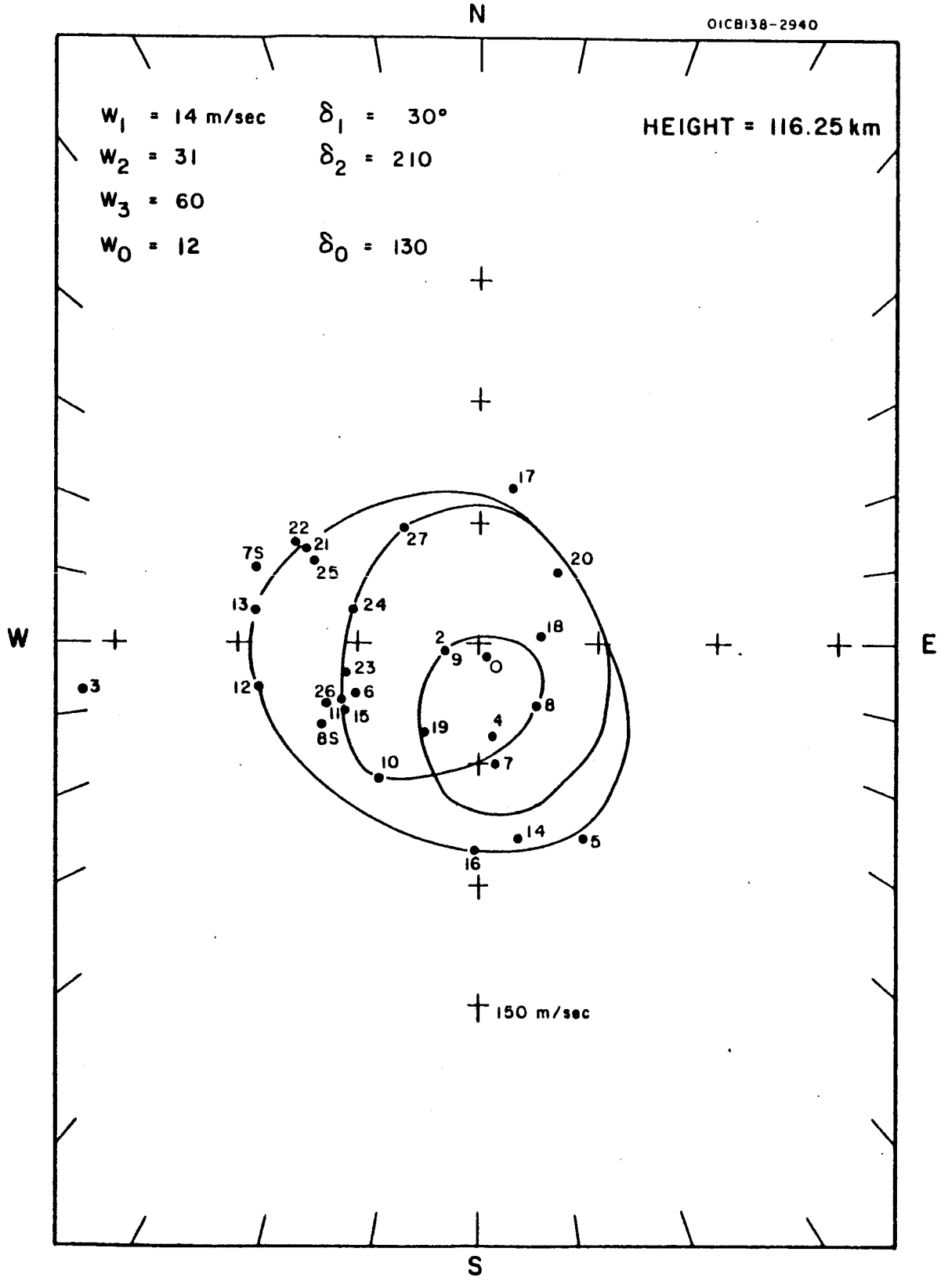

Figure 27. The pattern of wind structure as observed for a height of 116.25 km.

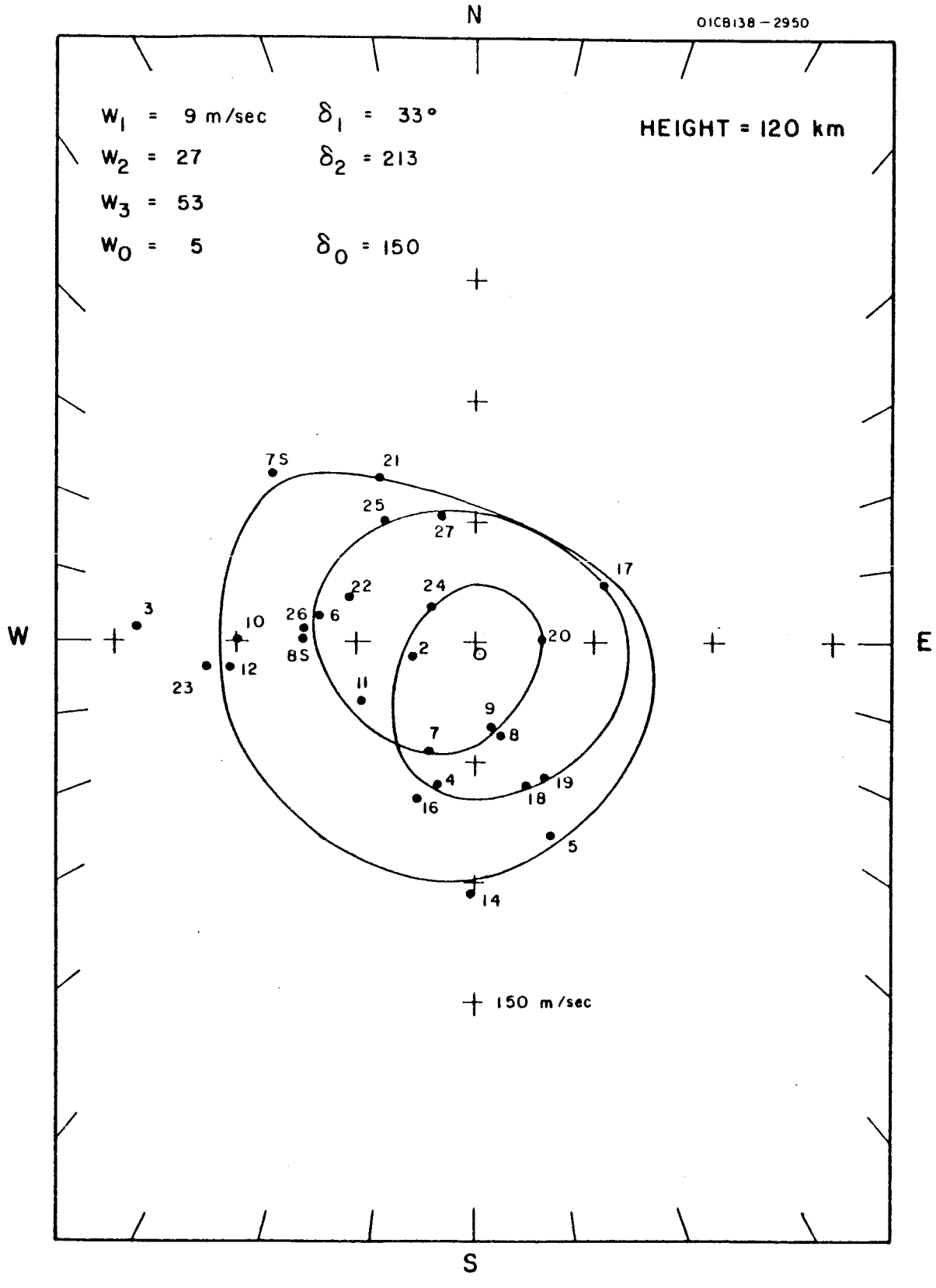

Figure 28. The pattern of wind structure as observed for a height of 120 km.

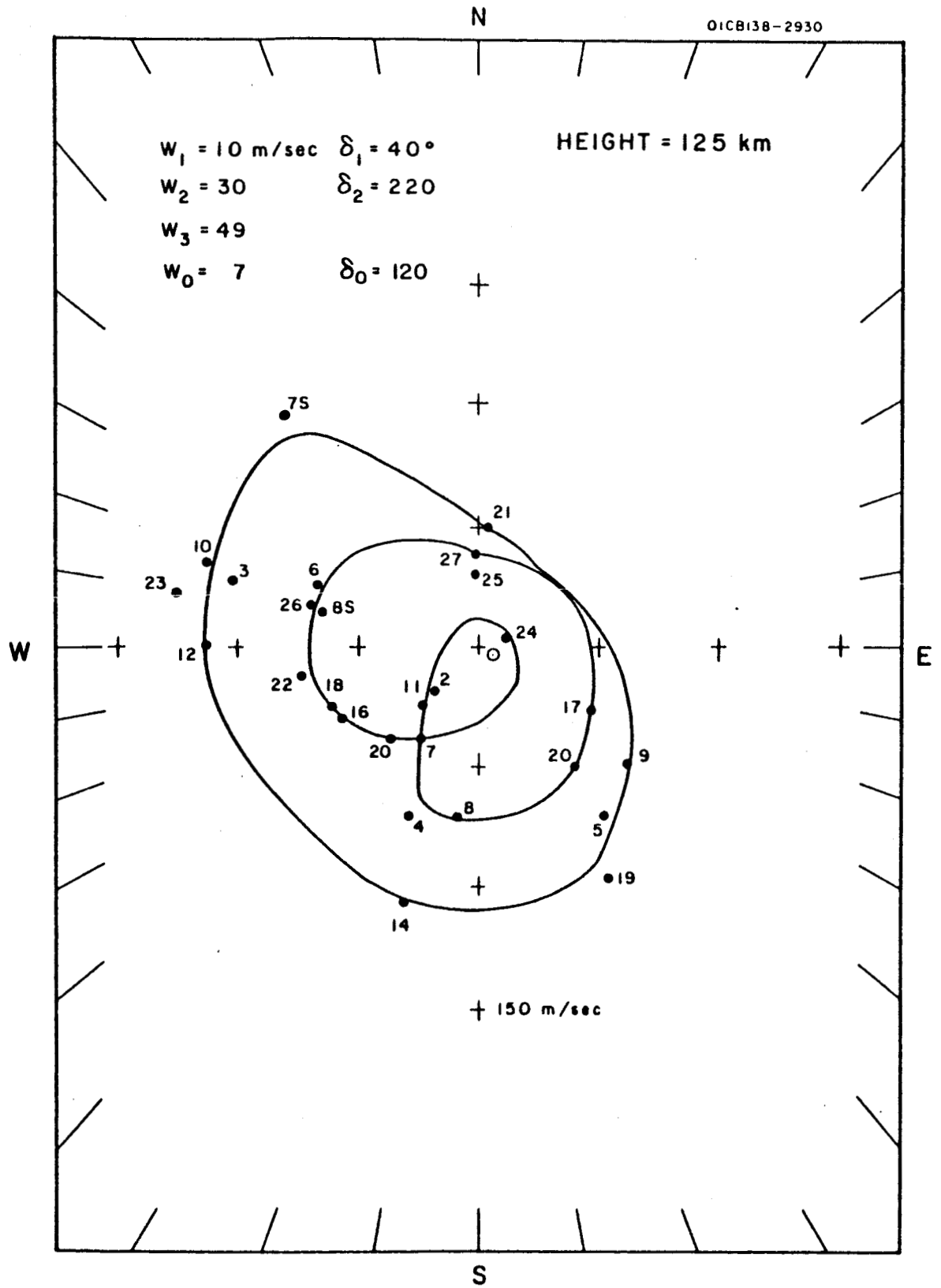

Figure 29. The pattern of wind structure as observed for a height of 125 km.

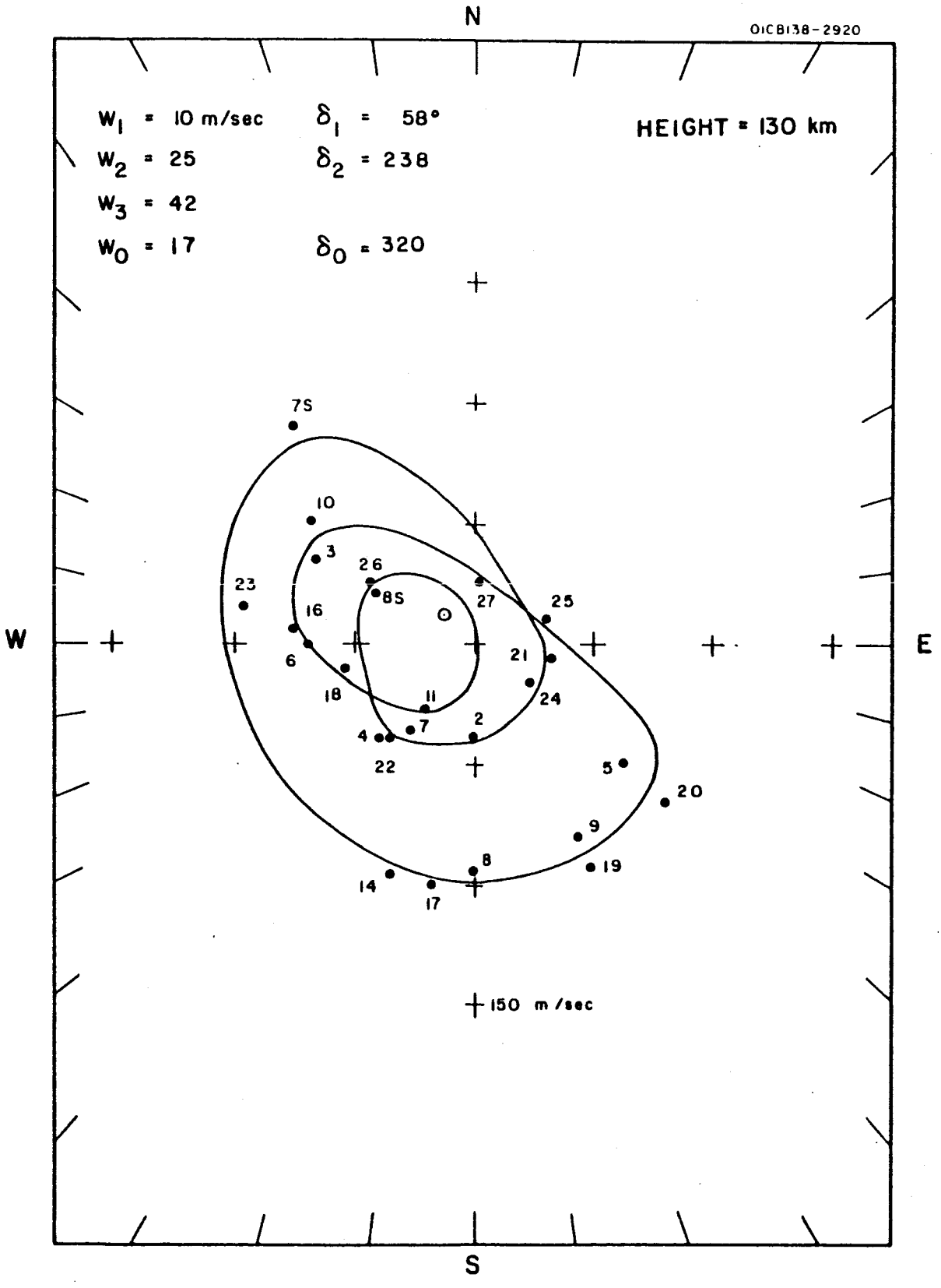

Figure 30. The pattern of wind structure as observed for a height of 130 km.

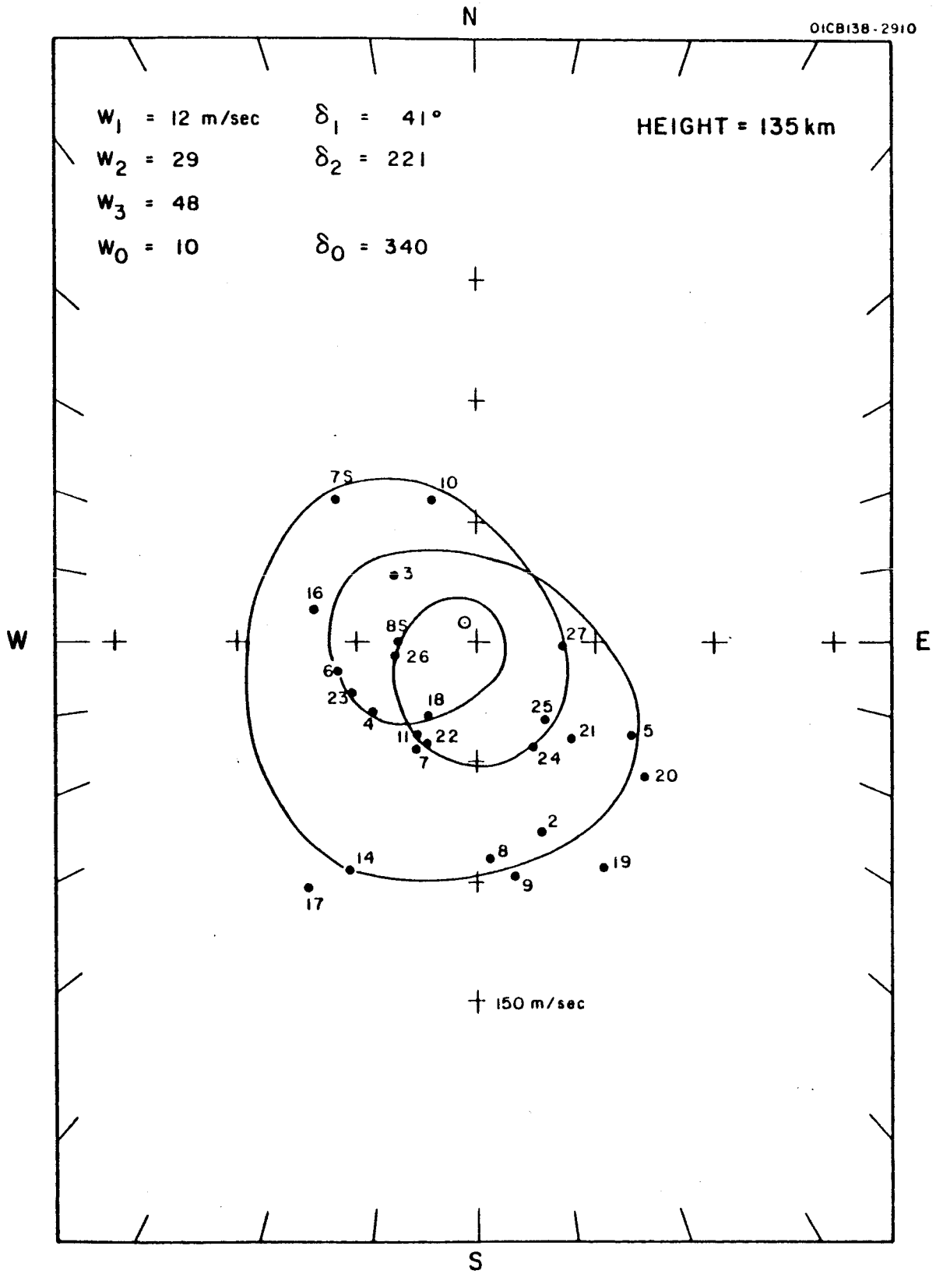

Figure 31. The pattern of wind structure as observed for a height of 135 km.

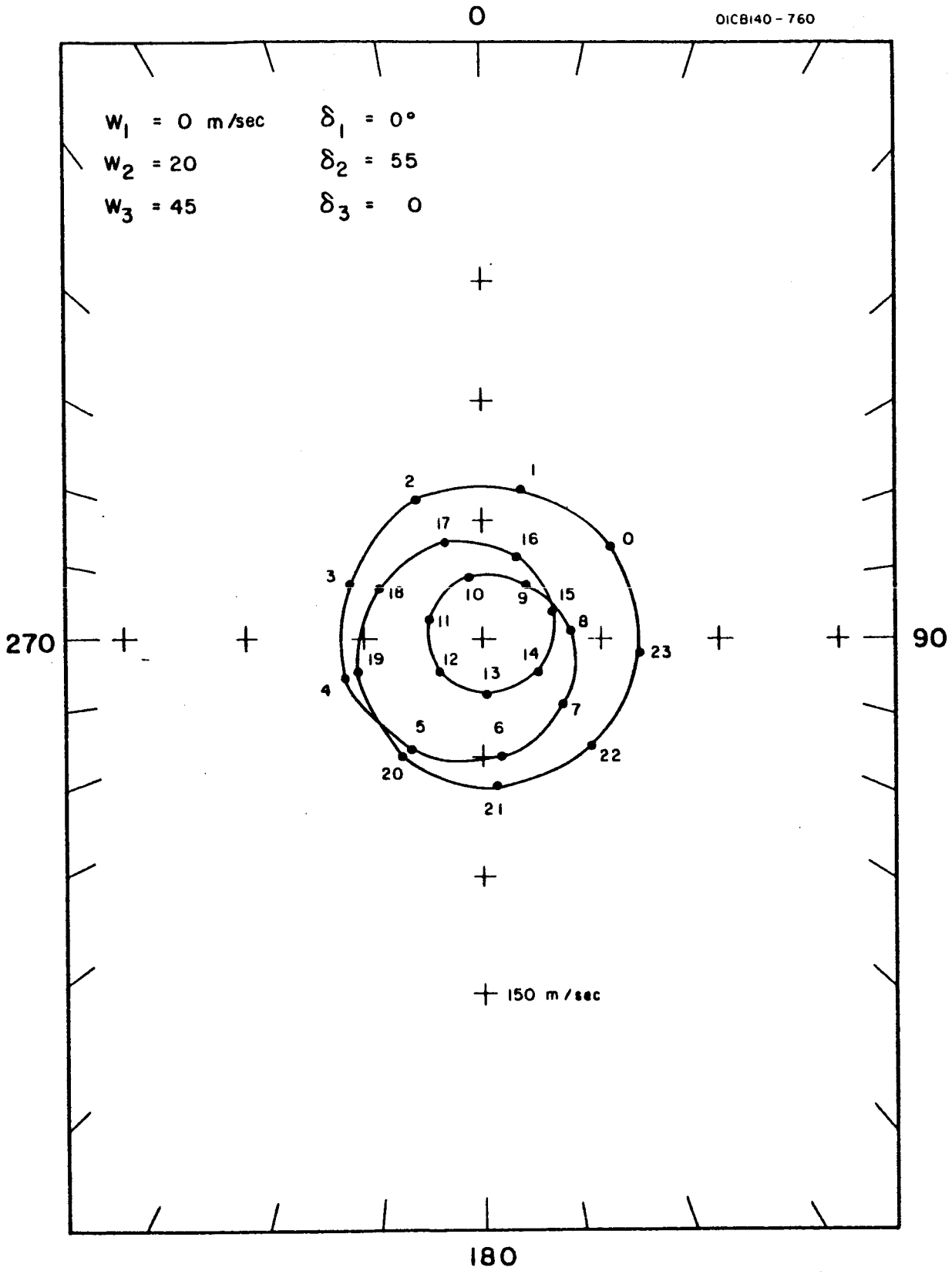

Figure 32. Theoretical figure drawn with $W_1 = 0$, $W_2 = 20$, and $W_3 = 45$ M/sec; $\delta_1 = 0$, $\delta_2 = 55$, and $\delta_3 = 0$ degress. The numbers represent the time scale in hours.

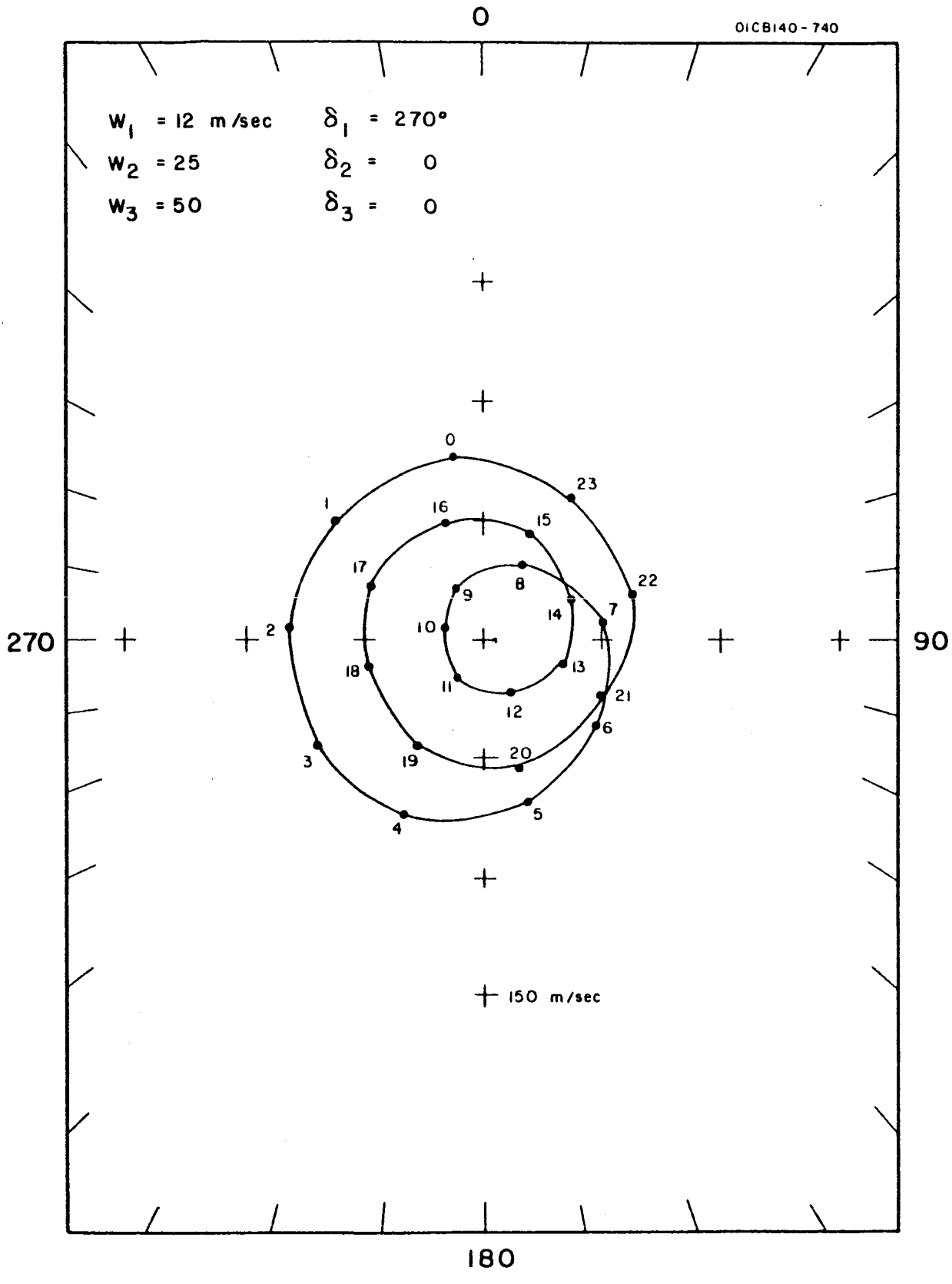

Figure 33. Theoretical figure drawn with W_1 = 12, W_2 = 25, and W_3 = 50 M/sec; δ_1 = 270, δ_2 = 0, and δ_3 = 0 degrees. The numbers represent the time scale in hours.

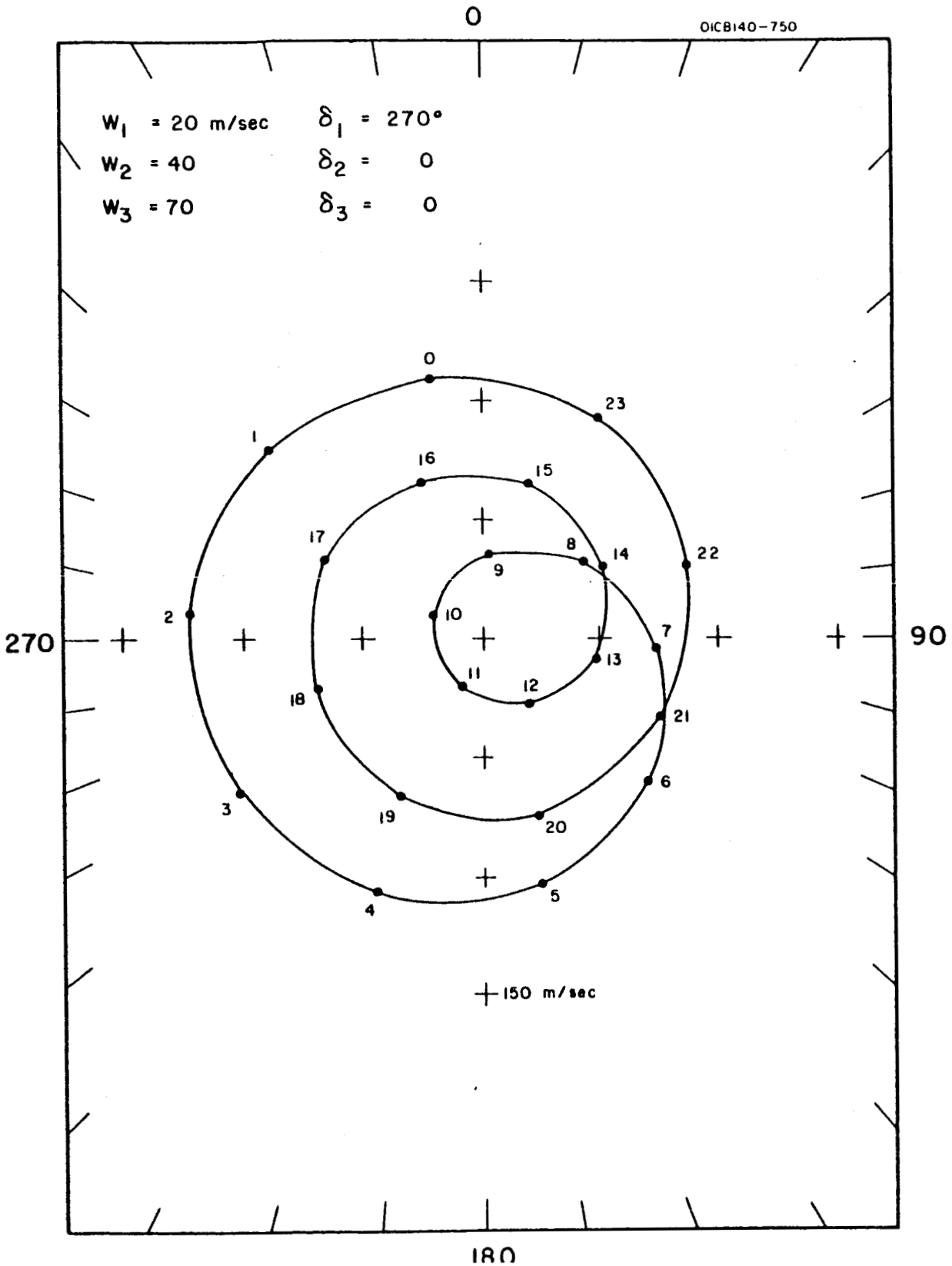

Figure 34. Theoretical figure drawn with $W_1 = 20$, $W_2 = 40$, and $W_3 = 70$ M/sec; $\delta_1 = 270$, $\delta_2 = 0$, and $\delta_3 = 0$ degrees. The numbers represent the time scale in hours.

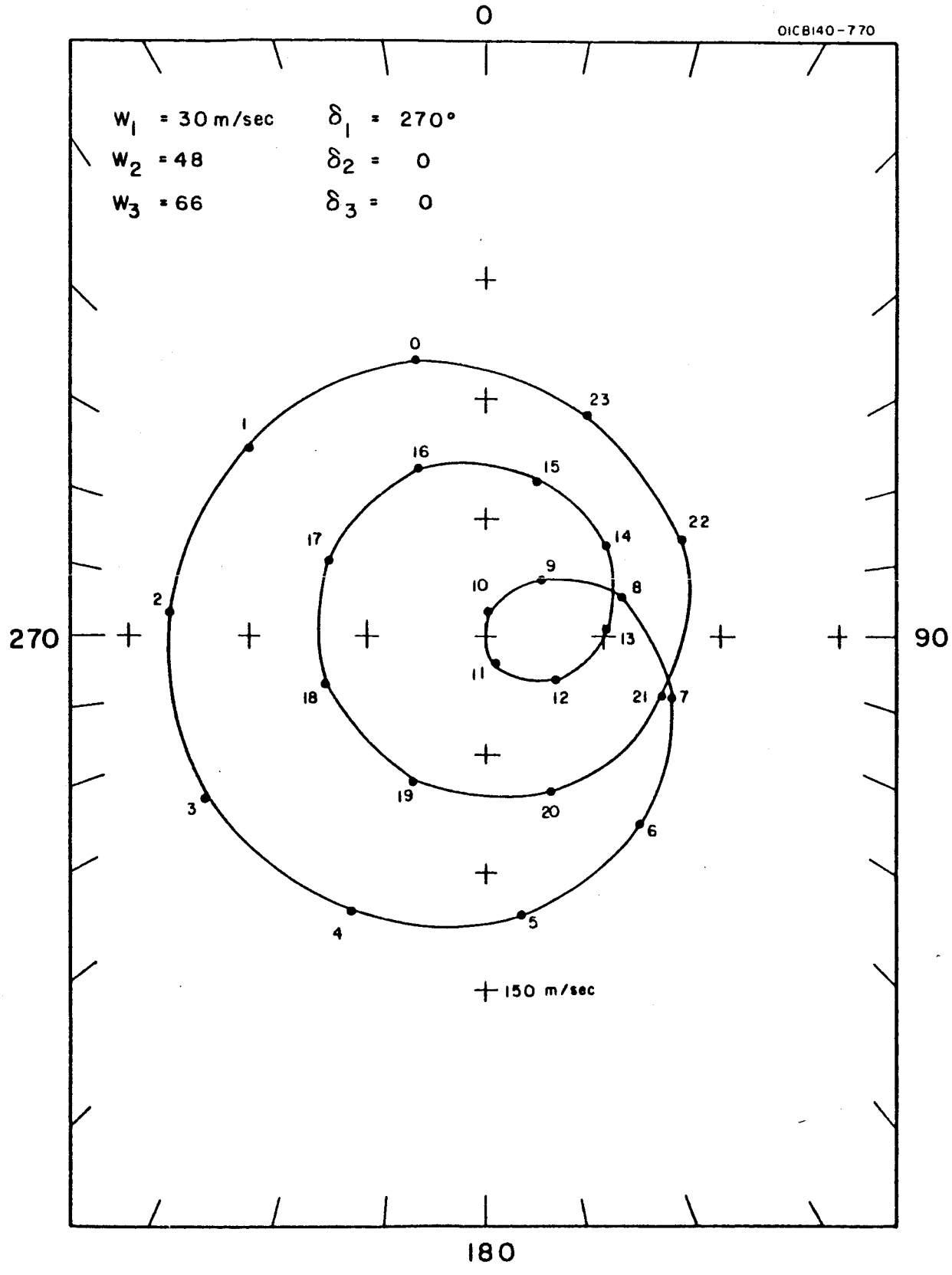

Figure 35. Theoretical figure drawn with W_1 = 30, W_2 = 48, and W_3 = 66 M/sec; δ_1 = 270, δ_2 = 0, and δ_3 = 0 degrees. The numbers represent the time scale in hours.

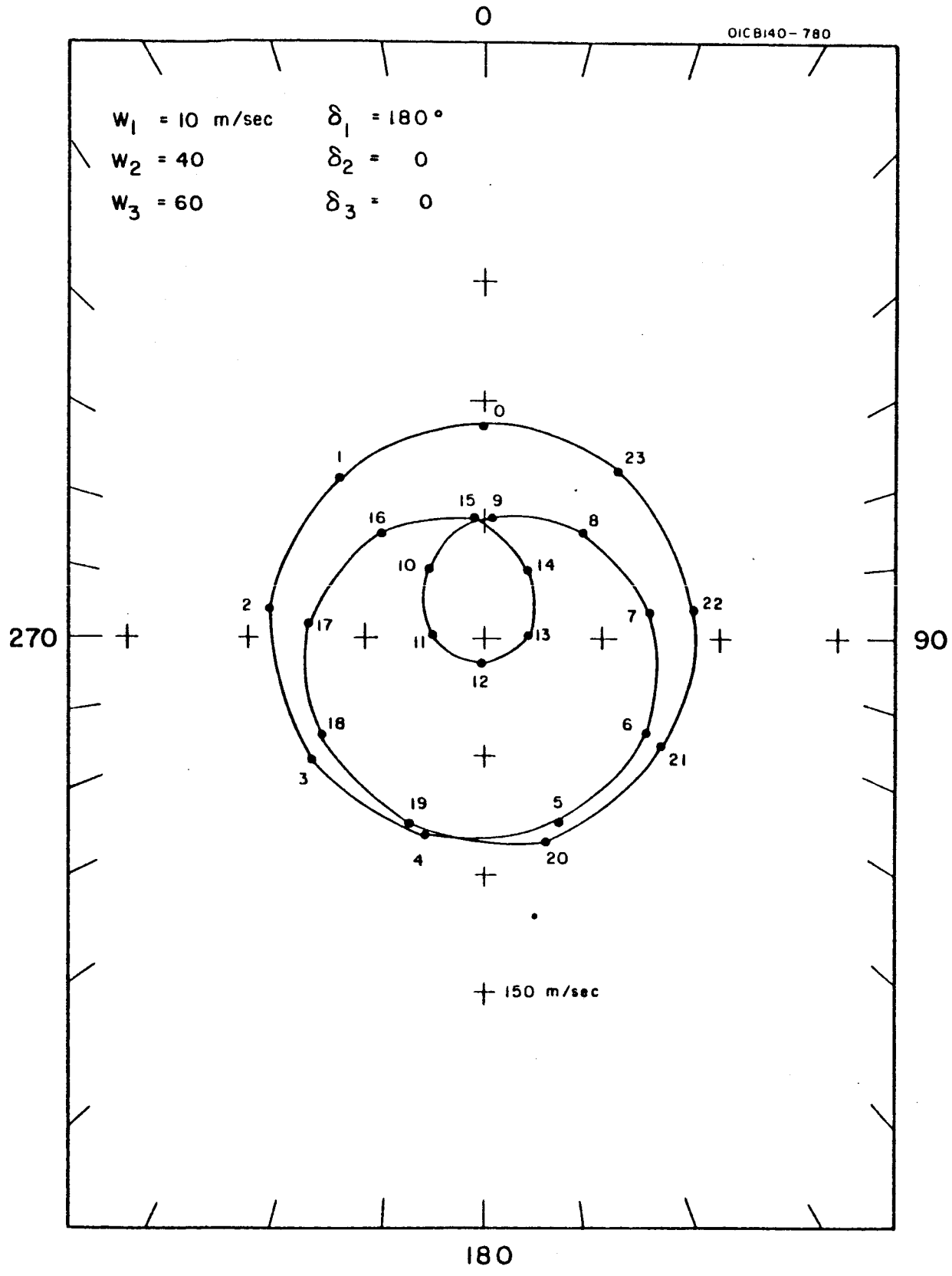

Figure 36. Theoretical figure drawn with W_1 = 10, W_2 = 40, and W_3 = 60 M/sec; δ_1 = 180, δ_2 = 0, and δ_3 = 0 degrees. The numbers represent the time scale in hours.

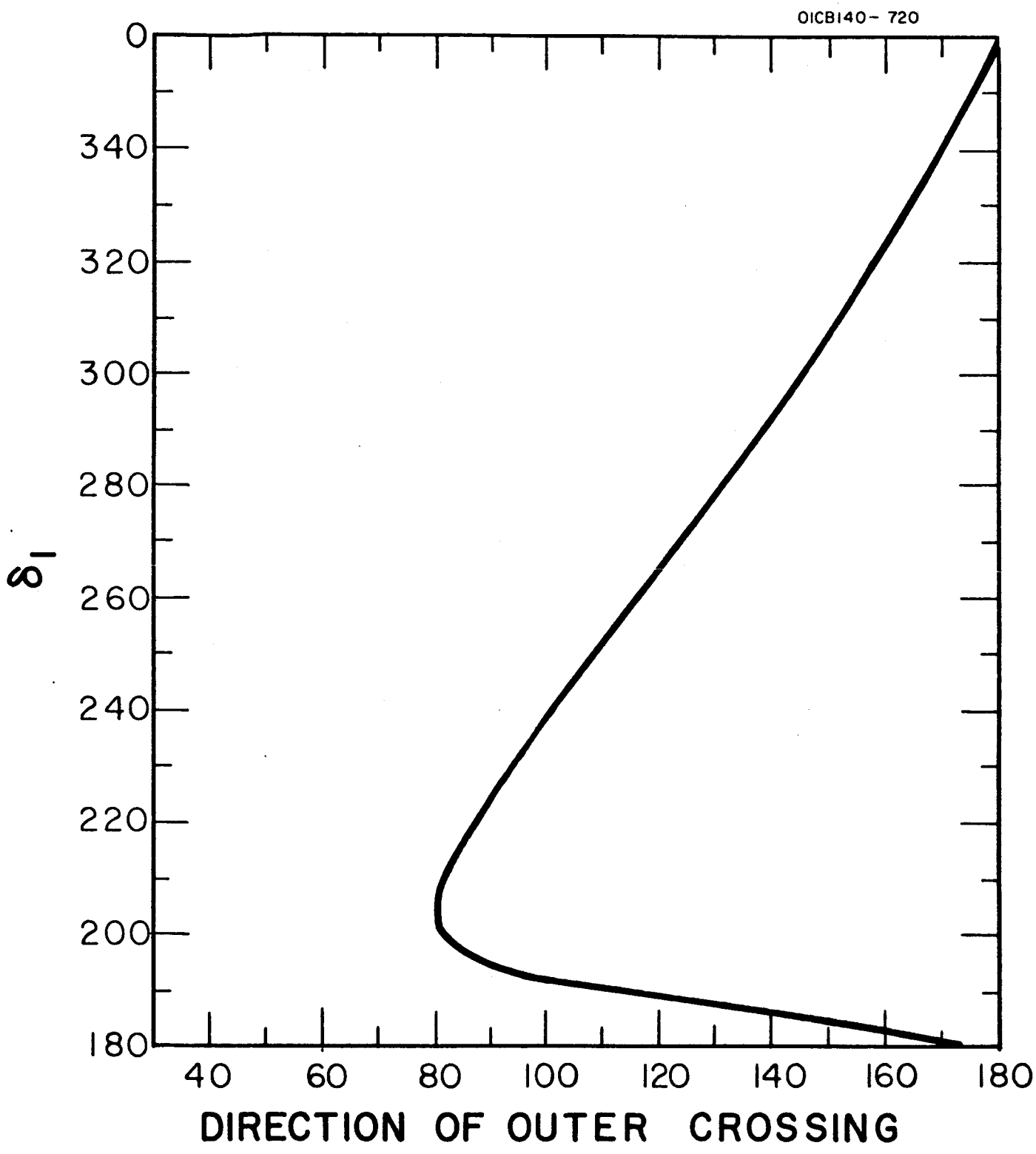

Figure 37. Direction of outer crossing as a function of δ_1 from theoretical figures similar to that of Figure 33.

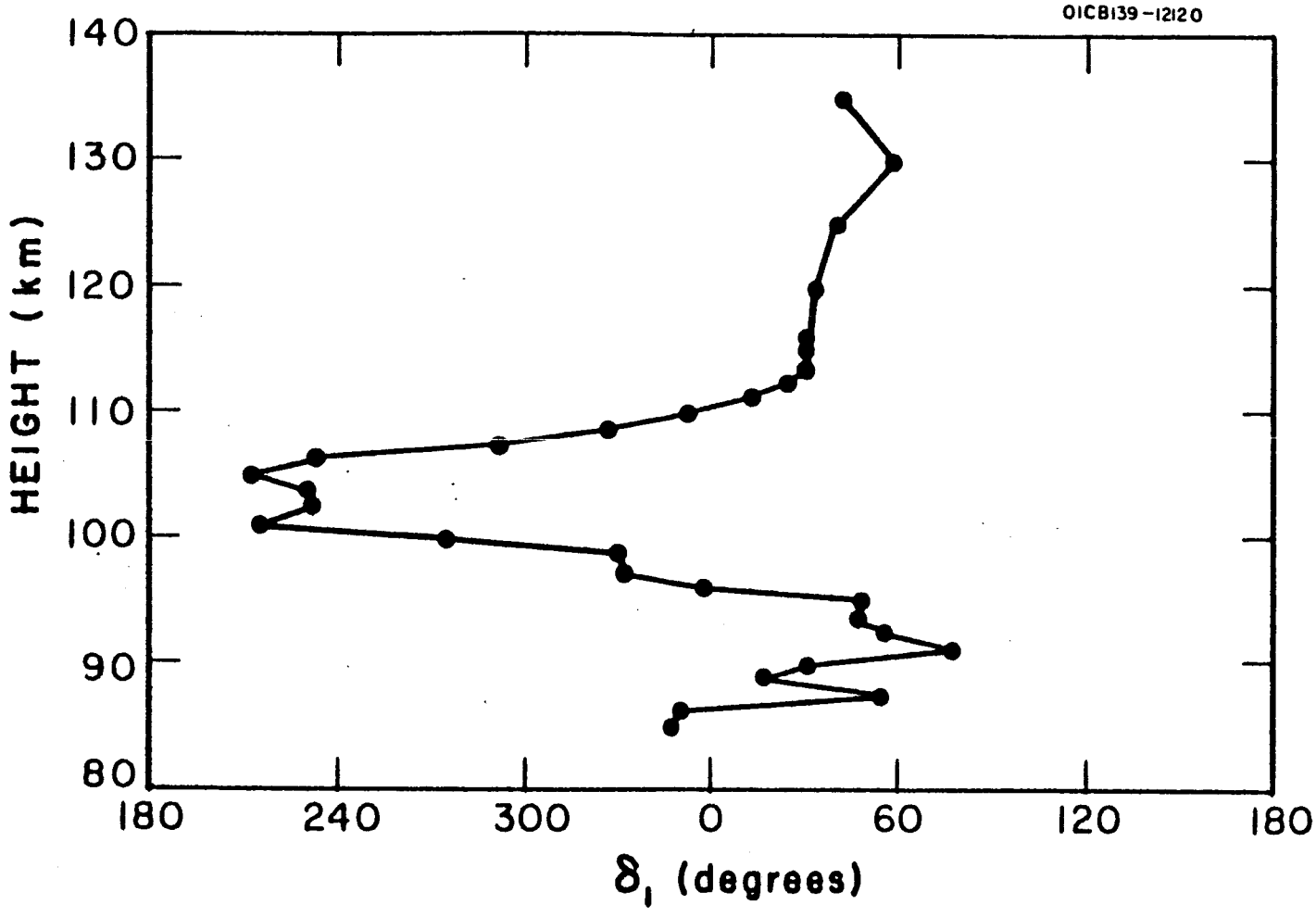

Figure 38. Observed values of δ_1 as a function of height.

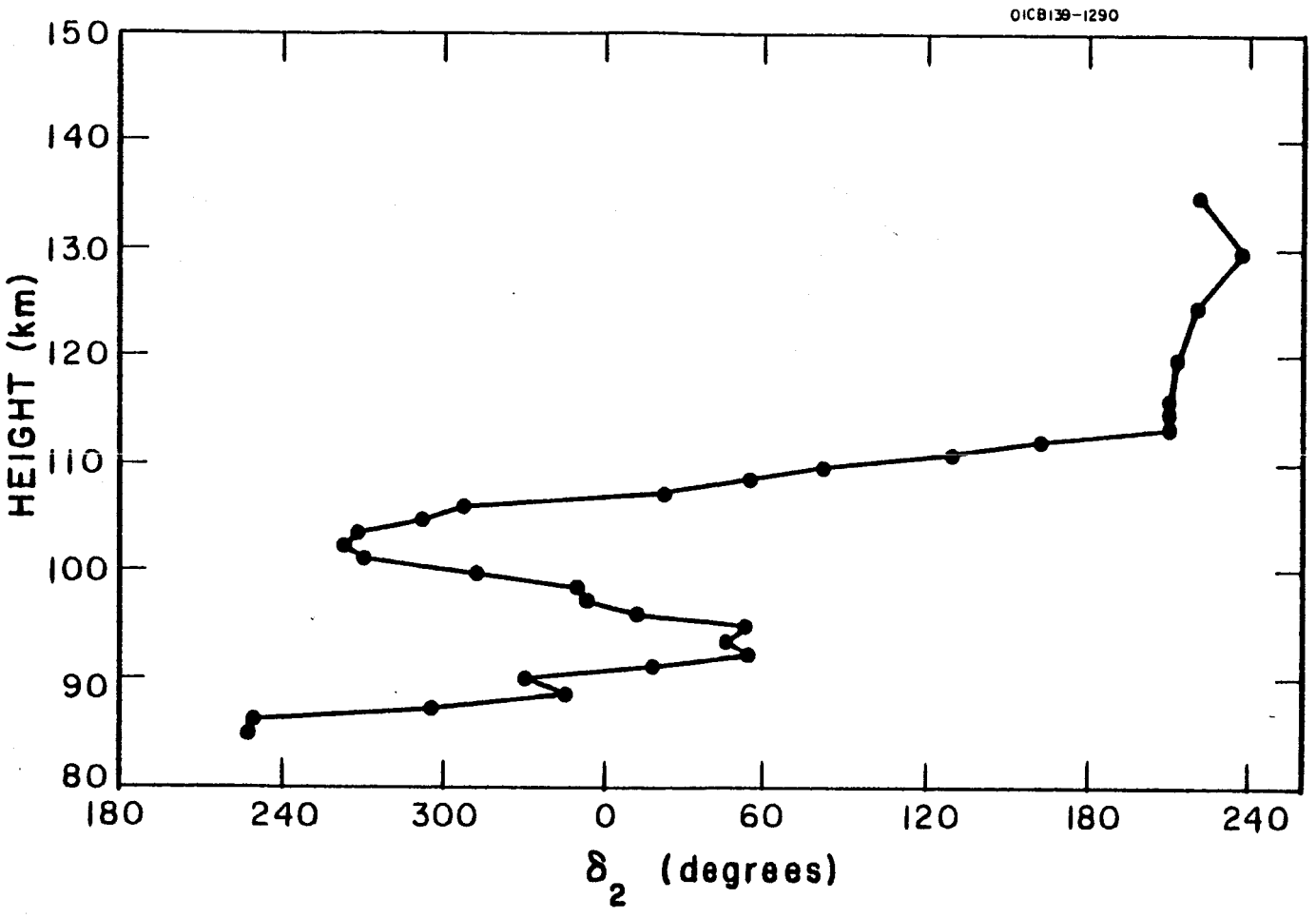

Figure 39. Observed values of δ_2 as a function of height.

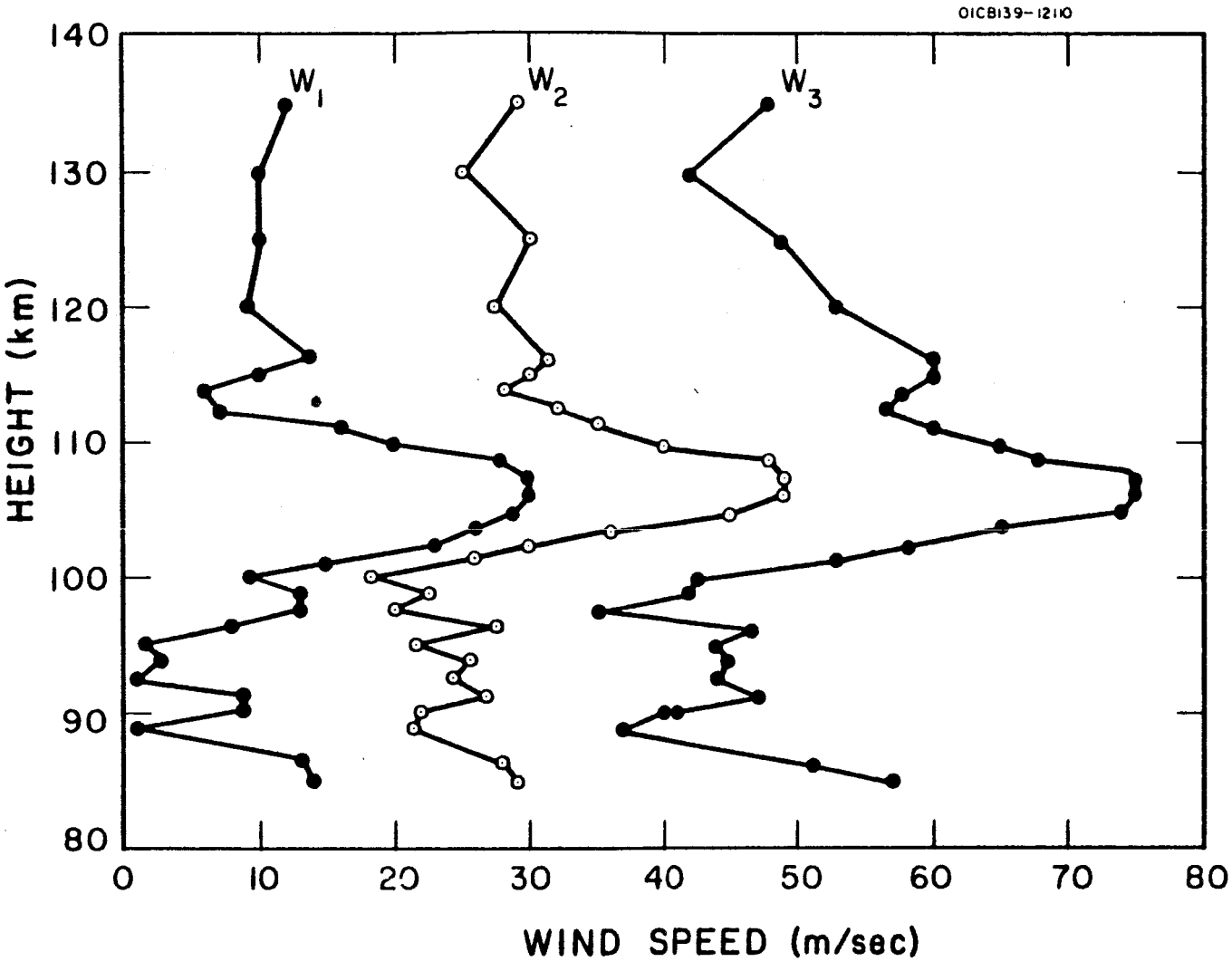

Figure 40. Observed values of W_1, W_2, and W_3 as a function of height.

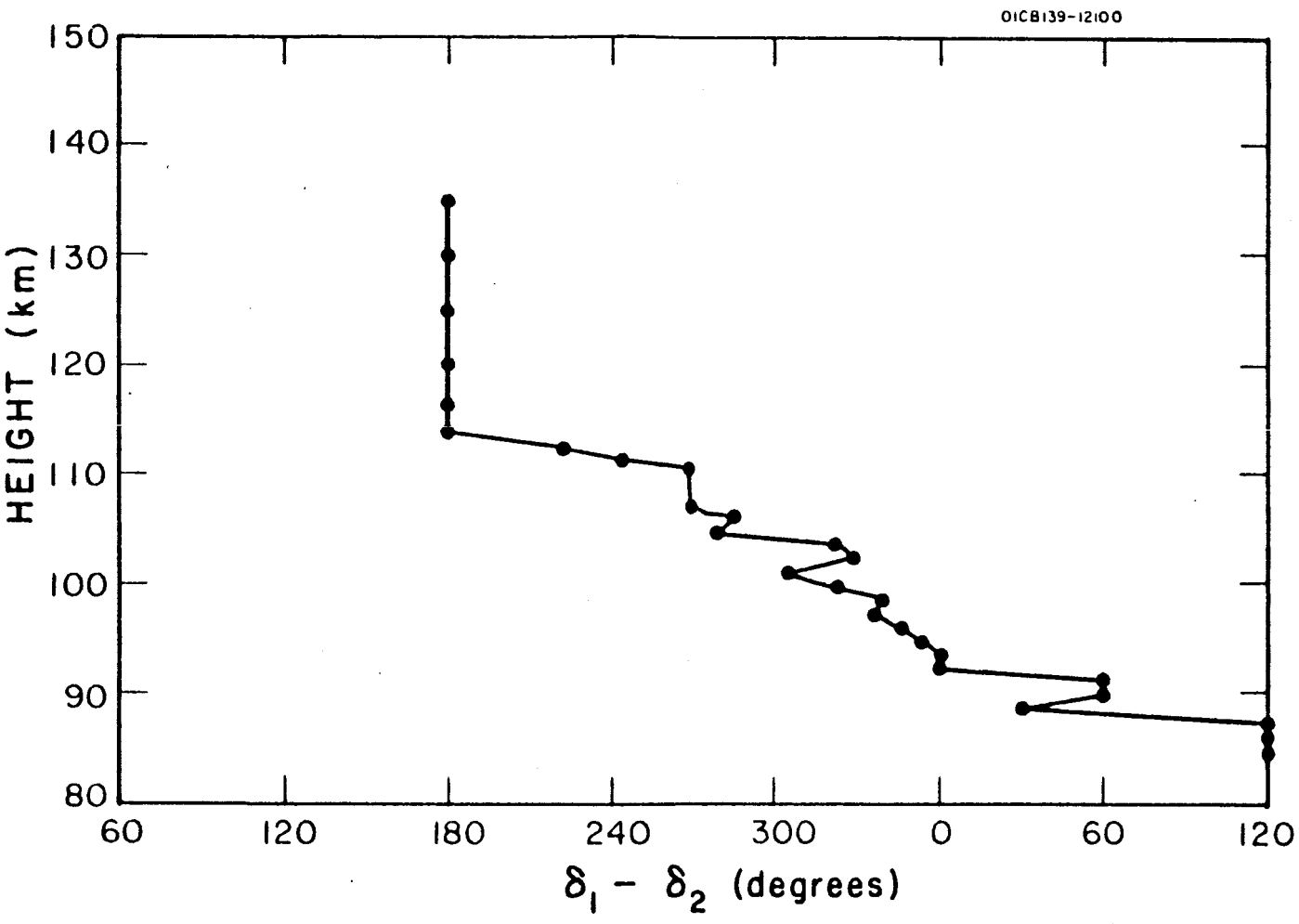

Figure 41. Observed values of δ_o as a function of height.

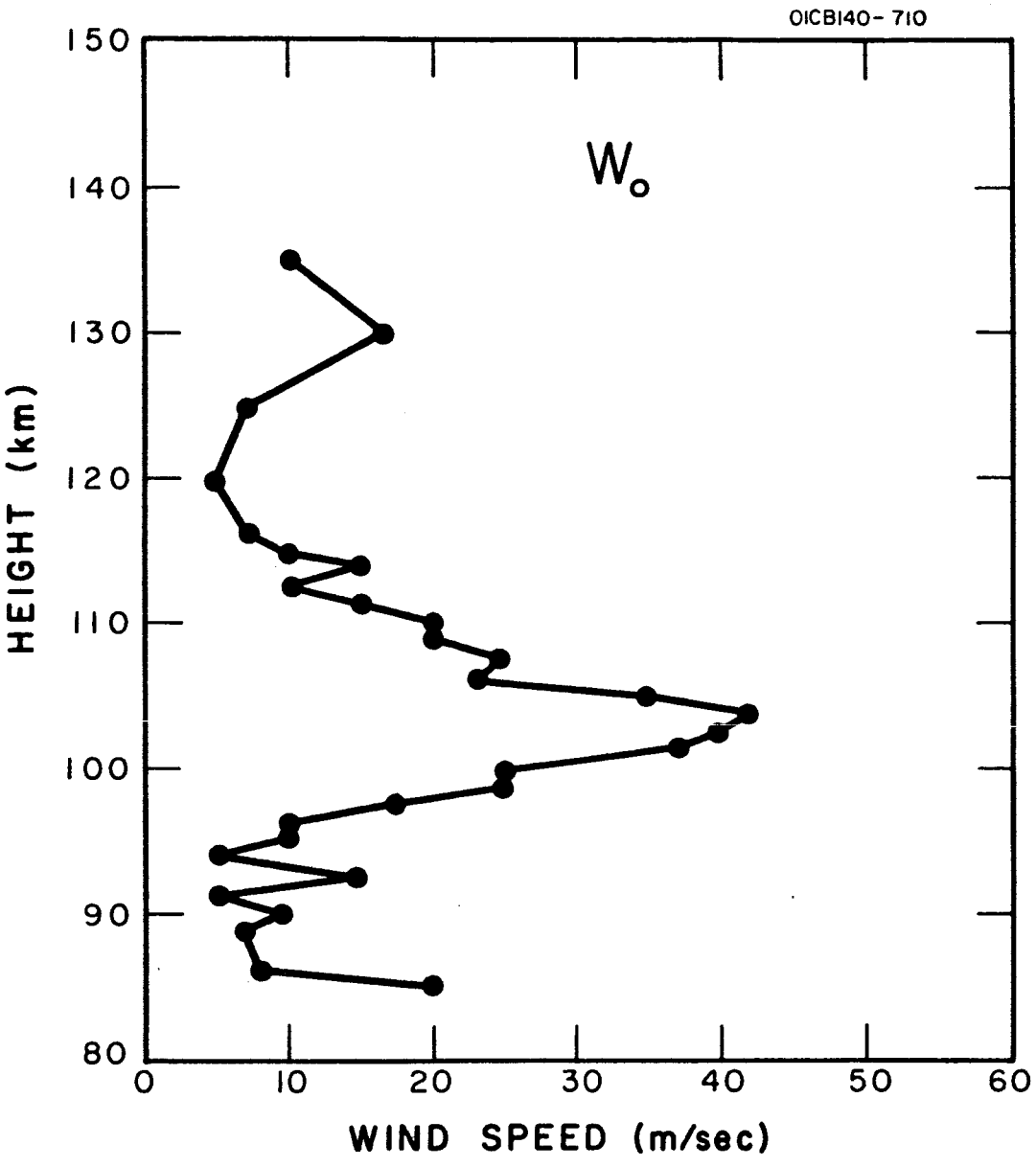

Figure 42. Observed values of W_o as a function of height.

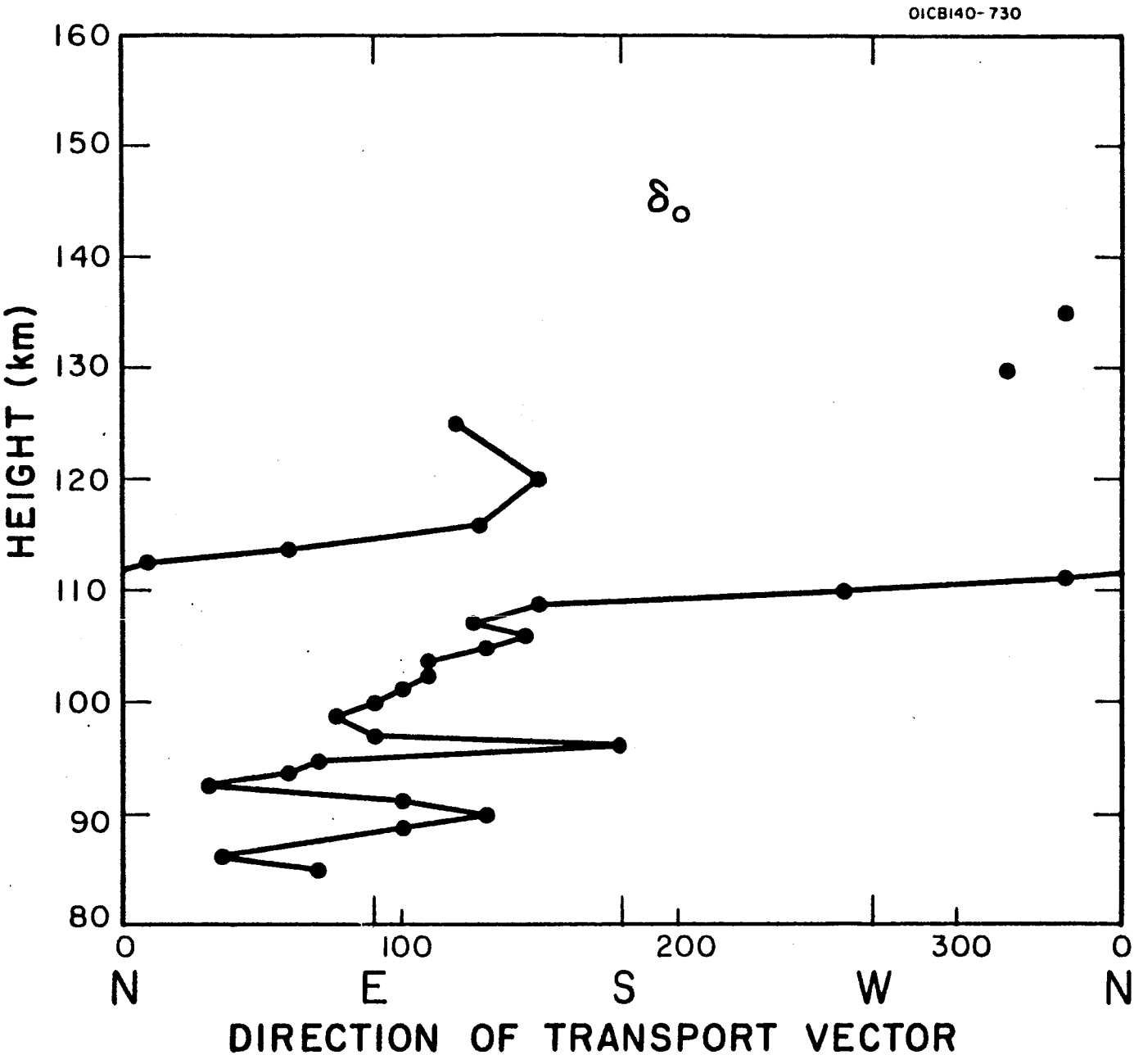

Figure 43. The difference in phase between δ_1 and δ_2 as a function of height.

REFERENCES

1. Geophysics Corporation of America, Final report for the period February 11, 1959 to February 11, 1960, NASA Contract No. NASw-25 Task II, Bedford, Massachusetts (1960).

2. Manring, E., Bedinger, J., Knaflich, H. and Lynch, R., "Upper Atmospheric Wind Profiles Determined from Three Rocket Experiments," NASA Contract No. NAS5-215, Tech. Report 61-1-N, Geophysics Corporation of America, Bedford, Massachusetts (February 1961).

3. Jenkins, R. and Manring, E., "The Design, Construction and Operation of Groundbased Tracking Equipment for Experiments Utilizing Optical Trace Materials to Study Atmospheric Parameters," NASA Contract No. NAS5-215, Tech. Report 61-2-N, Geophysics Corporation of America, Bedford, Massachusetts (March 1961).

4. Levy, R. J. and Manring, E. R., "Photography of Luminous Extended Objects Against a Twilight Sky," NASA Contract No. NAS5-215, Tech. Report 61-4-N, Geophysics Corporation of America, Bedford, Massachusetts (March 1961).

5. Manring, E., Bedinger, J. and Knaflich, H., "Some Measurements of Winds and of the Coefficient of Diffusion in the Upper Atmosphere," Space Research II, Proceedings of the Second International Space Science Symposium Florence, April 10-14, 1961, p. 1107-1124, edited by H. C. van de Hulst, C. de Jager, and A. F. Moore, North-Holland Publishing Co., Amsterdam (1961).

6. Manring, E., Bedinger, J. and Knaflich, H., "Measurement of Winds in the Upper Atmosphere during April 1961," J. Geophys. Res. 67, 3923-3925 (1962).

7. Geophysics Corporation of America, "Study of Winds, Diffusion, and Expansion of Gases in the Upper Atmosphere," Final Report on Contract NAS5-215, NASA Contract No. NAS5-215, Tech. Report 62-13-N, Bedford, Massachusetts (October 1962).

8. Geophysics Corporation of America, "Study of Winds, Diffusion, and Expansion of Gases in the Upper Atmosphere," Final Report on Contract NASw-396, NASA Contract No. NASw-396, Tech. Report 62-16-N, Bedford, Massachusetts (May 1962).

9. Webb, W. L., Christensen, W. I., Varner, E. P. and Spurling, J. P., "Inter-Range Instrumentation Group Participation in the Meteorological Rocket Network," Bull. Am. Meteorol. Soc. 43, 640-649 (1962).

REFERENCES (Continued)

10. Greenhow, J. S. and Neufeld, E. L., "Winds in the Upper Atmosphere," Quart. J. Roy. Meteorol. Soc. 87, 472 (1961).

11. Elford, W. G., "A Study of Winds Between 80 and 100 km in Medium Latitudes," Planetary Space Sci. 1, 94 (1959).

12. Broglio, Luigi, "La seconda fase del programma italiano di ricerca mediante razzi sonda," Scoula D'Ingegneria Aeronautica, Via Eudossiana 18, Rome (1961).

13. Broglio, Luigi, "The Italian Fifth Cycle of Experiments by Sounding Rockets Using Sodium Cloud Technique," Italian Committee for Space Research, National Council of Research (1963).

14. Nordberg, W. and Smith, W., "Preliminary Measurements of Temperatures and Winds Above 50 km over Wallops Island, Virginia," NASA, Tech. Note, D-1694 (1963).

15. Smith, J. W., "Cape Canaveral Wind Summary Surface to 84 km," NASA, MTP-AERO-62-3, Marshall Space Flight Center, Huntsville, Alabama (January 17, 1962).

16. Kiss, E., "Annotated Bibliography of Rocket Meteorology," Meteorological and Geoastrophysical Abstracts 11, 1480-1535 (1960).

17. Murgatroyd, R. J., "Winds and Temperature Between 20-100 km," Quart. J. Roy. Meteorol. Soc. 83, 417-458 (1957).

18. Batten, E. S., "A Model of the Annual Temperature Variations at 30°N between 30 and 60 km," RM-3564-PR, The Rand Corporation, Santa Monica, California (1963).

19. Finger, F. G., Teweles, S. and Mason, R. B., "Synoptic Analysis Based on Meteorological Rocketsonde Data," J. Geophys. Res. 68, 1377-1399 (1963).

20. Greenhow, J. S. and Lovell, A. C. B., "The Upper Atmosphere and Meteors," Physics of the Upper Atmosphere, p. 513-549, edited by J. A. Ratcliffe, Academic Press, New York (1960).

21. Liller, W. and Whipple, F. L., "High-Altitude Winds by Meteor-train Photography," Special Supplement to J. Atmospheric and Terrest. Phys. 1, 112-130 (1954).

22. Hines, C. O., "Internal Atmospheric Gravity Waves at Ionospheric Heights," Canad. J. Phys. 38, 1441 (1960).

REFERENCES (Continued)

23. Siebert, M., "Atmospheric Tides," Advances in Geophysics 7, 105-187, Academic Press, New York (1961).

24. Butler, S. T. and Small, K. A., "The Excitation of Atmospheric Oscillations," Proc. Roy. Soc. A 274, 91-121 (1963).

25. Edwards, H. D., Cooksey, M. M., Justus, C. G., Fuller, R. N., Albritton, D. L. and Rosenberg, N. W., "Upper-Atmosphere Wind Measurements Determined from 12 Rocket Experiments," J. Geophys. Res. 68, 3021-3032 (1963).

26. Rosenberg, N. W., Edwards, H. D. and Wright, J. W., "Ionospheric Winds: Motions into Night and Sporadic E Correlations," to be published in Space Research IV, North-Holland Publishing Co., Amsterdam.

27. Edwards, H. D., Justus, C. G. and Kurts, D. C., "Upper Atmosphere Winds for Evening Twilight," submitted to J. Geophys. Res. for publication.

APPENDIX A

Wind measurements from 22 sodium vapor trails over Wallops Island are included. A plot of both wind speed and direction of trail transport is given as a function of altitude for each trail. The time, date and altitude range is shown on each plot. The figure numbers correspond to flight numbers in Table 2 of this report.

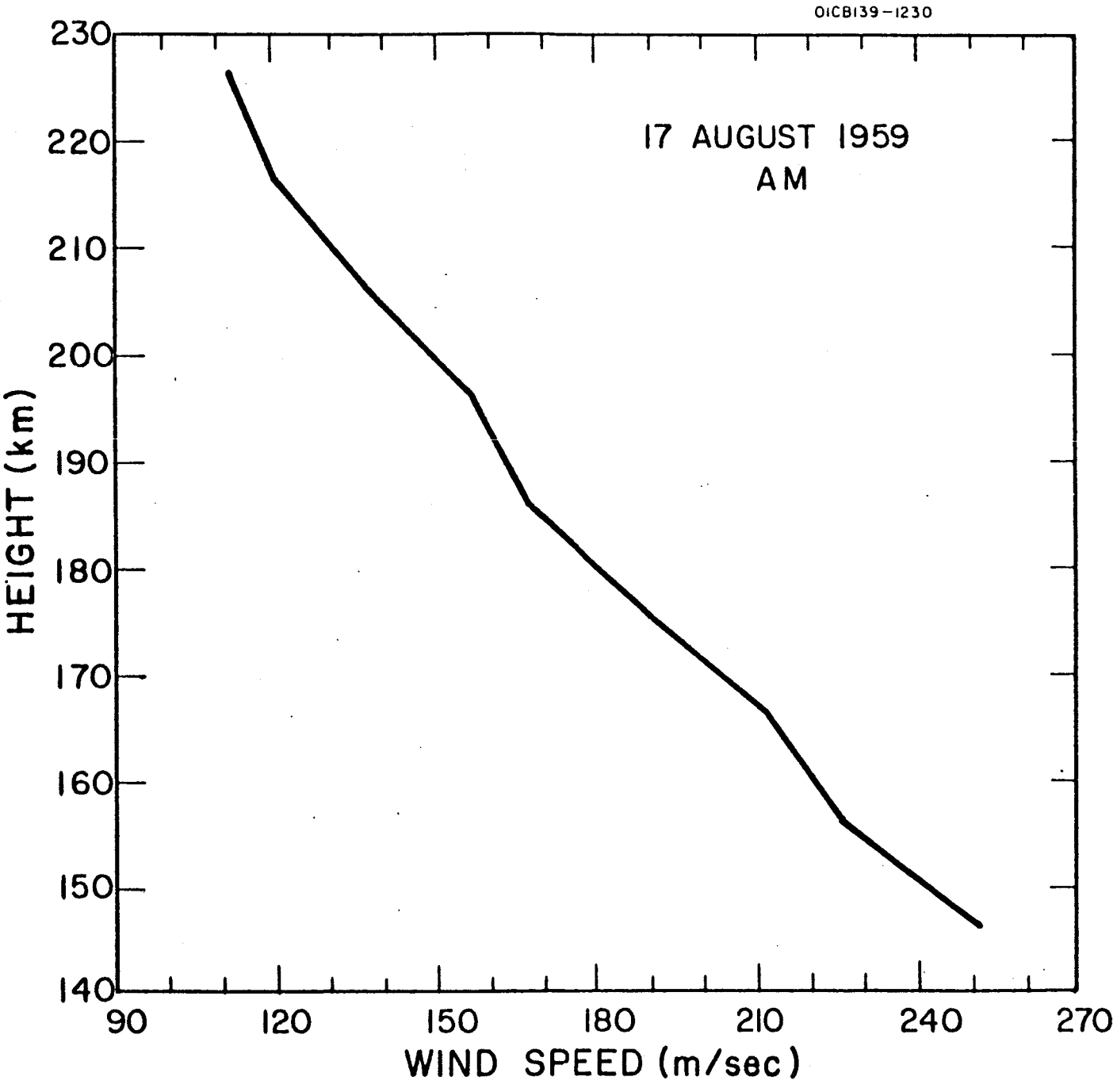

Figure A.1a. Wind speed as a function of height for morning twilight of 17 August 1959.

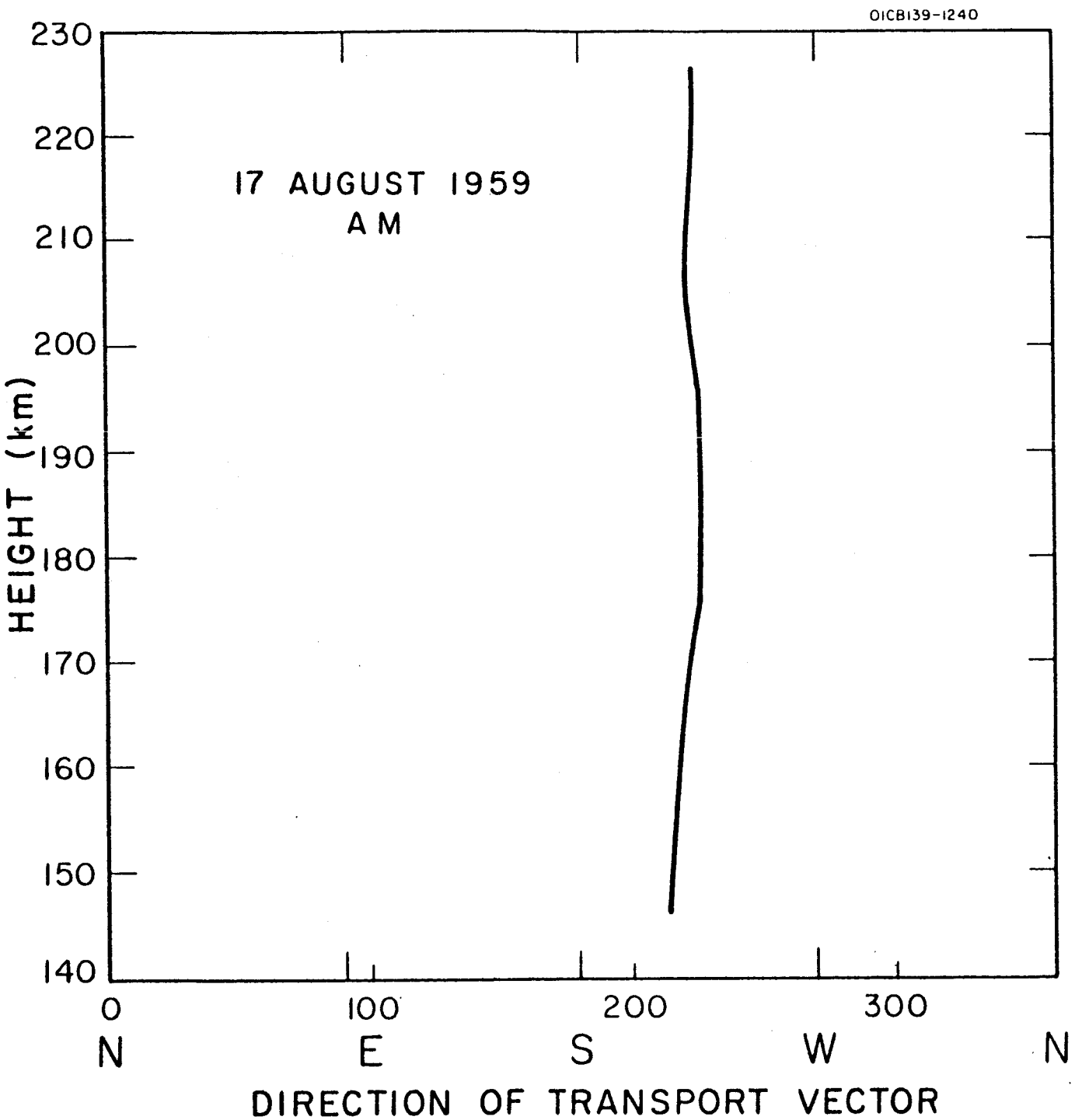

Figure A.1b. Direction of transport vector as a function of height for morning twilight of 17 August 1959.

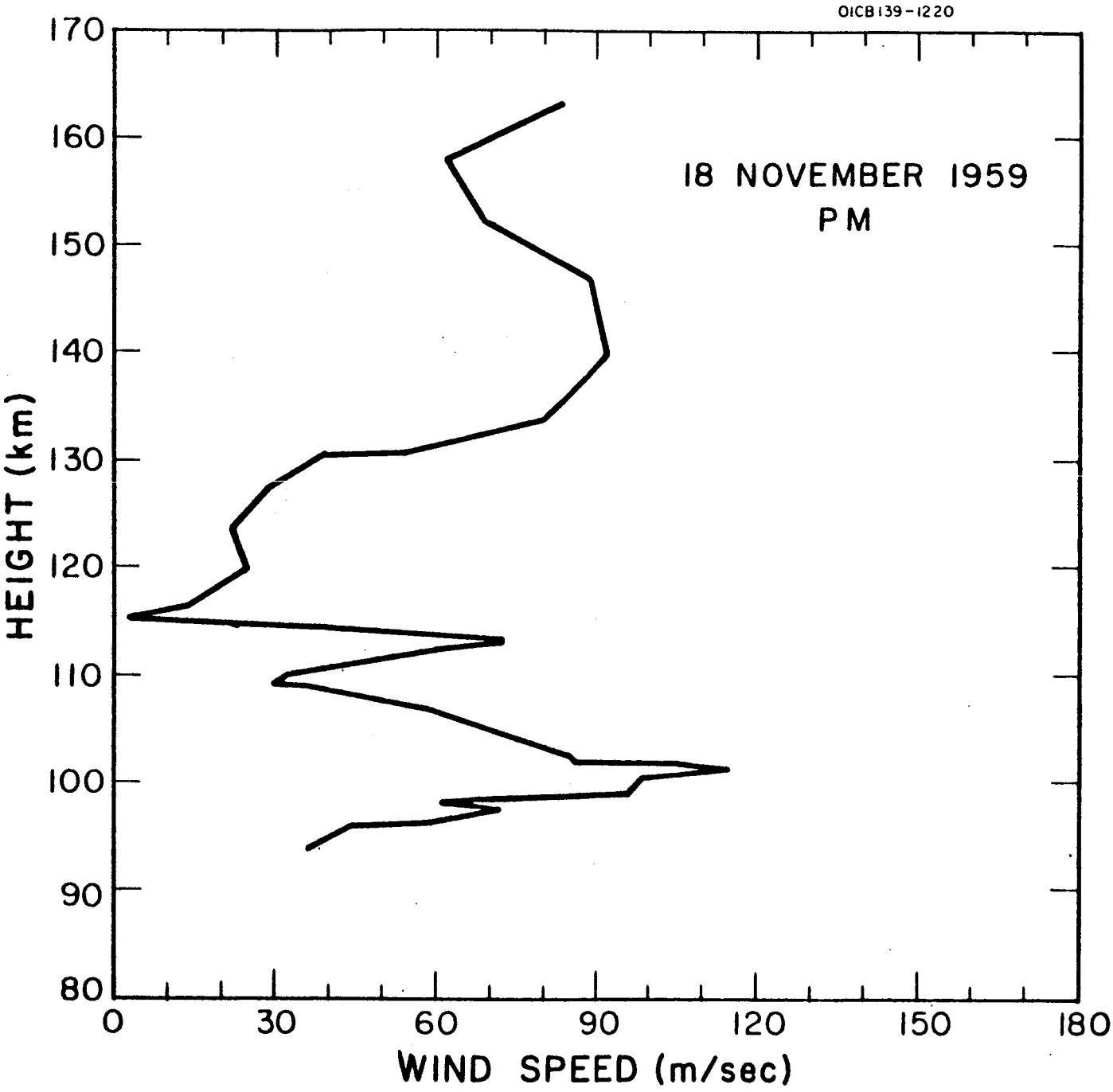

Figure A.2a. Wind speed as a function of height for evening twilight of 18 November 1959.

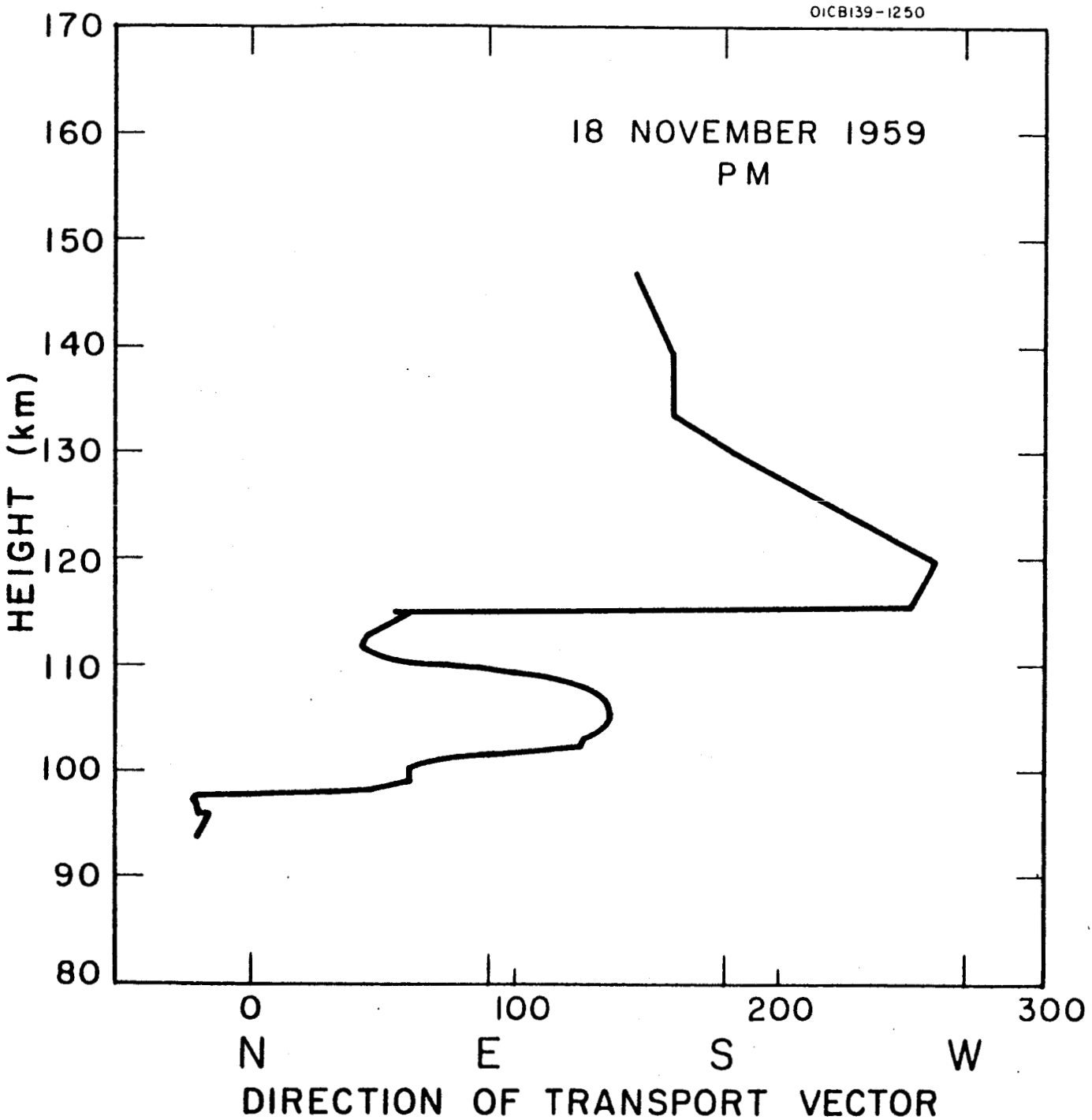

Figure A.2b. Direction of transport vector as a function of height for evening twilight of 18 November 1959.

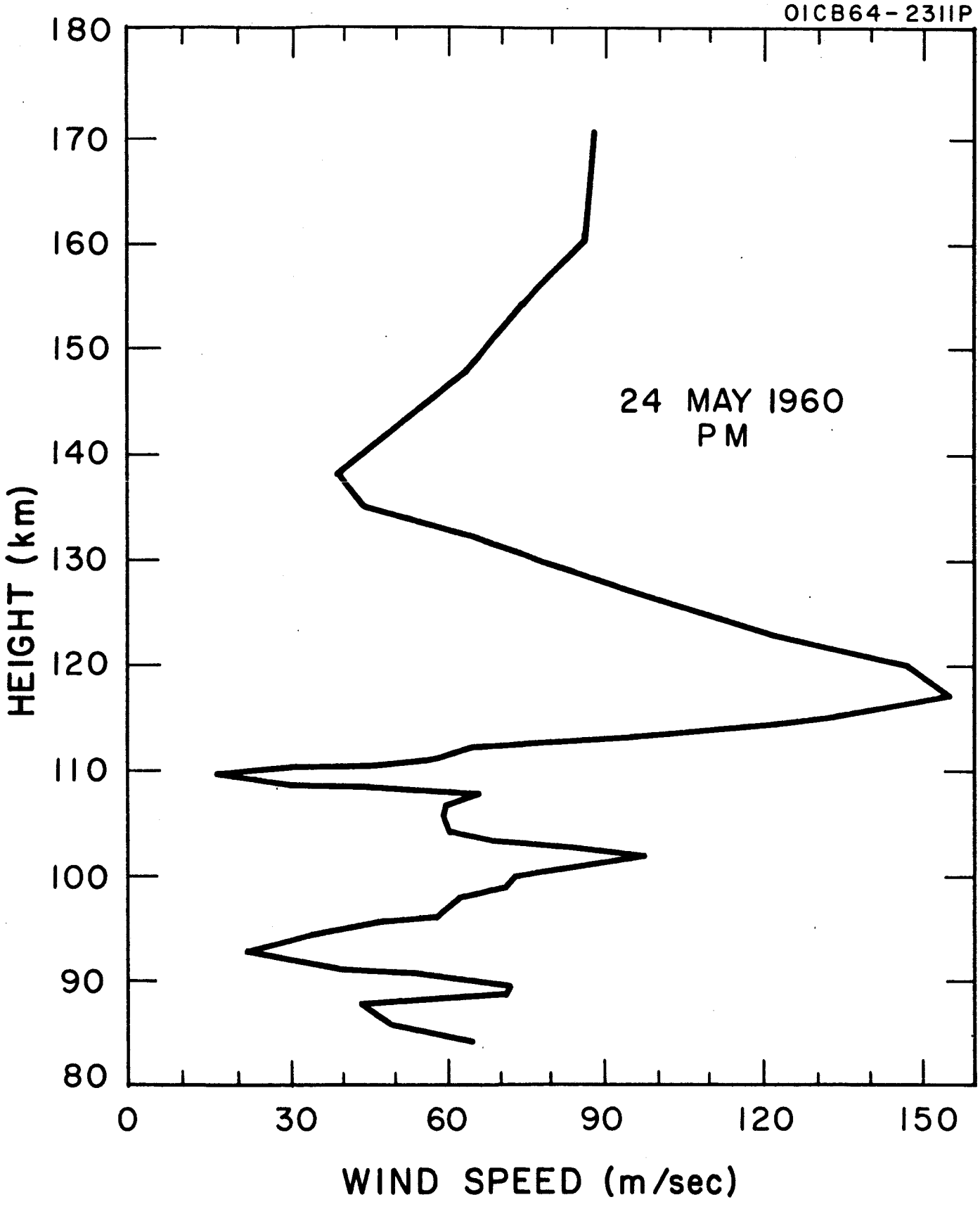

Figure A.3a. Wind speed as a function of height for evening twilight of 24 May 1960.

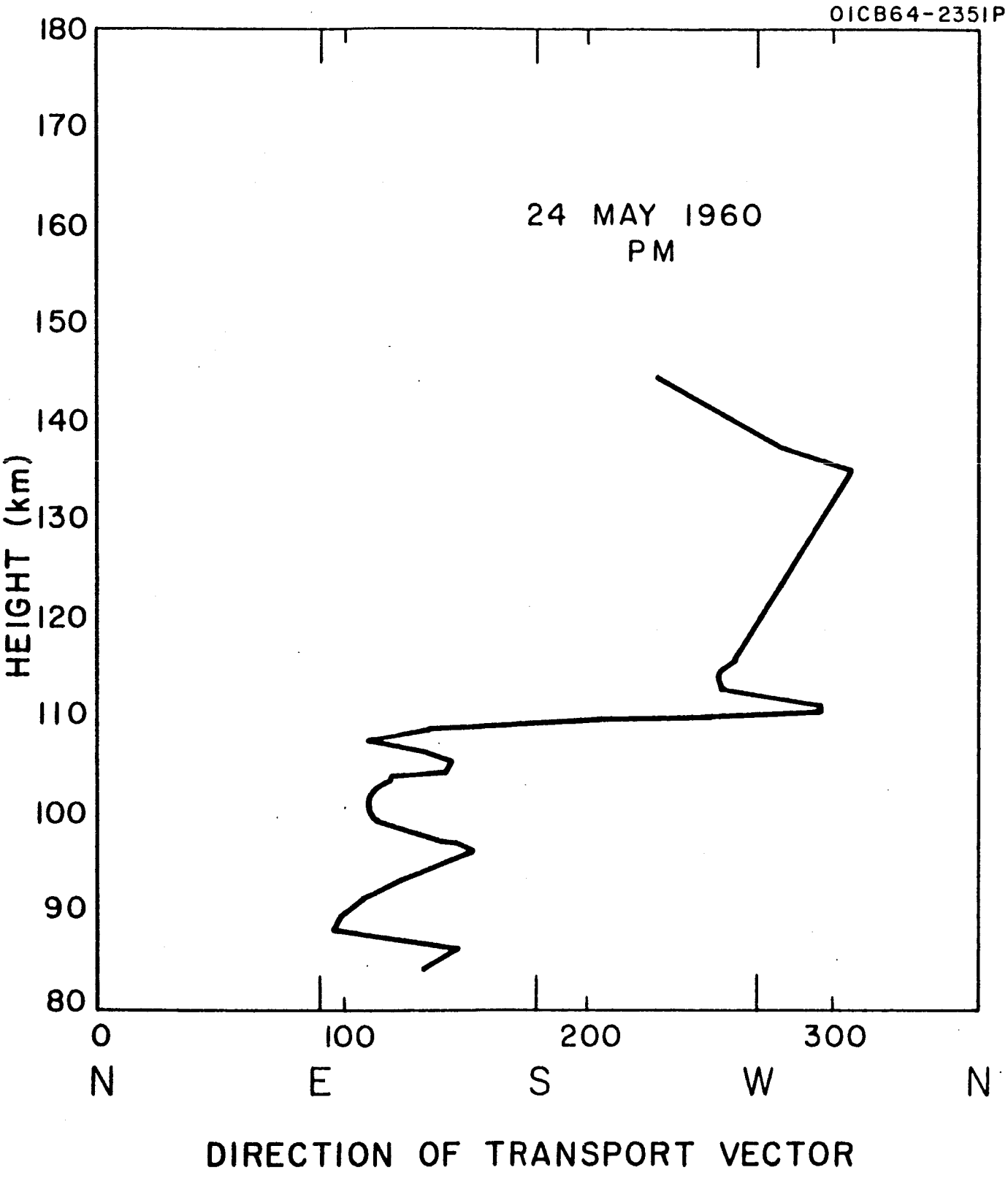

Figure A.3b. Direction of transport vector as a function of height for evening twilight of 24 May 1960.

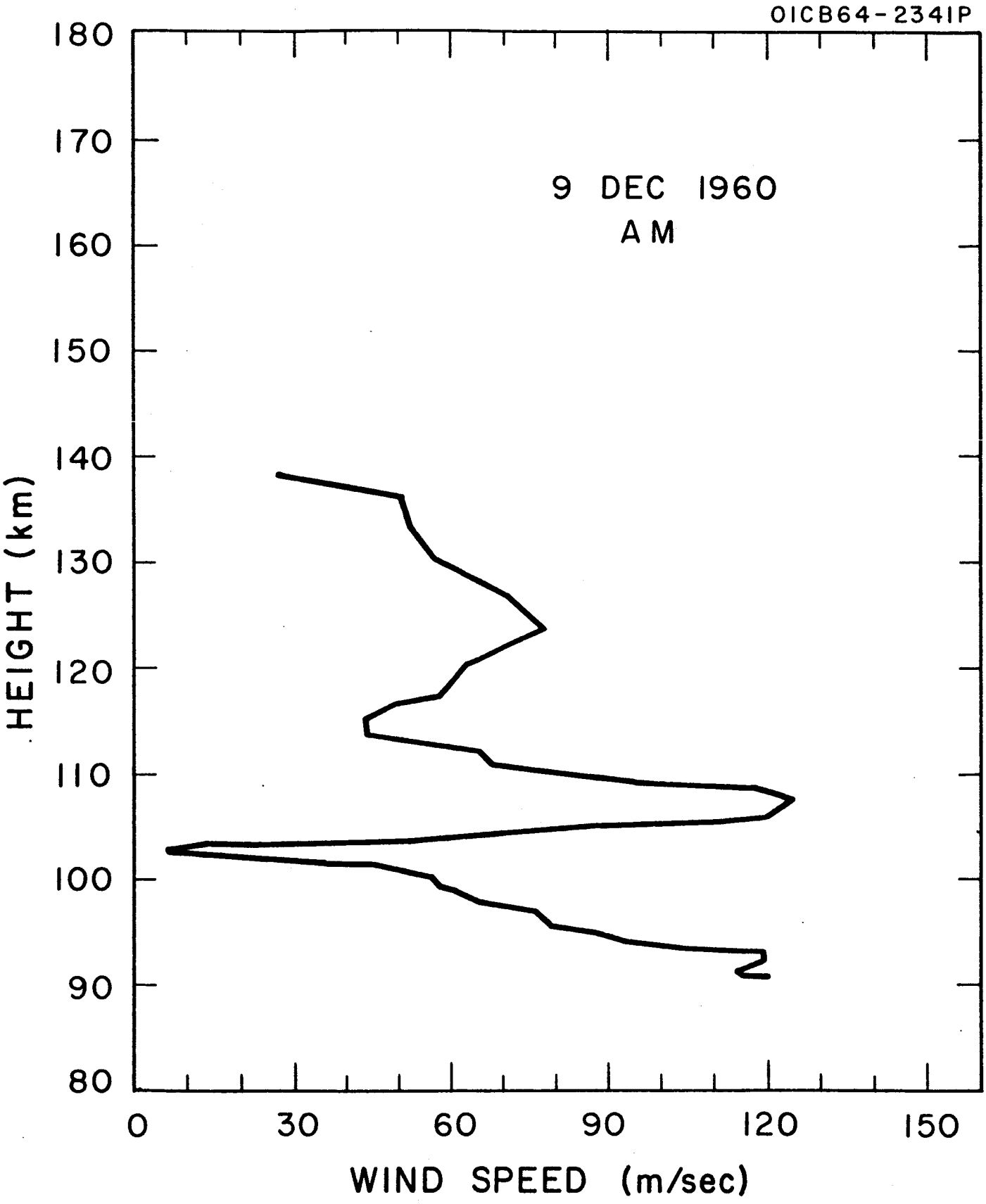

Figure A.4a. Wind speed as a function of height for morning twilight of 9 December 1960.

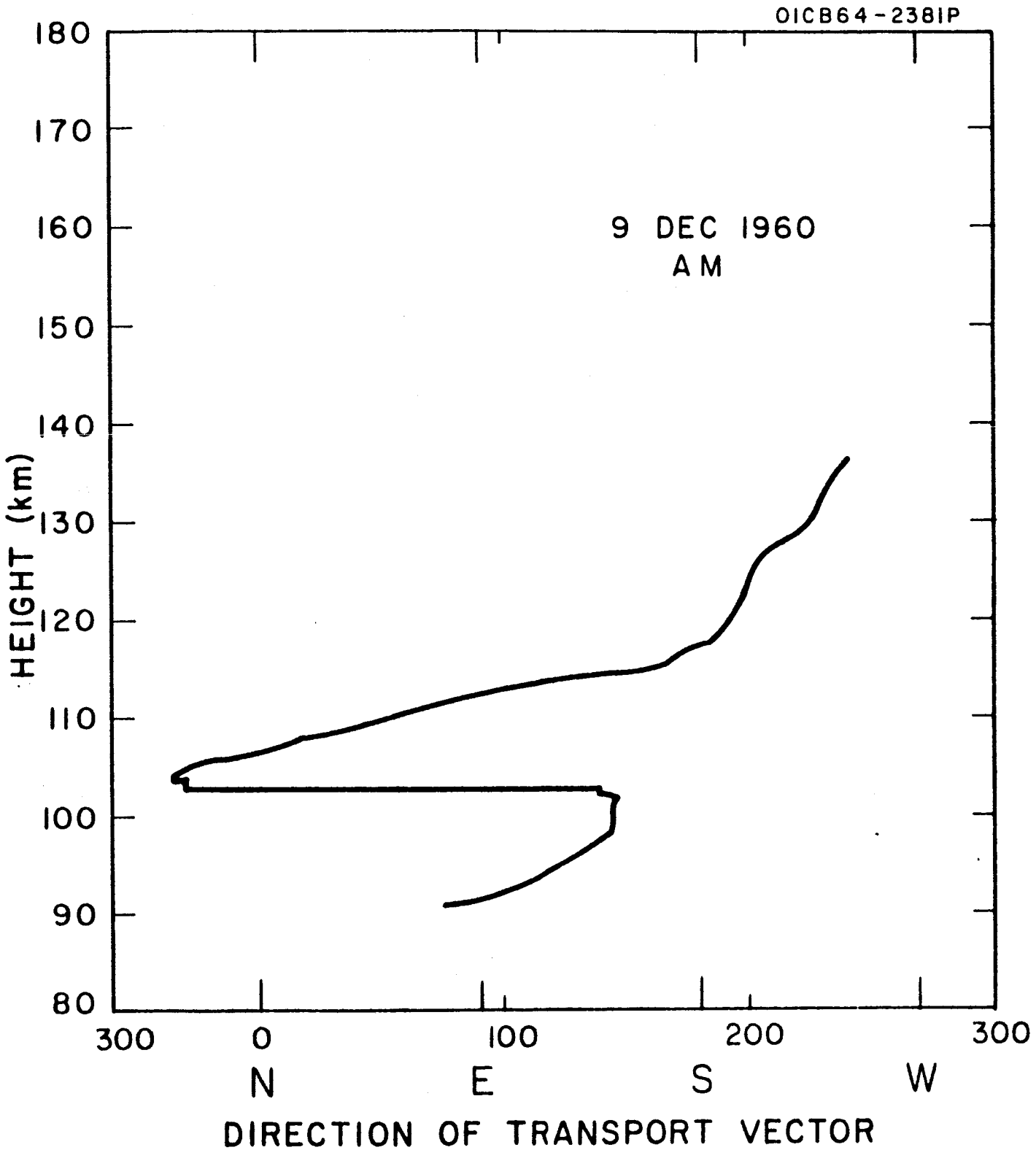

Figure A.4b. Direction of transport vector as a function of height for morning twilight of 9 December 1960.

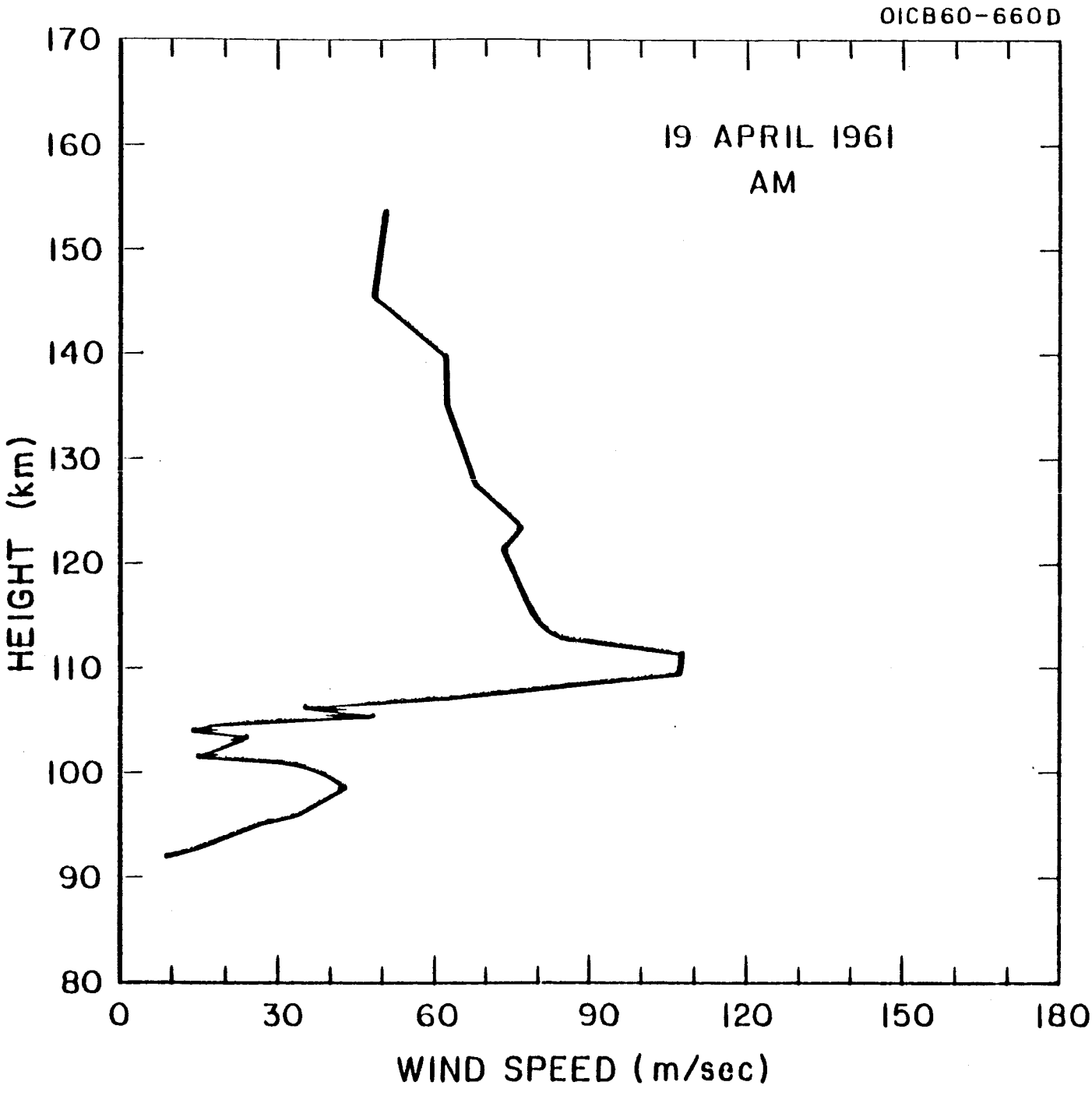

Figure A.5a. Wind speed as a function of height for morning twilight of 19 April 1961.

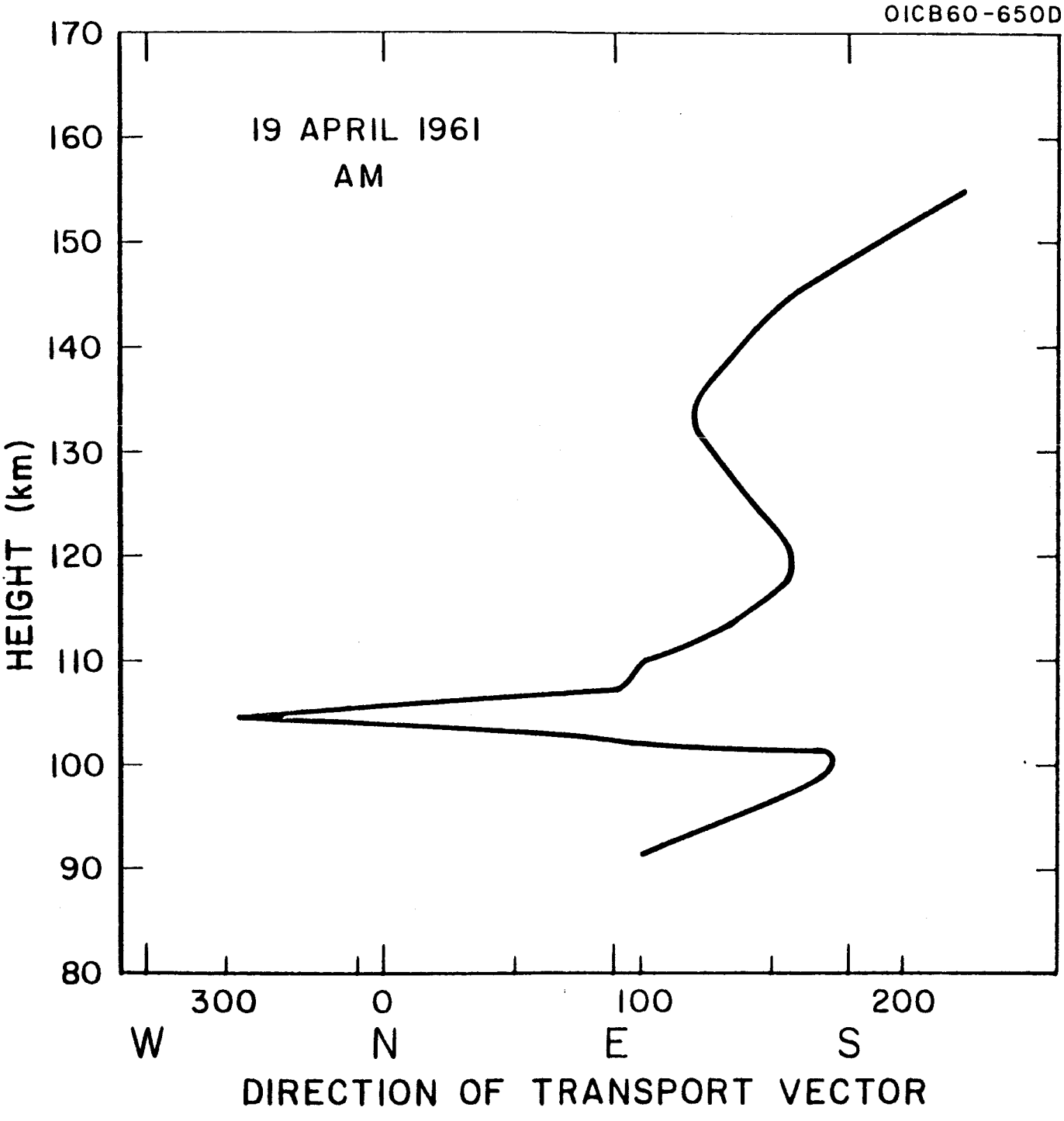

Figure A.5b. Direction of transport vector as a function of height for morning twilight of 19 April 1961.

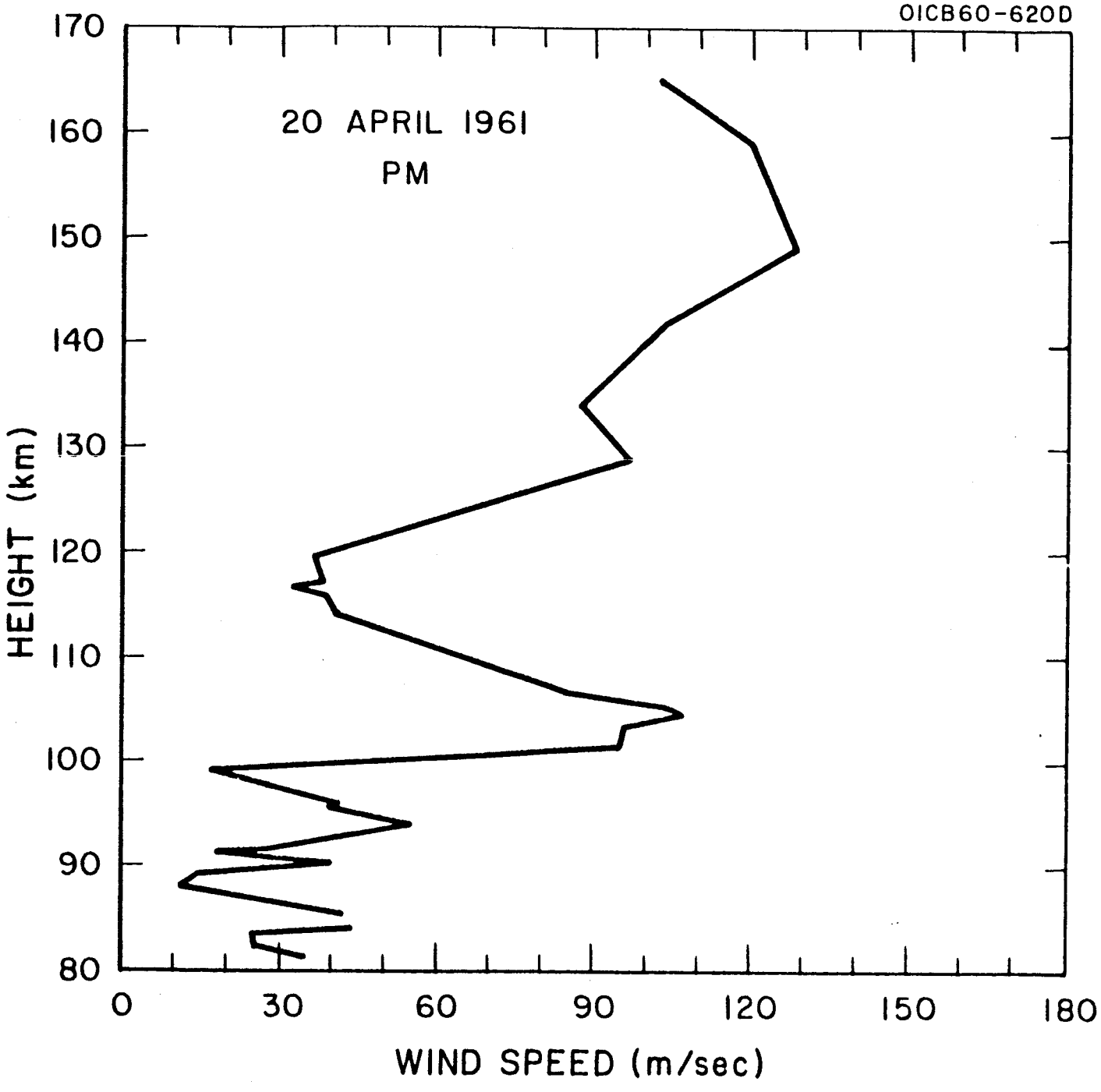

Figure A.8a. Wind speed as a function of height for evening twilight of 20 April 1961.

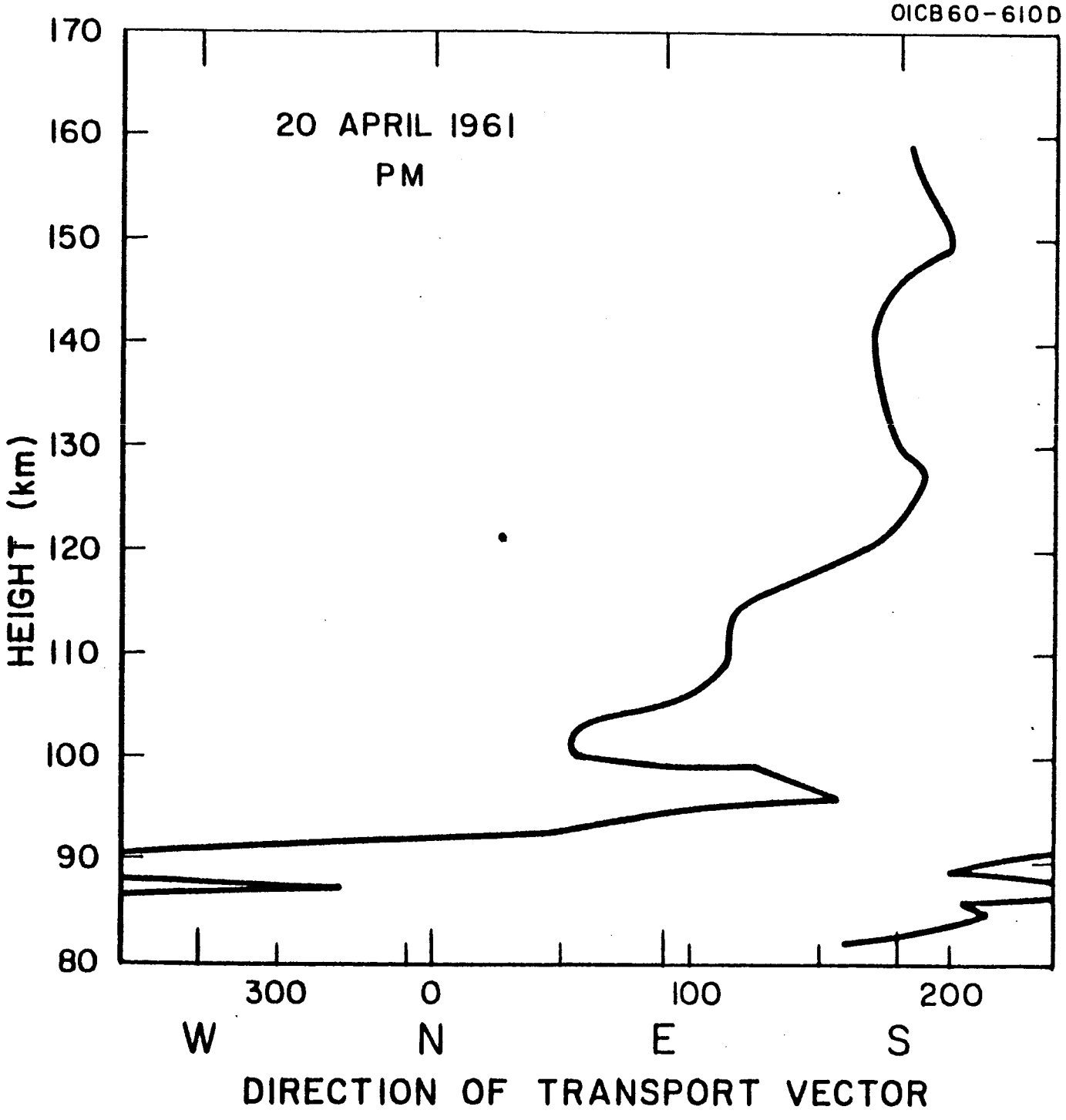

Figure A.8b. Direction of transport vector as a function of height for evening twilight of 20 April 1961.

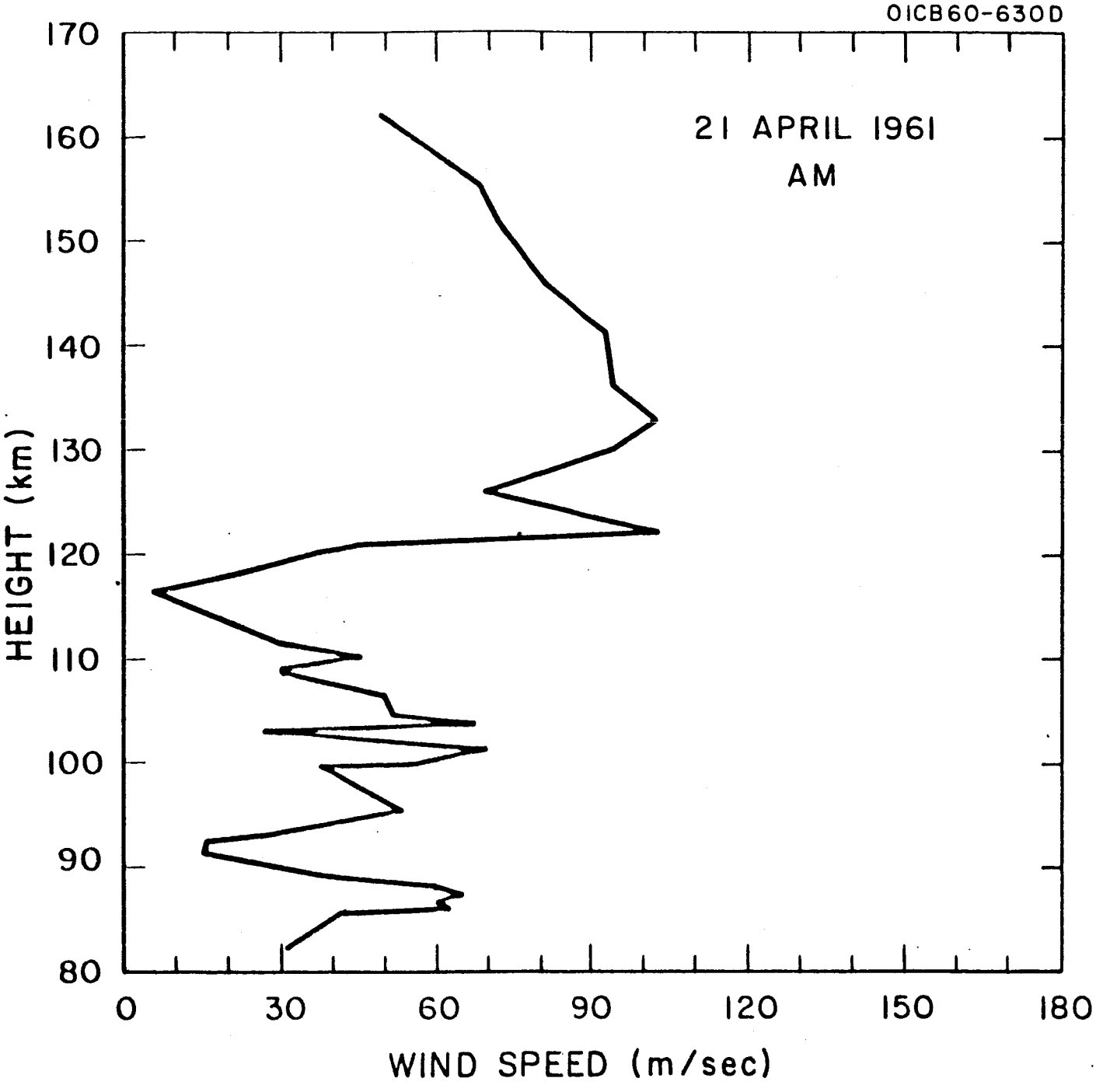

Figure A.9a. Wind speed as a function of height for morning twilight of 21 April 1961.

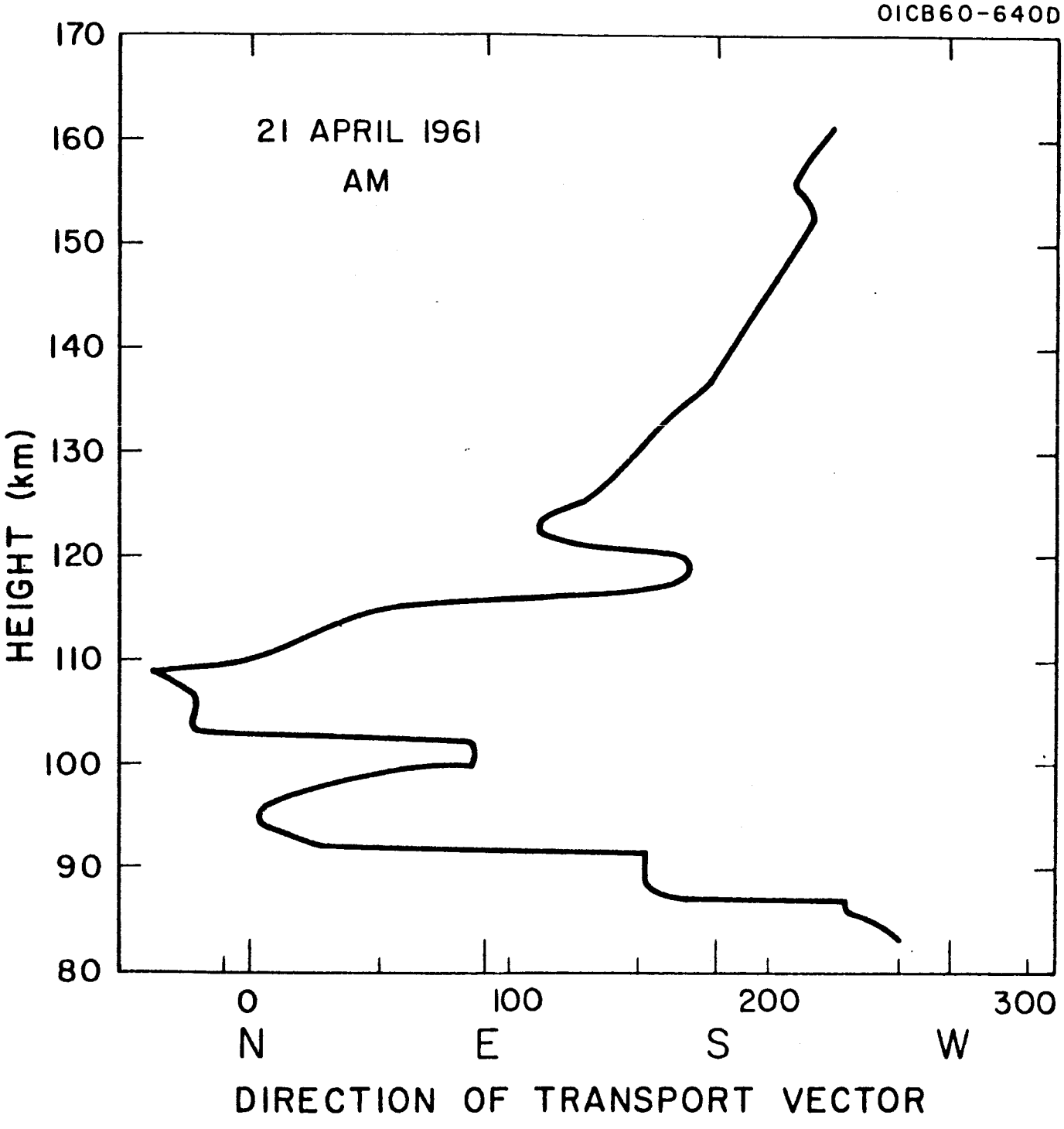

Figure A.9b. Direction of transport vector as a function of height for morning twilight of 21 April 1961.

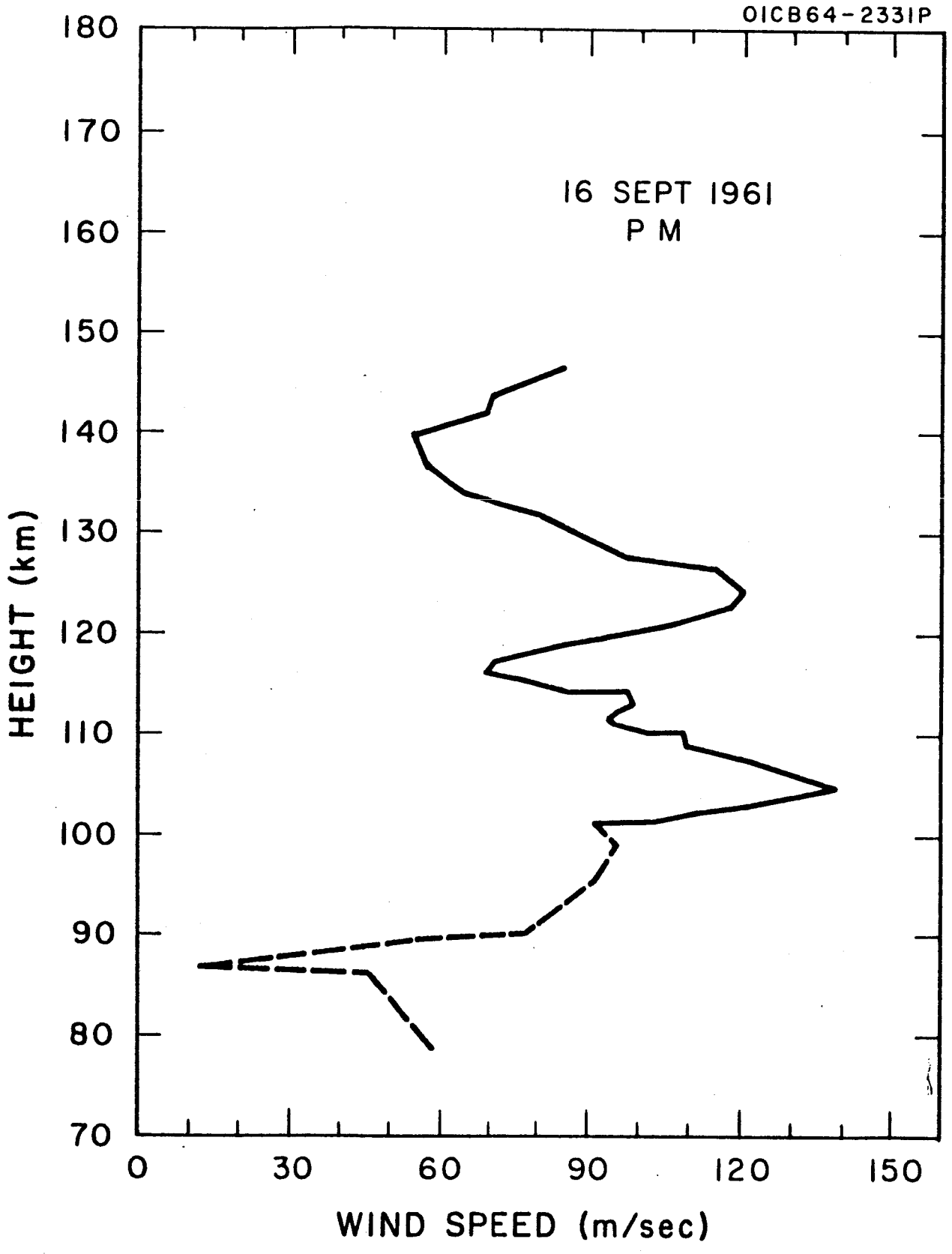

Figure A.10a. Wind speed as a function of height for evening twilight of 16 September 1961.

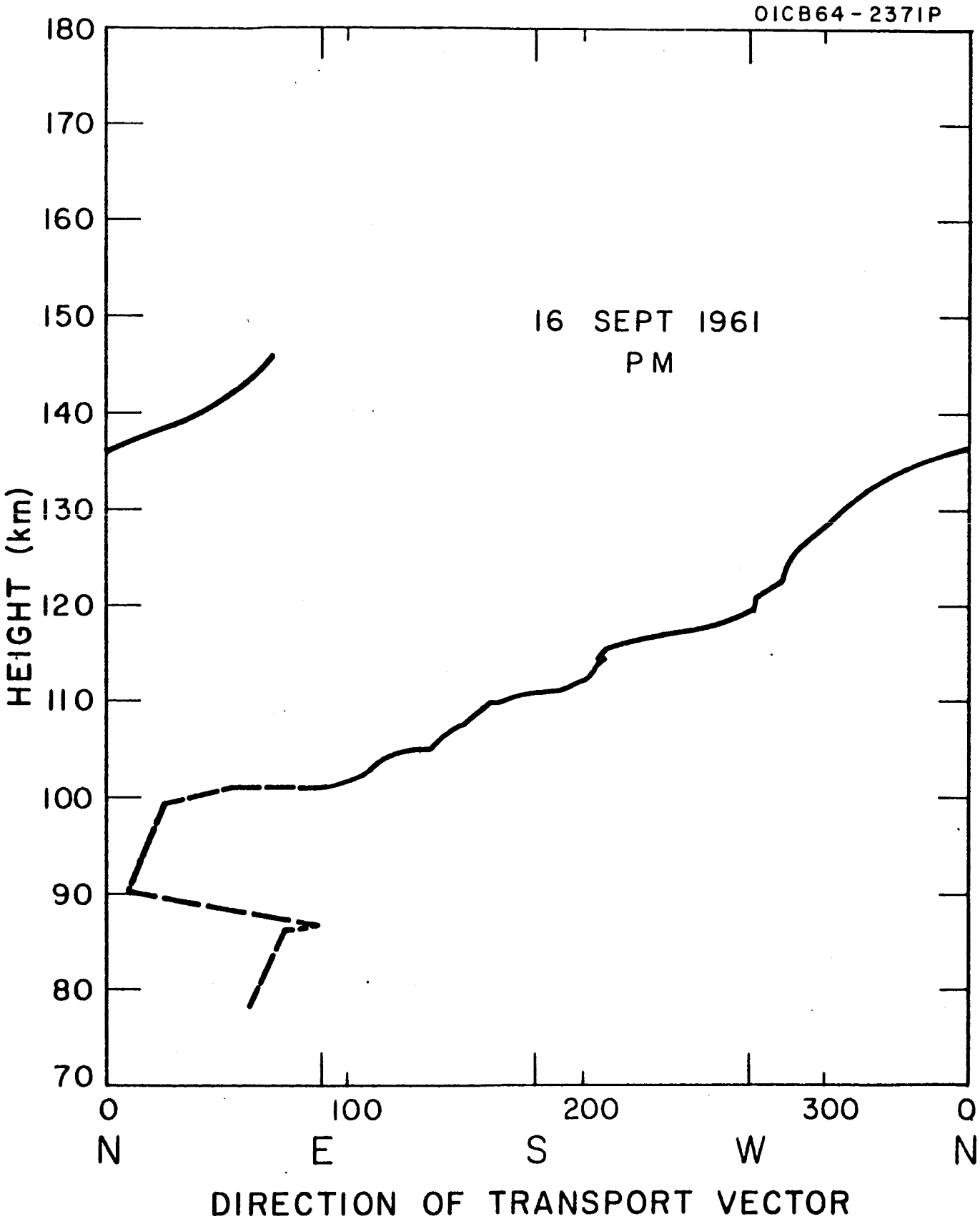

Figure A.10b. Direction of transport vector as a function of height for evening twilight of 16 September 1961.

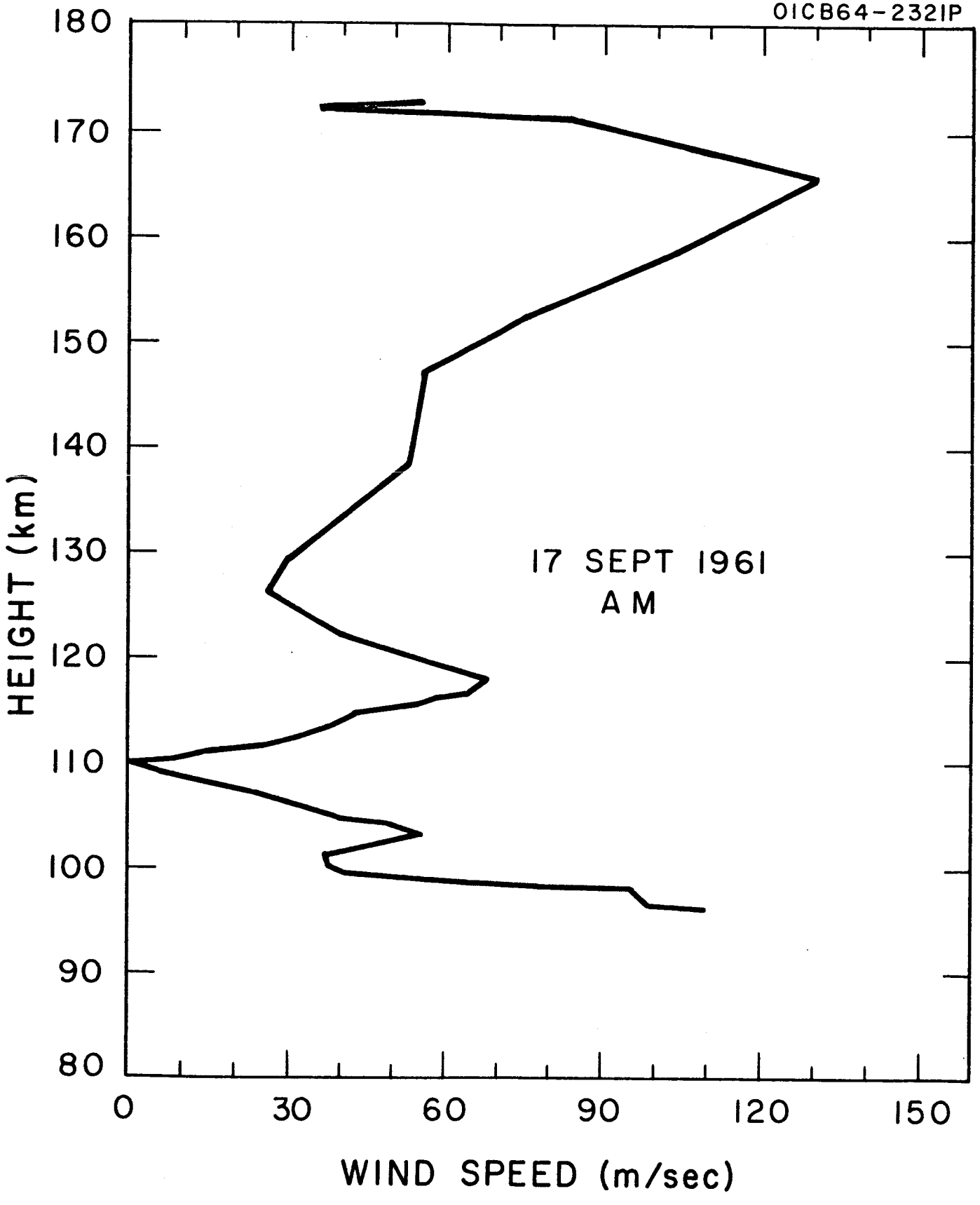

Figure A.11a. Wind speed as a function of height for morning twilight of 17 September 1961.

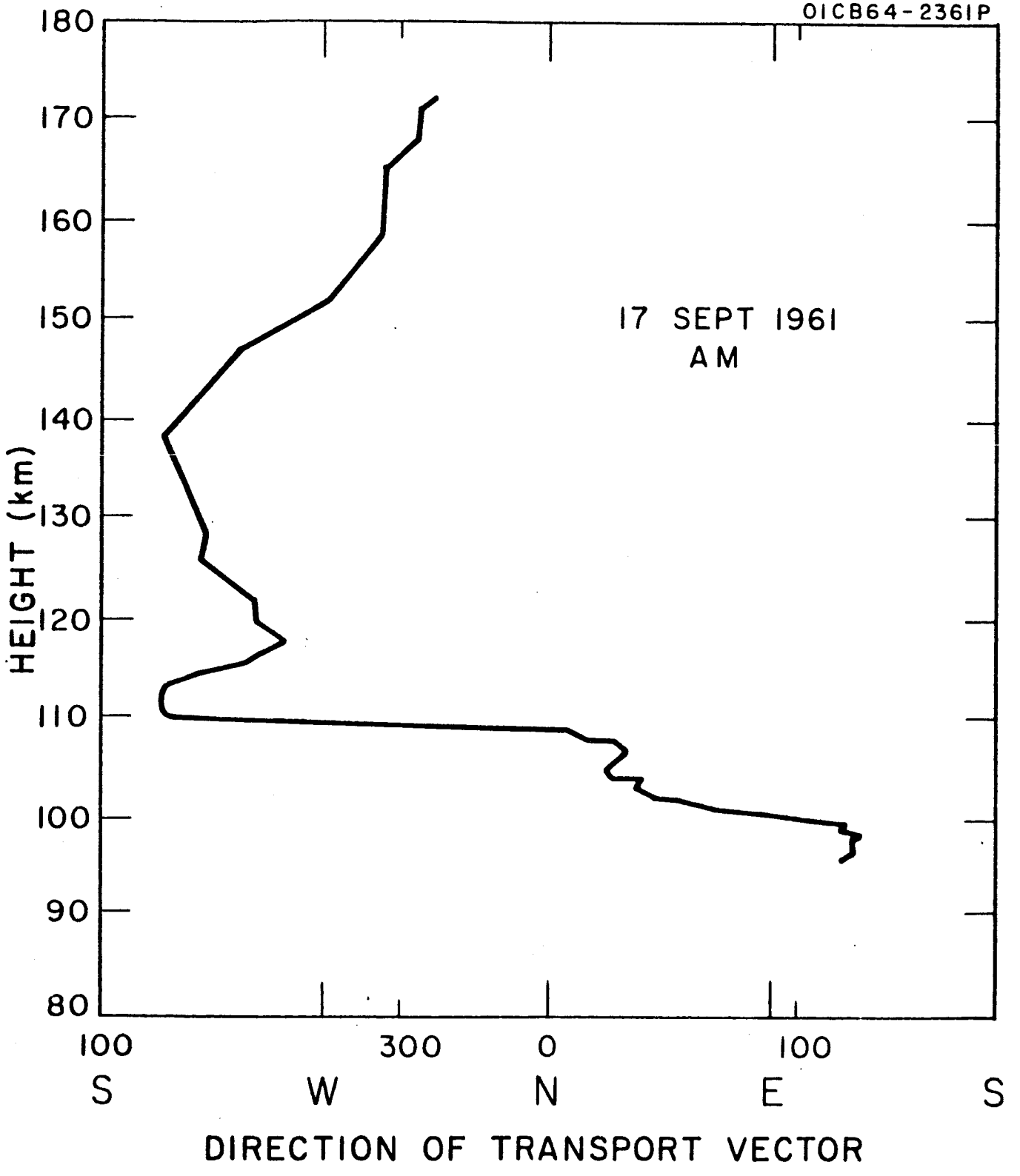

Figure A.11b. Direction of transport vector as a function of height for morning twilight of 17 September 1961.

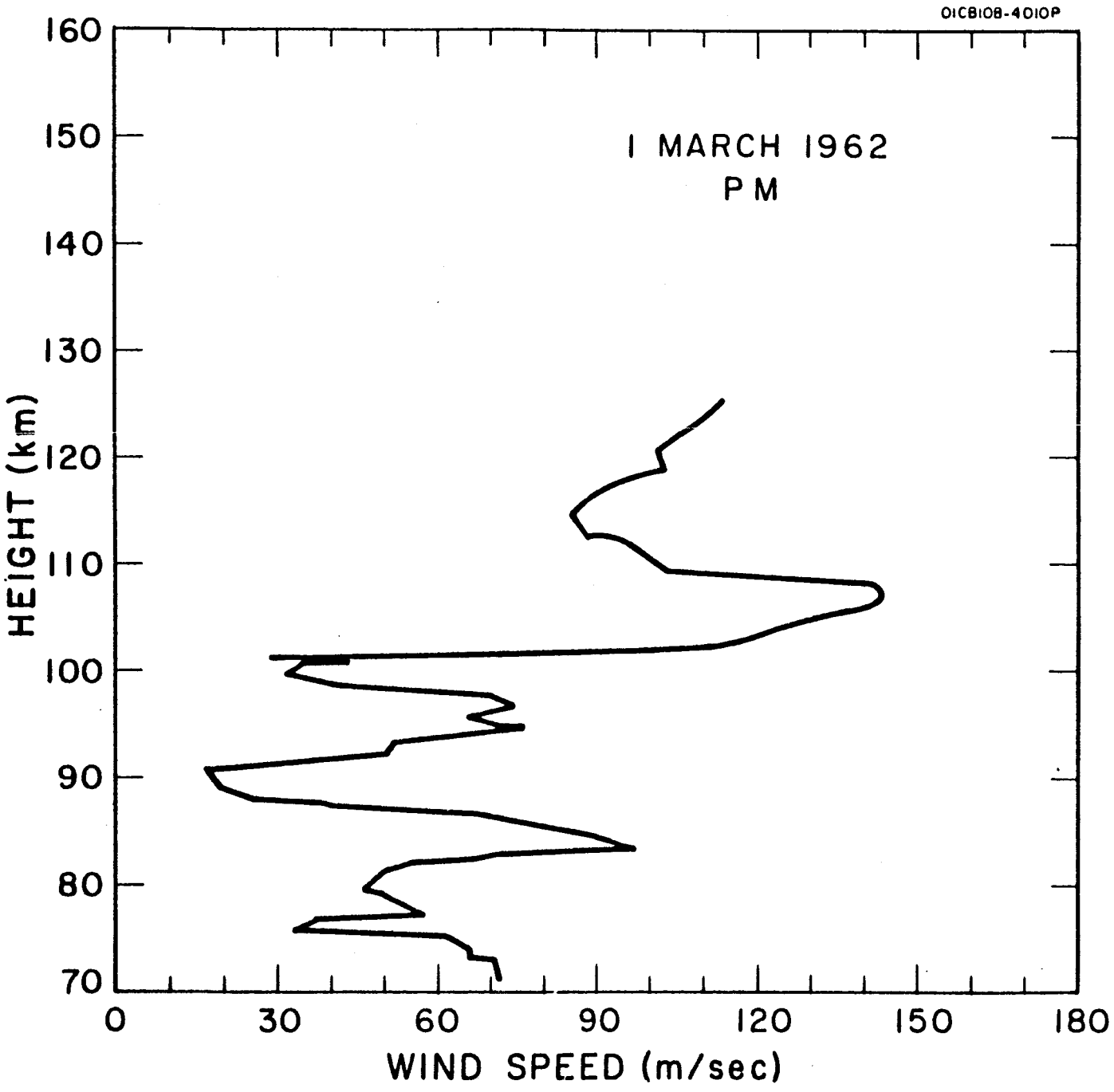

Figure A.12a. Wind speed as a function of height for evening twilight of 1 Marcy 1962.

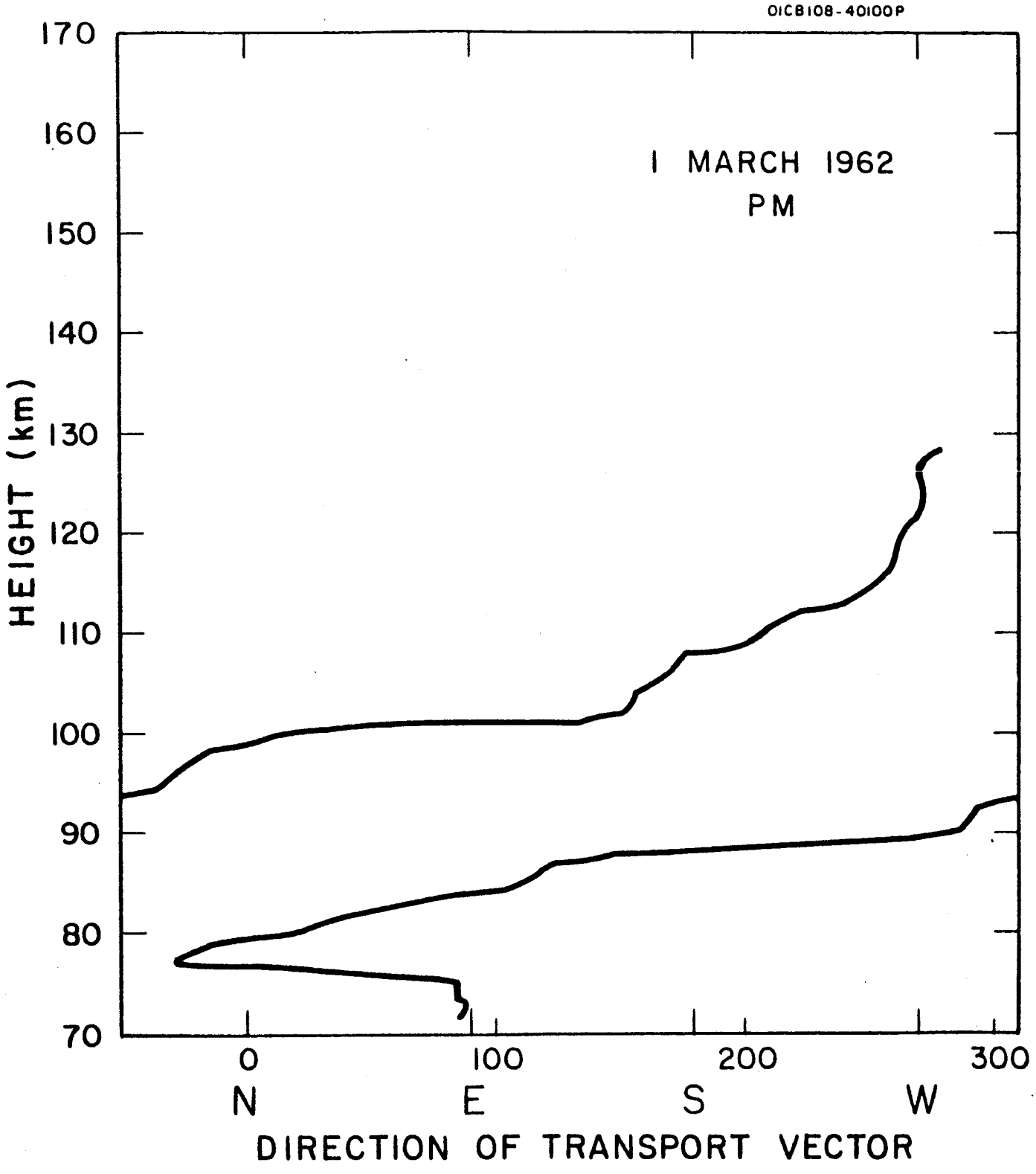

Figure A.12b. Direction of transport vector as a function of height for evening twilight of 1 March 1962.

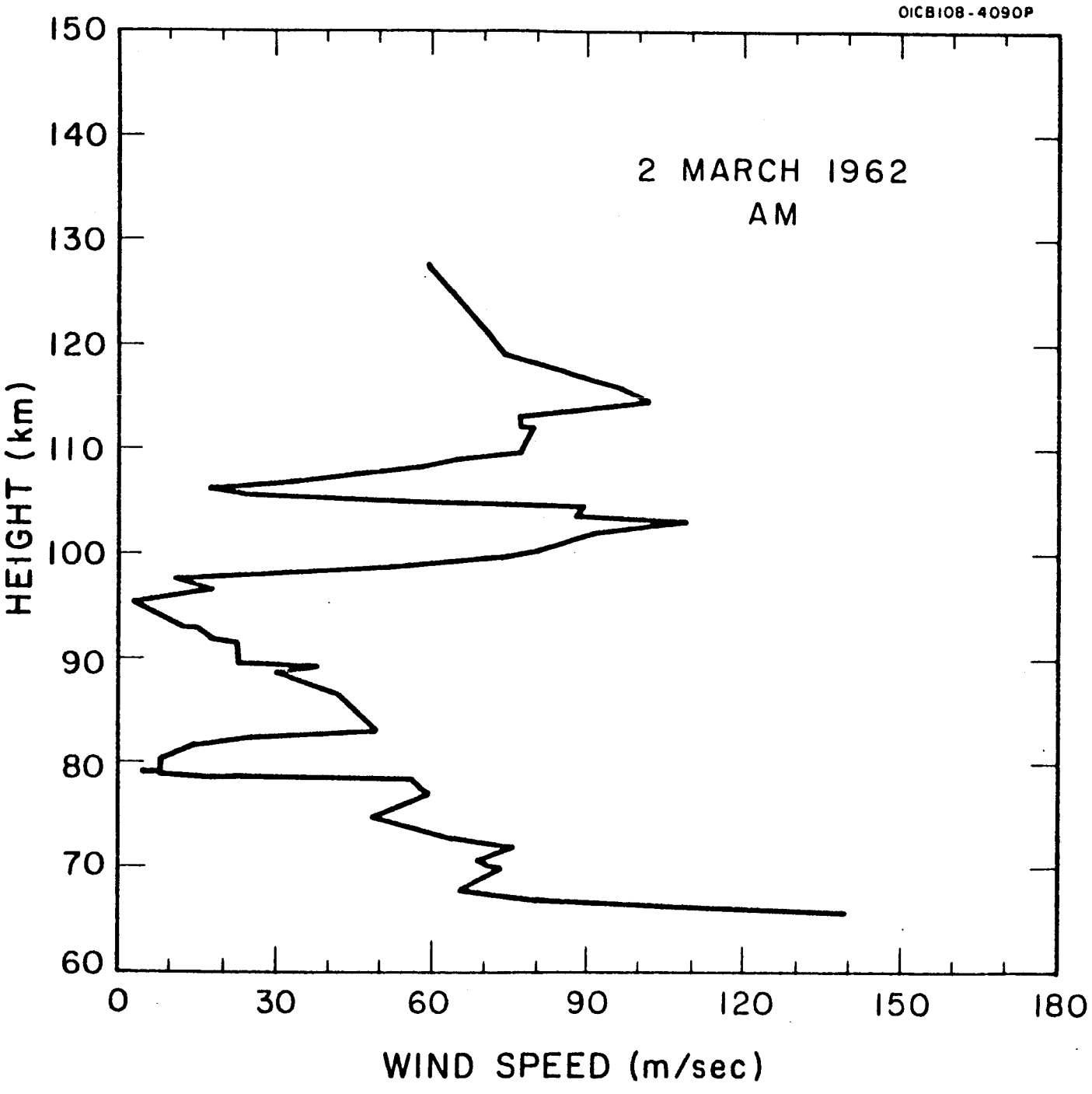

Figure A.13a. Wind speed as a function of height for morning twilight of 2 March 1962.

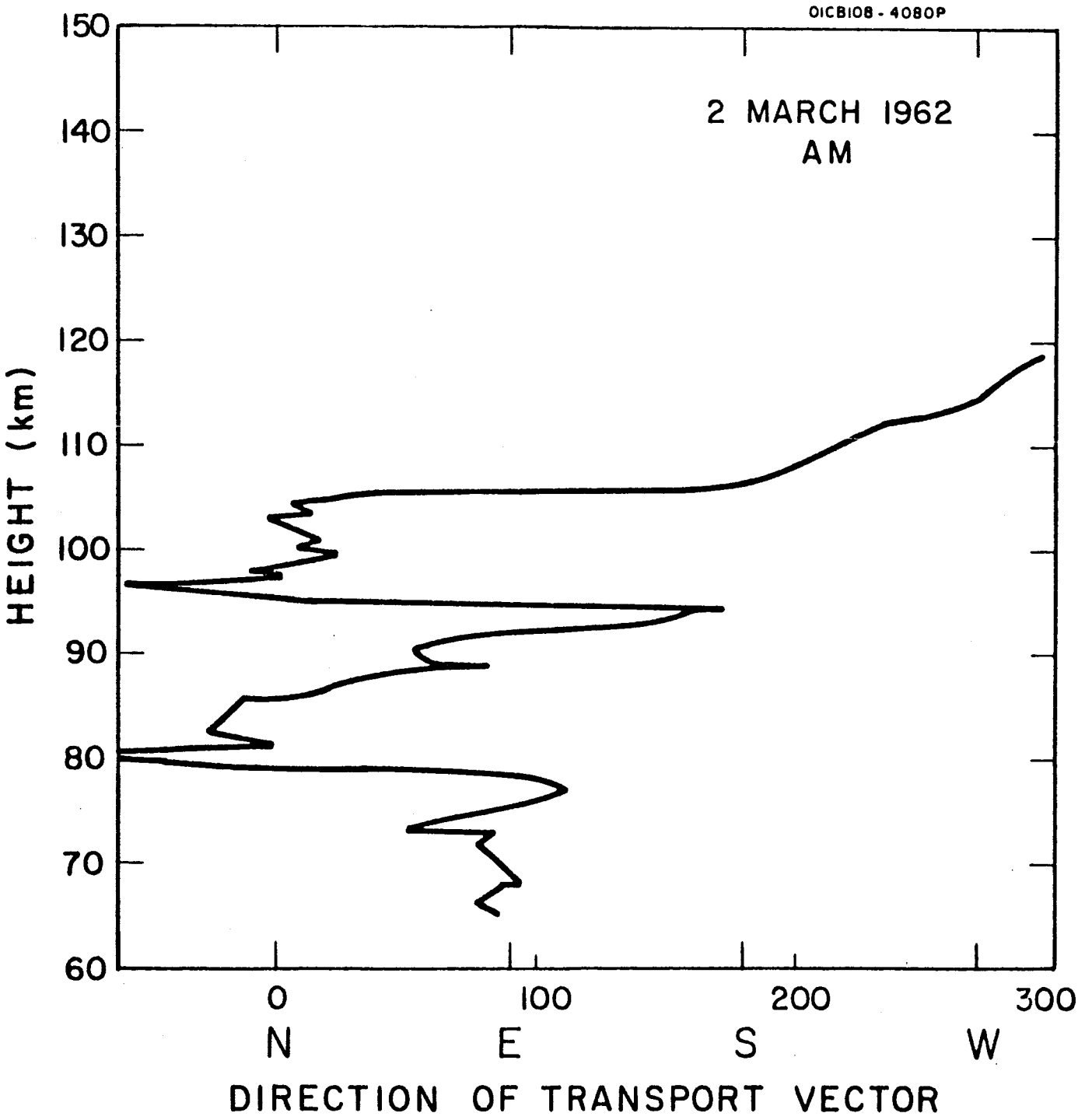

Figure A.13b. Direction of transport vector as a function of height for morning twilight of 2 March 1962.

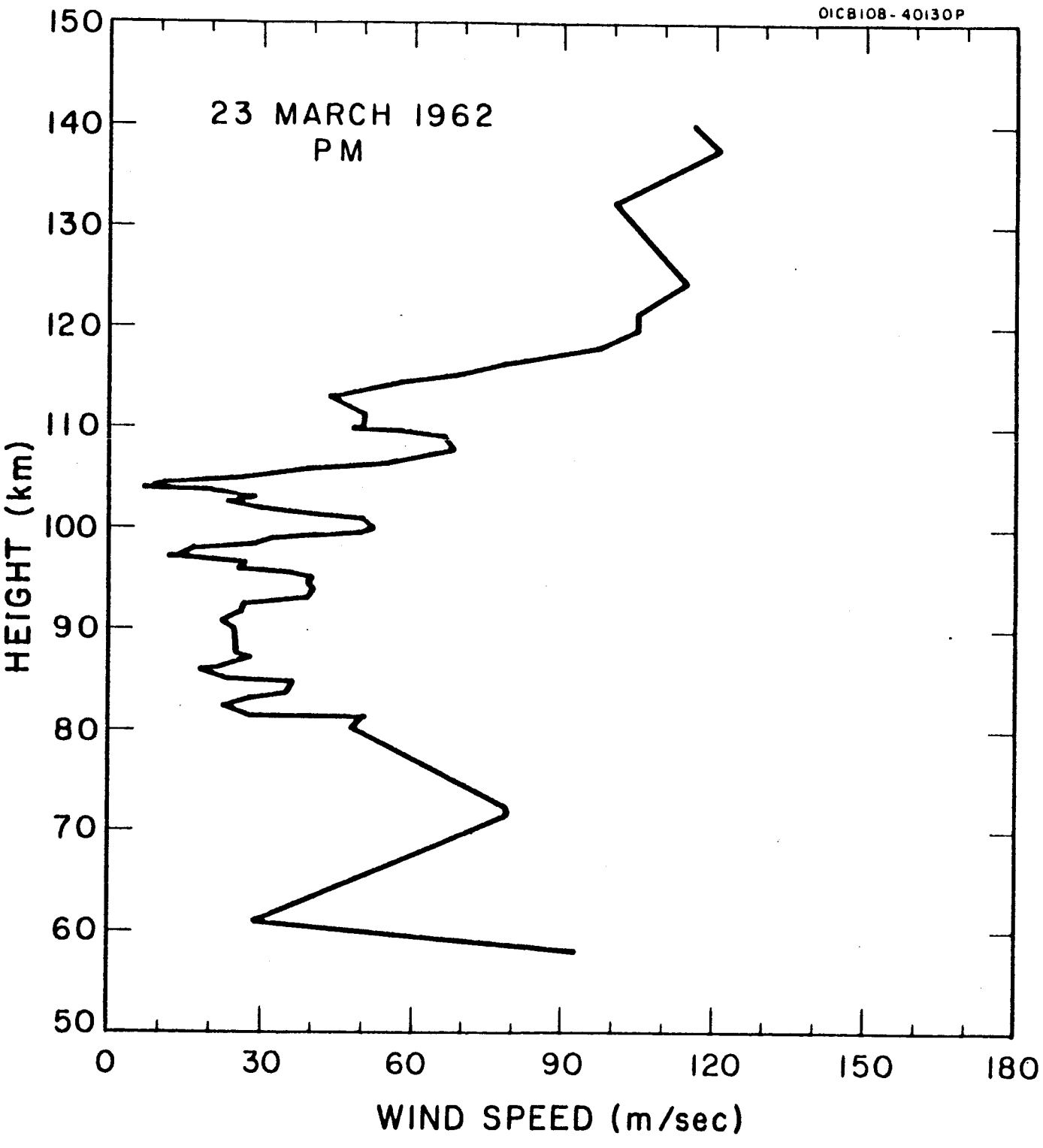

Figure A.14a. Wind speed as a function of height for evening twilight of 23 March 1962.

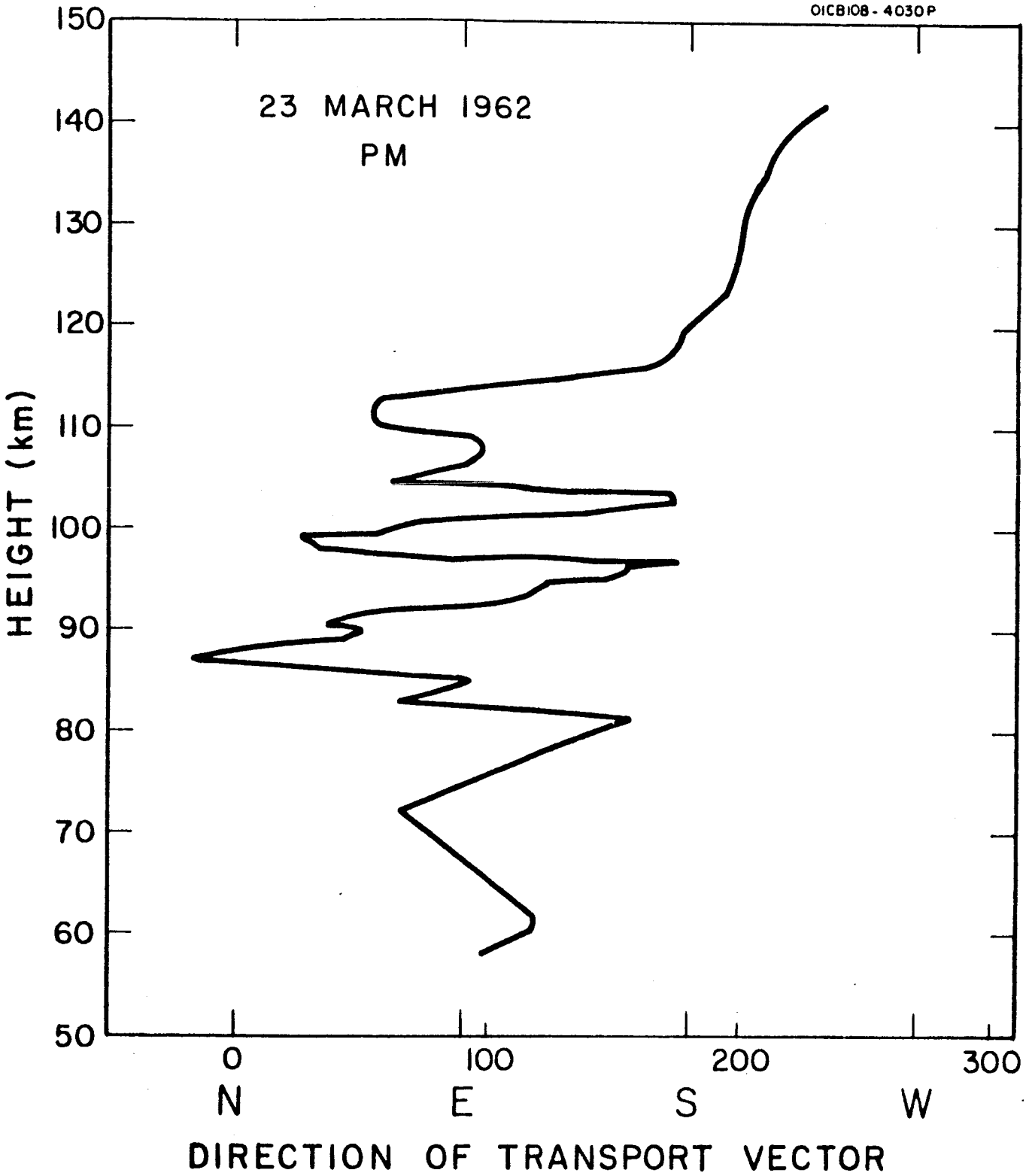

Figure A.14b. Direction of transport vector as a function of height for evening twilight of 23 March 1962.

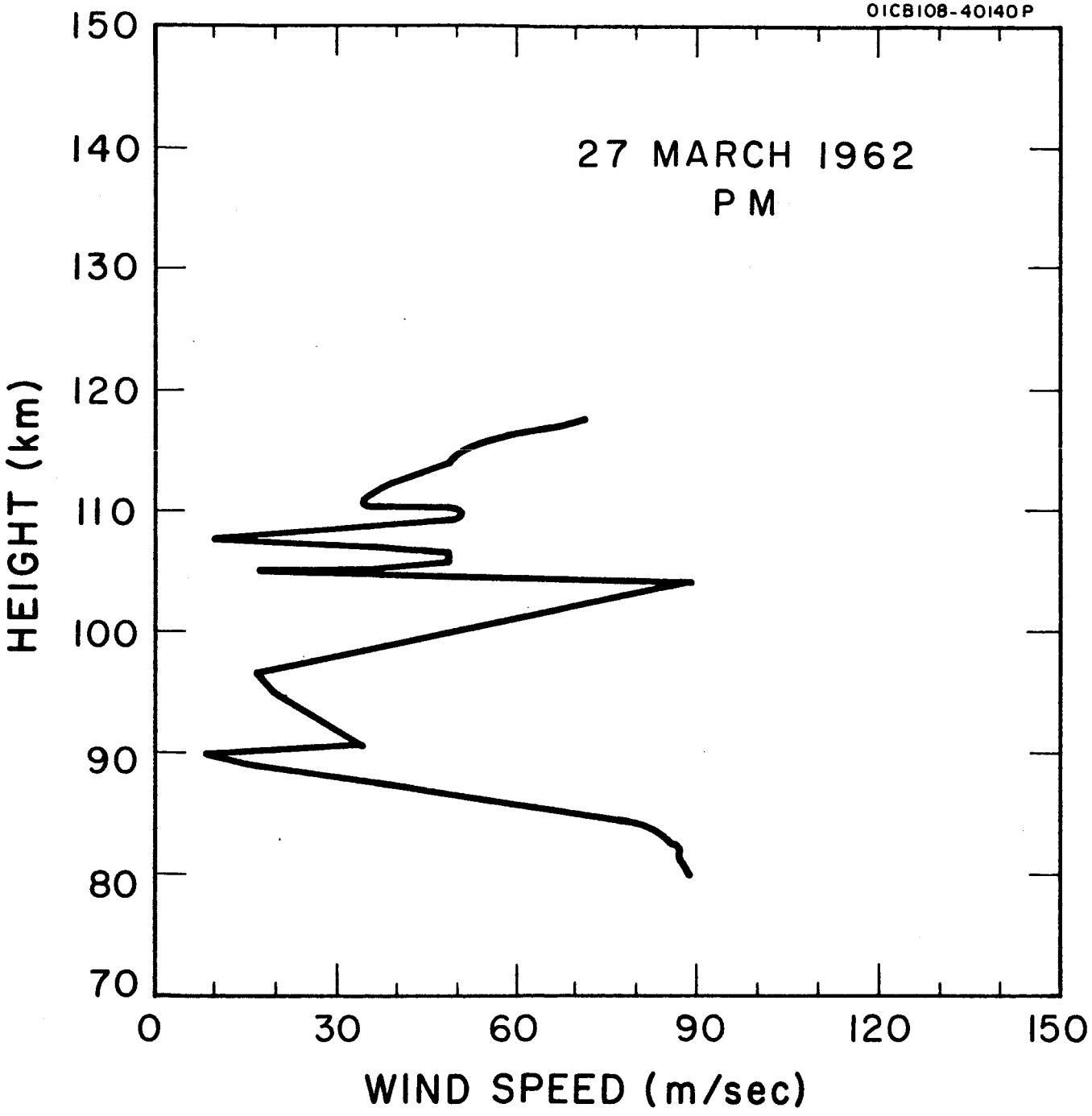

Figure A.15a. Wind speed as a function of height for evening twilight of 27 Marcy 1962.

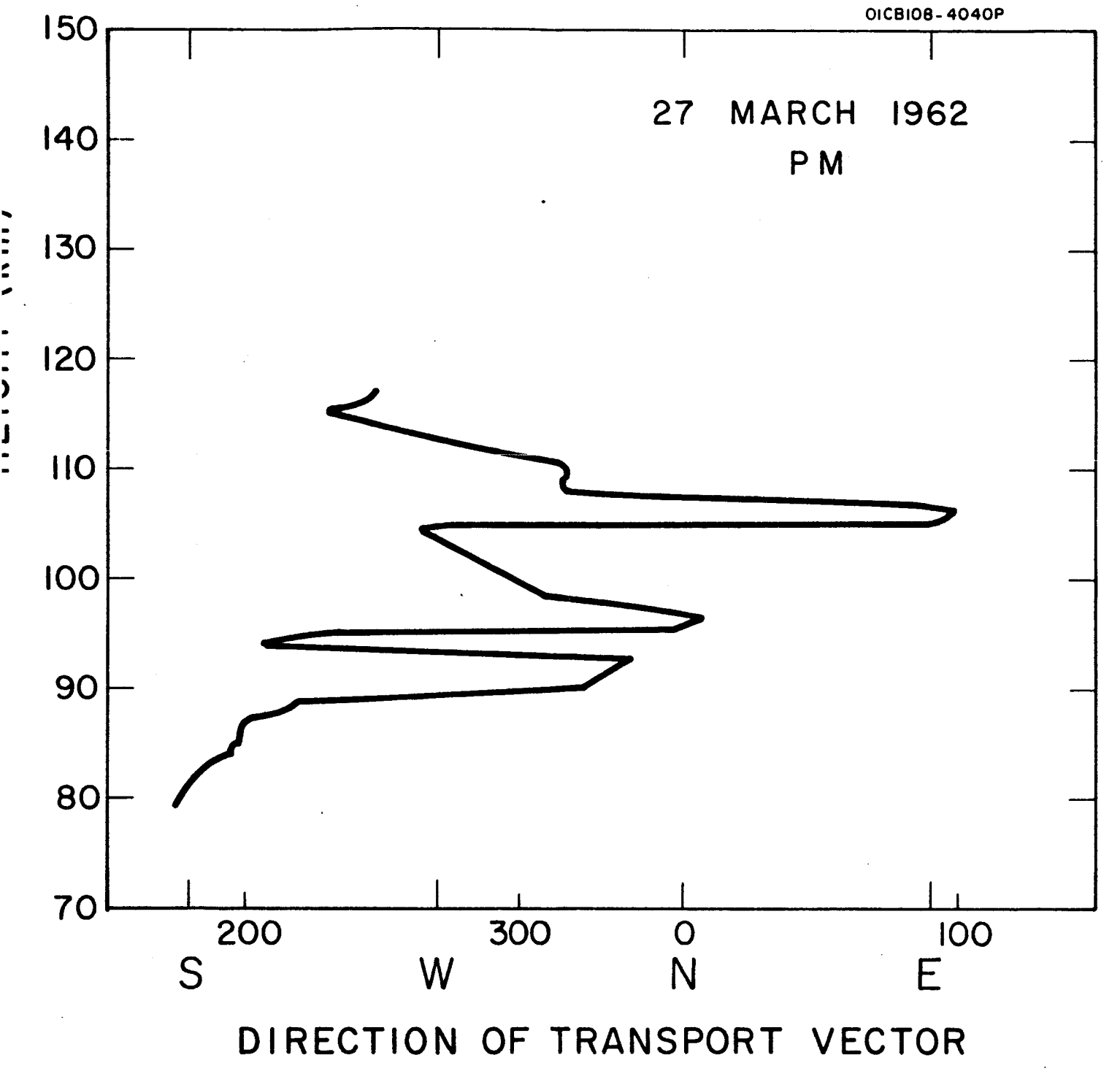

Figure A.15b. Direction of transport vector as a function of height for evening twilight of 27 March 1962.

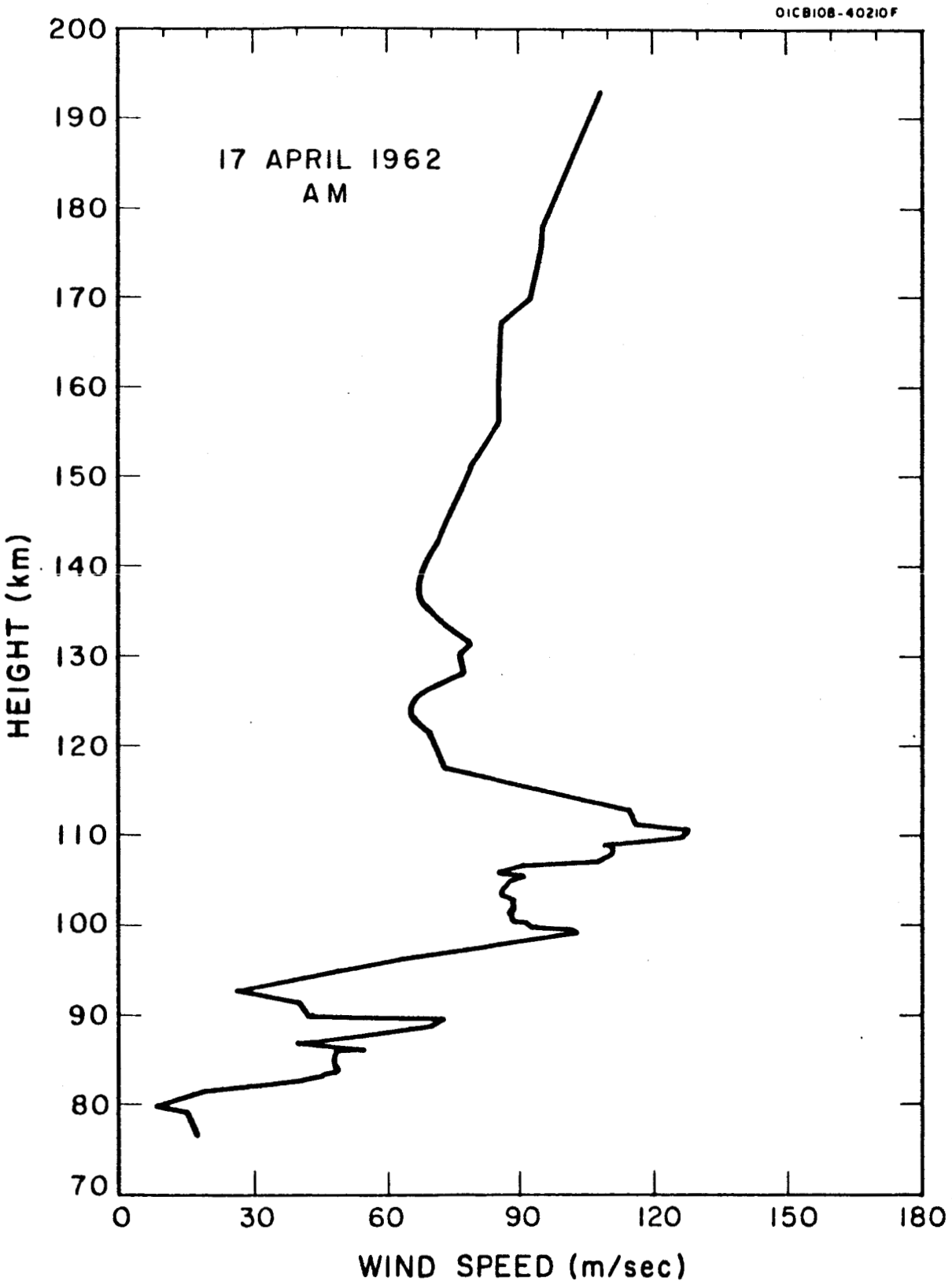

Figure A.16a. Wind speed as a function of height for morning twilight of 17 April 1962.

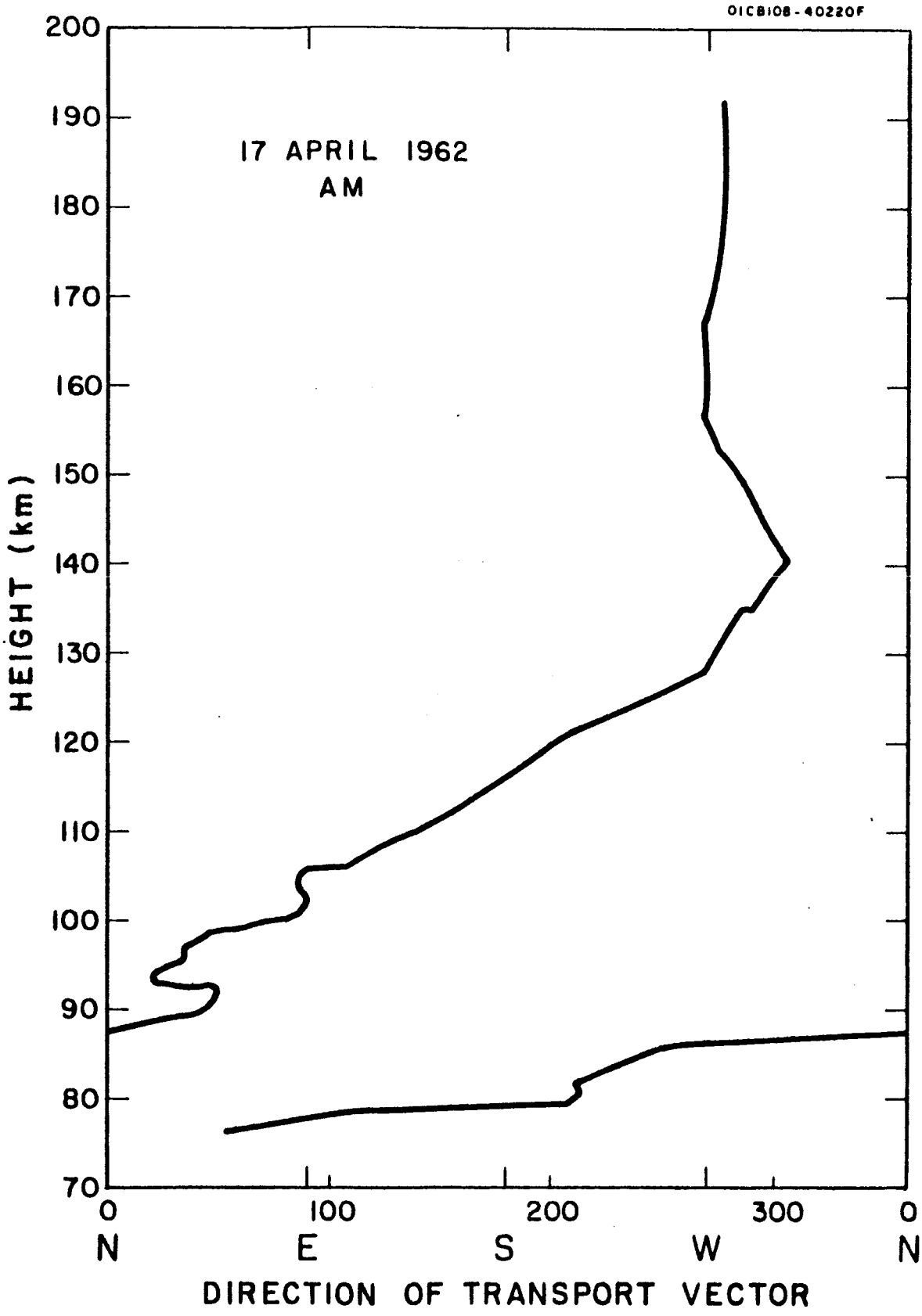

Figure A.16b. Direction of transport vector as a function of height for morning twilight of 17 April 1962.

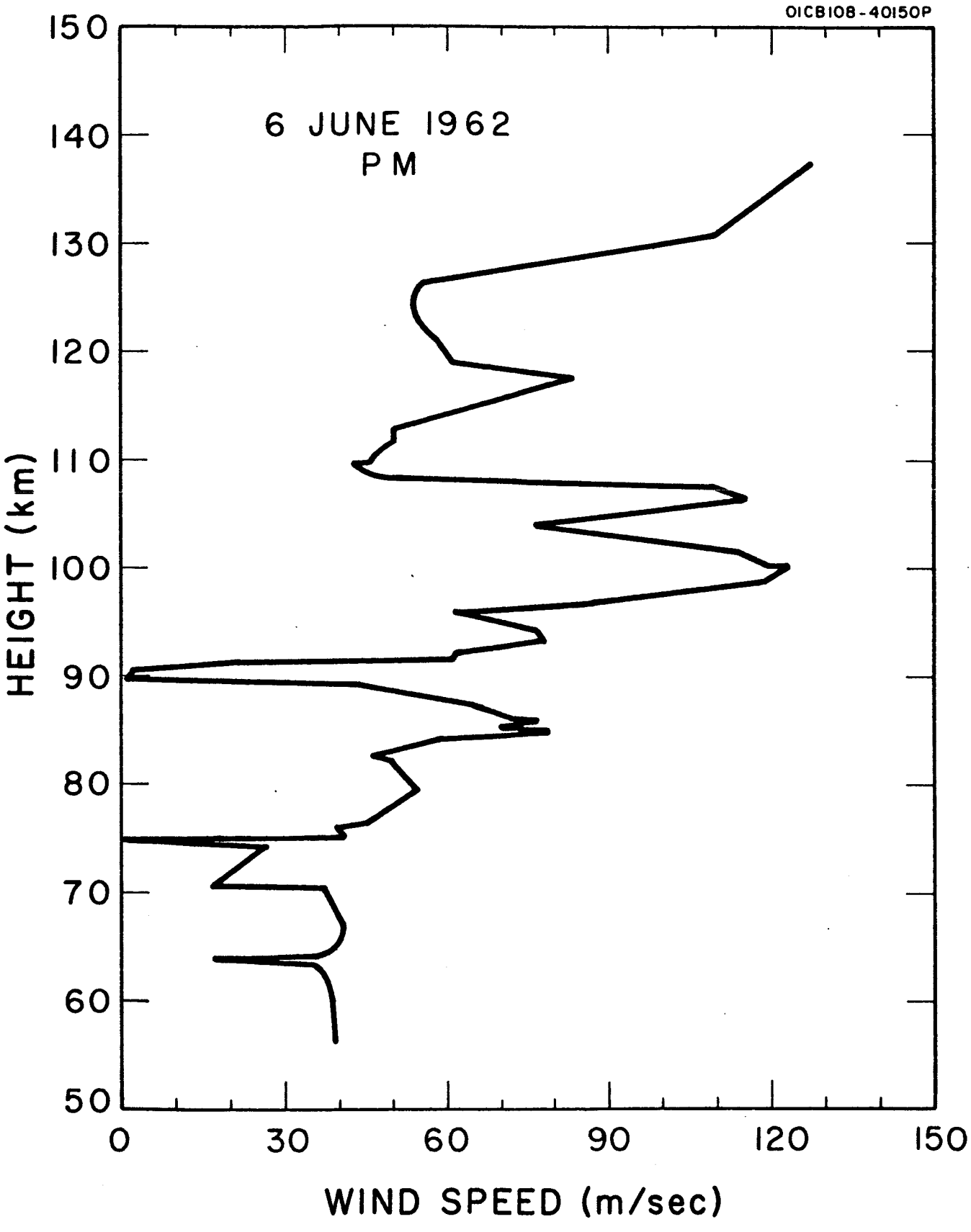

Figure A.17a. Wind speed as a function of height for evening twilight of 6 June 1962.

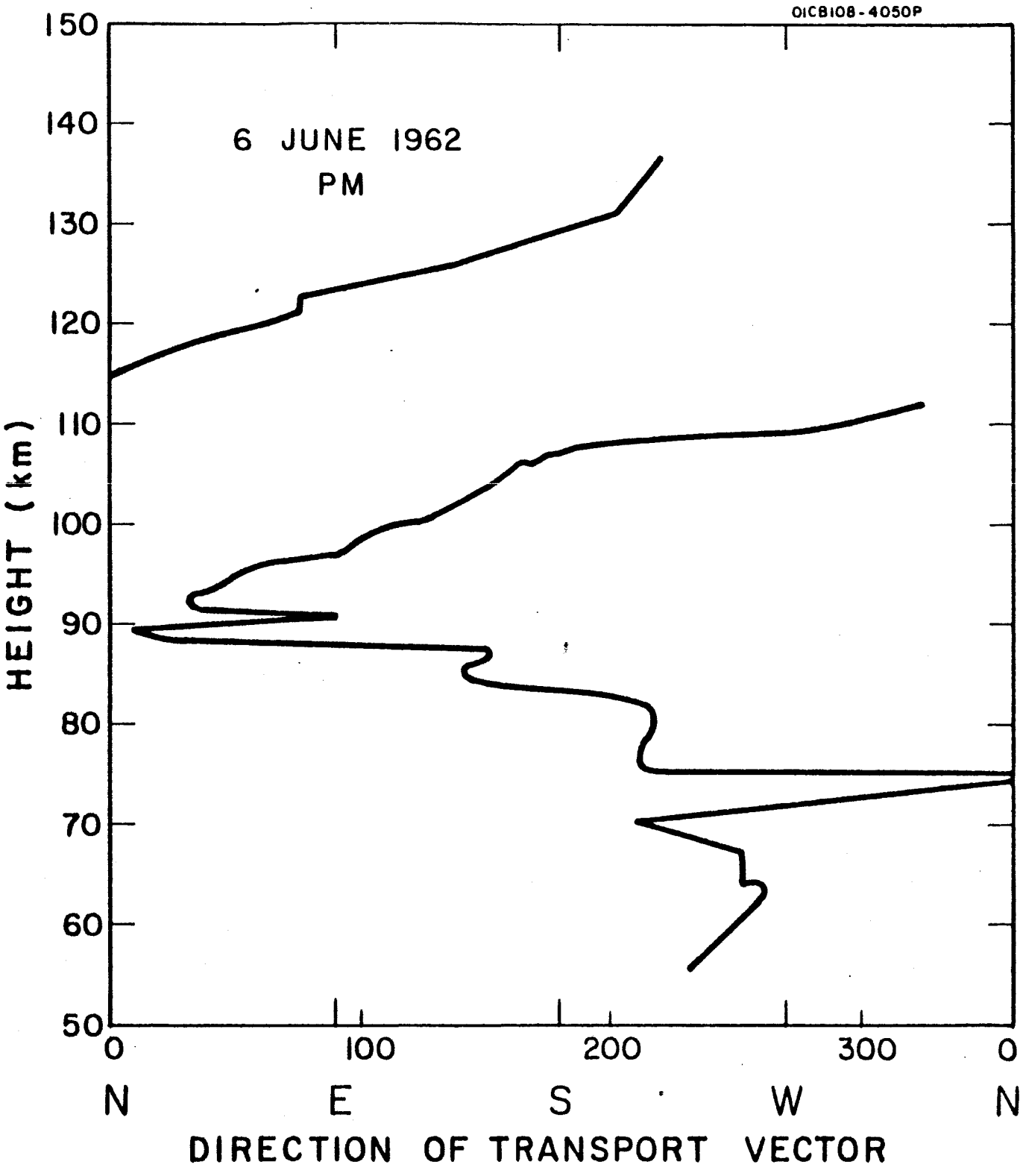

Figure A.17b. Direction of transport vector as a function of height for evening twilight of 6 June 1962.

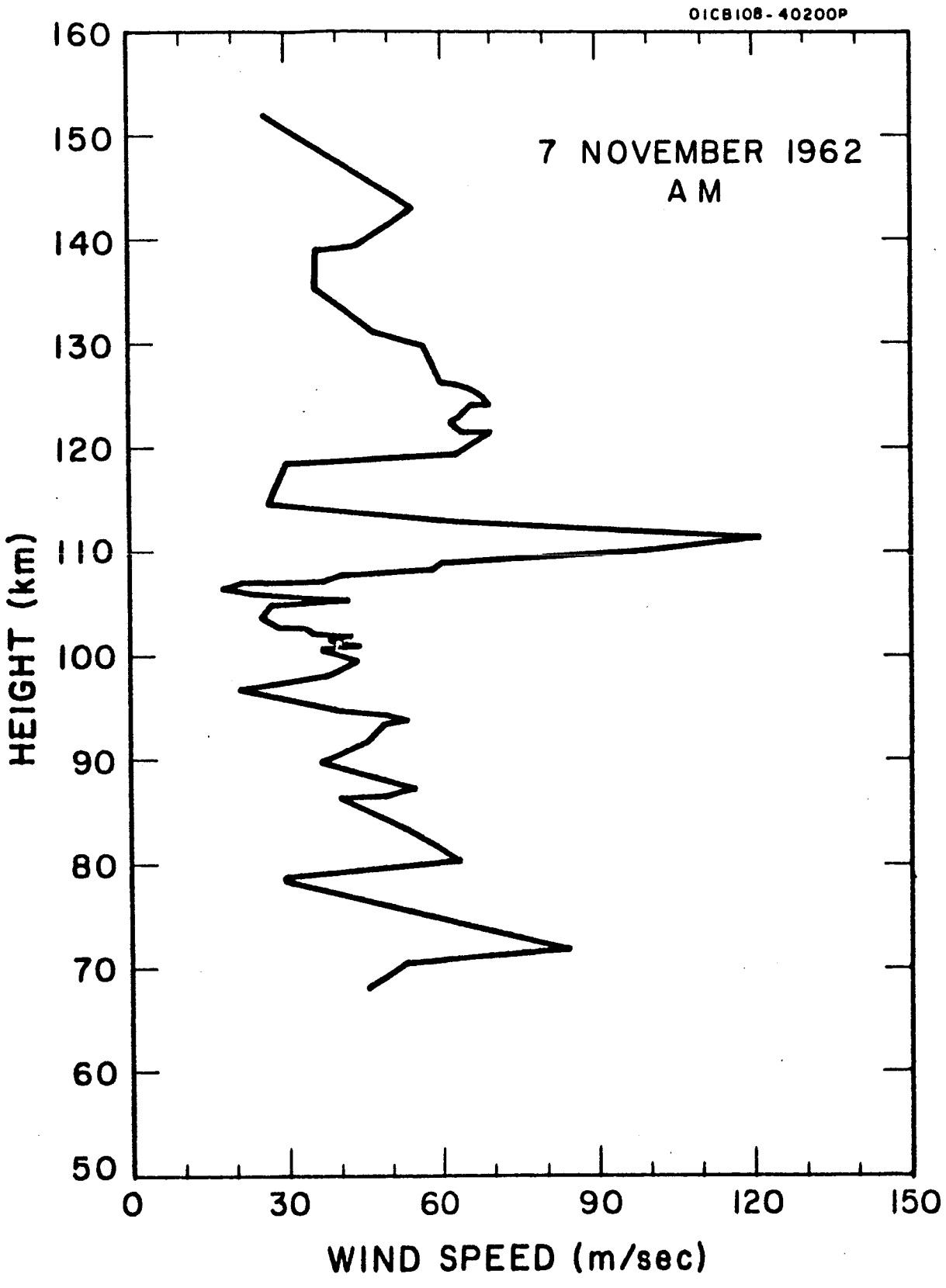

Figure A.18a. Wind speed as a function of height for morning twilight of 7 November 1962.

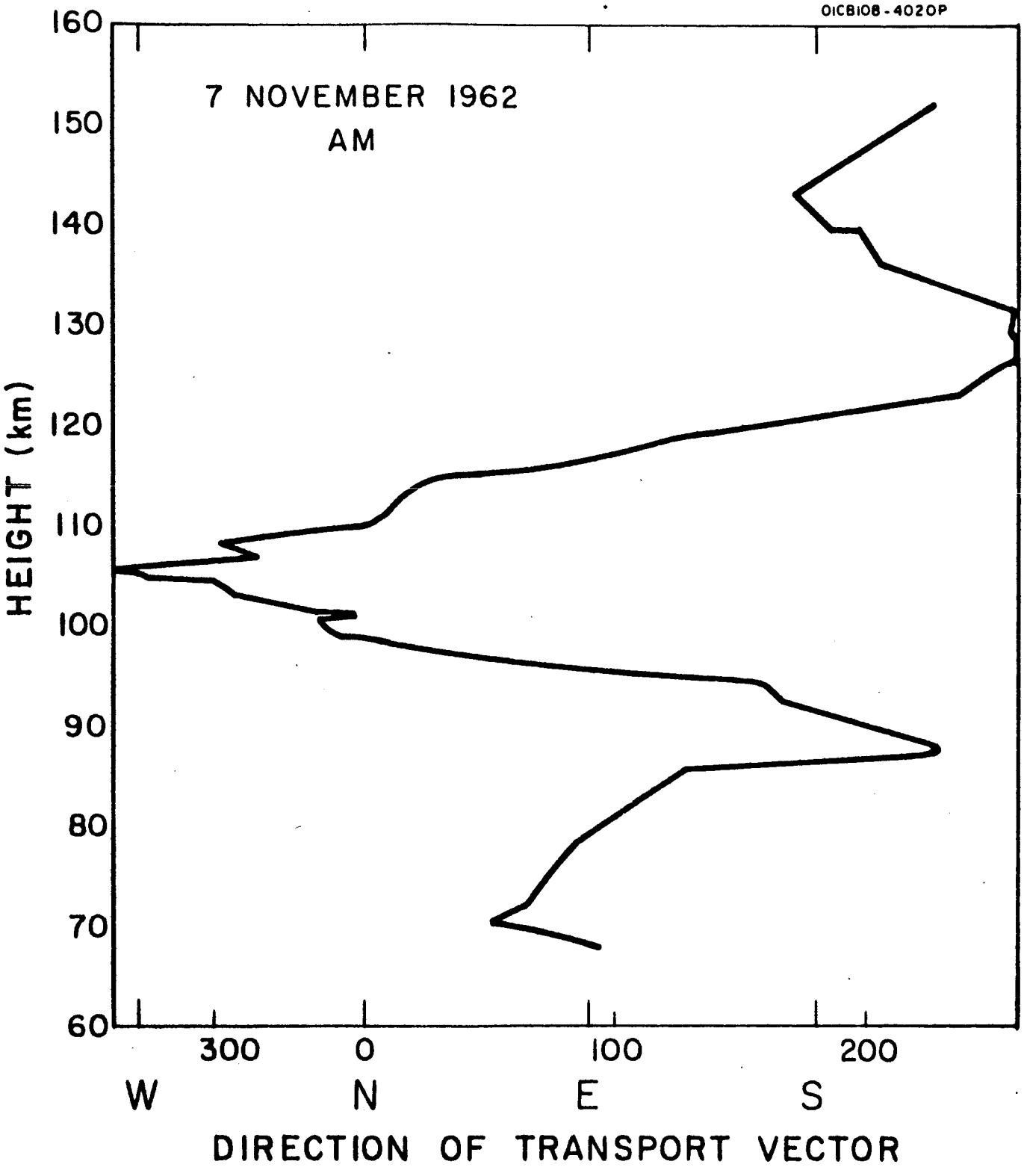

Figure A.18b. Direction of transport vector as a function of height for morning twilight of 7 November 1962.

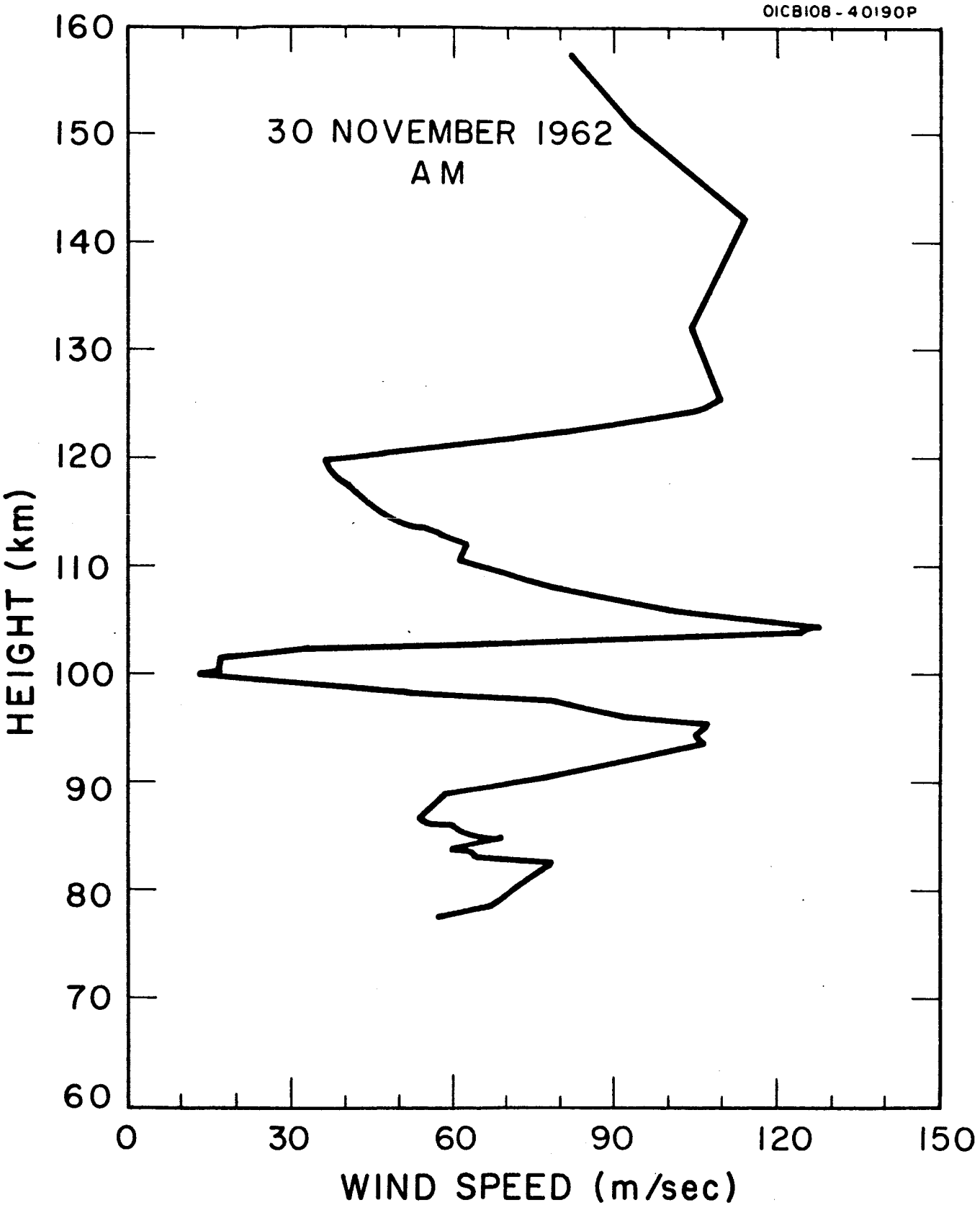

Figure A.19a. Wind speed as a function of height for morning twilight of 30 November 1962.

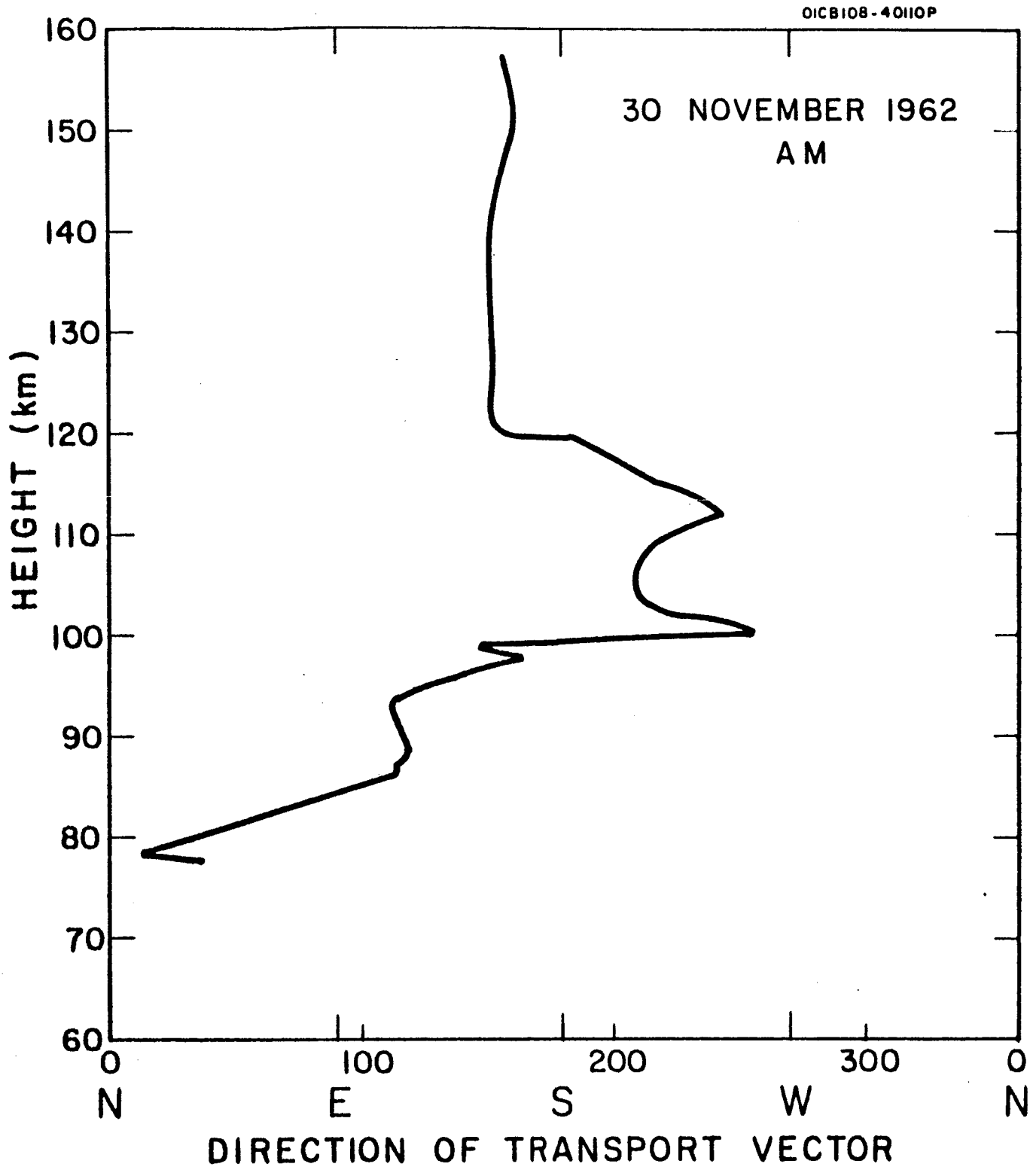

Figure A.19b. Direction of transport vector as a function of height for morning twilight of 30 November 1962.

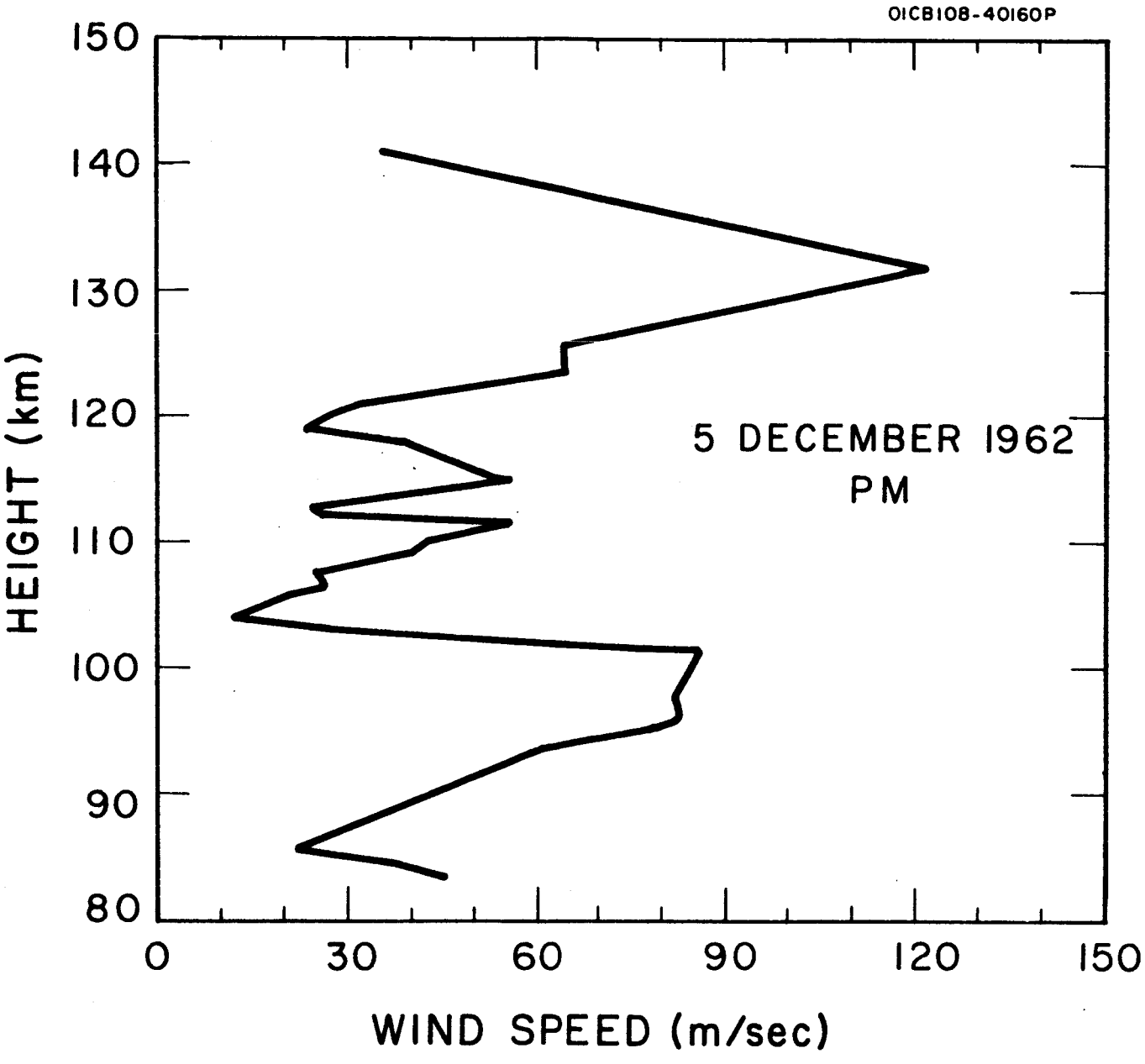

Figure A.20a. Wind speed as a function of height for evening twilight of 5 December 1962.

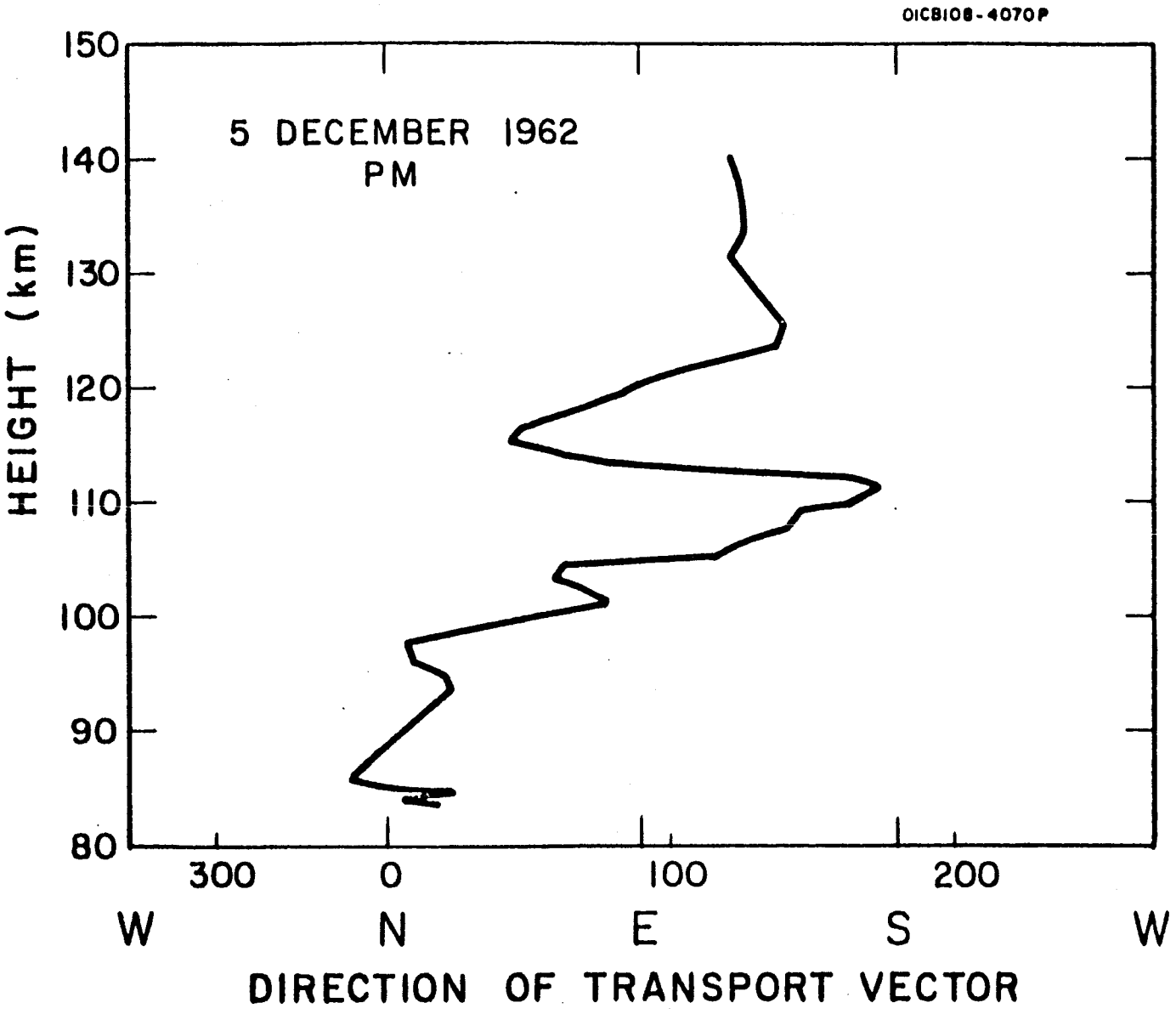

Figure A.20b. Direction of transport vector as a function of height for evening twilight of 5 December 1962.

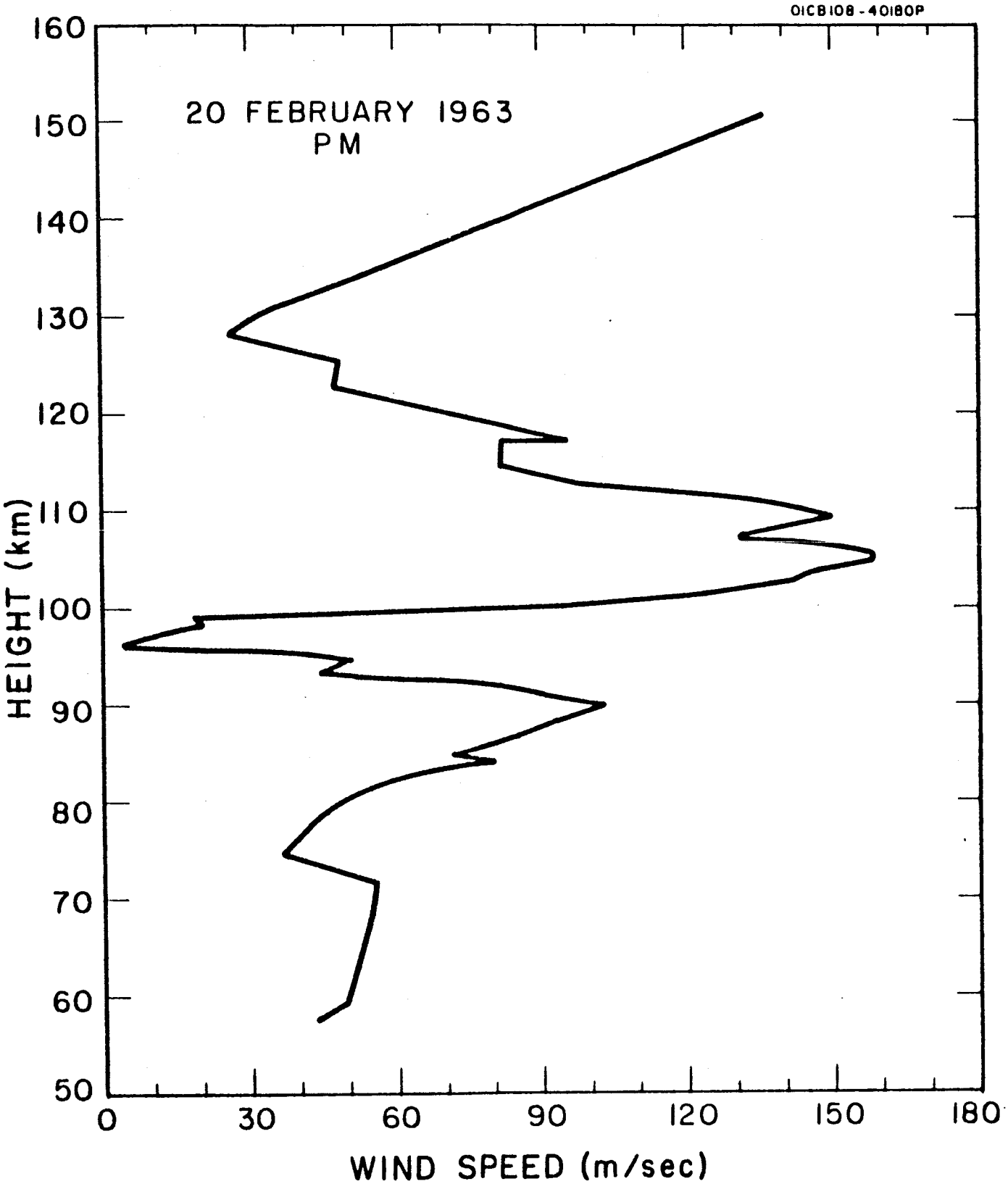

Figure A.21a. Wind speed as a function of height for evening twilight of 20 February 1963.

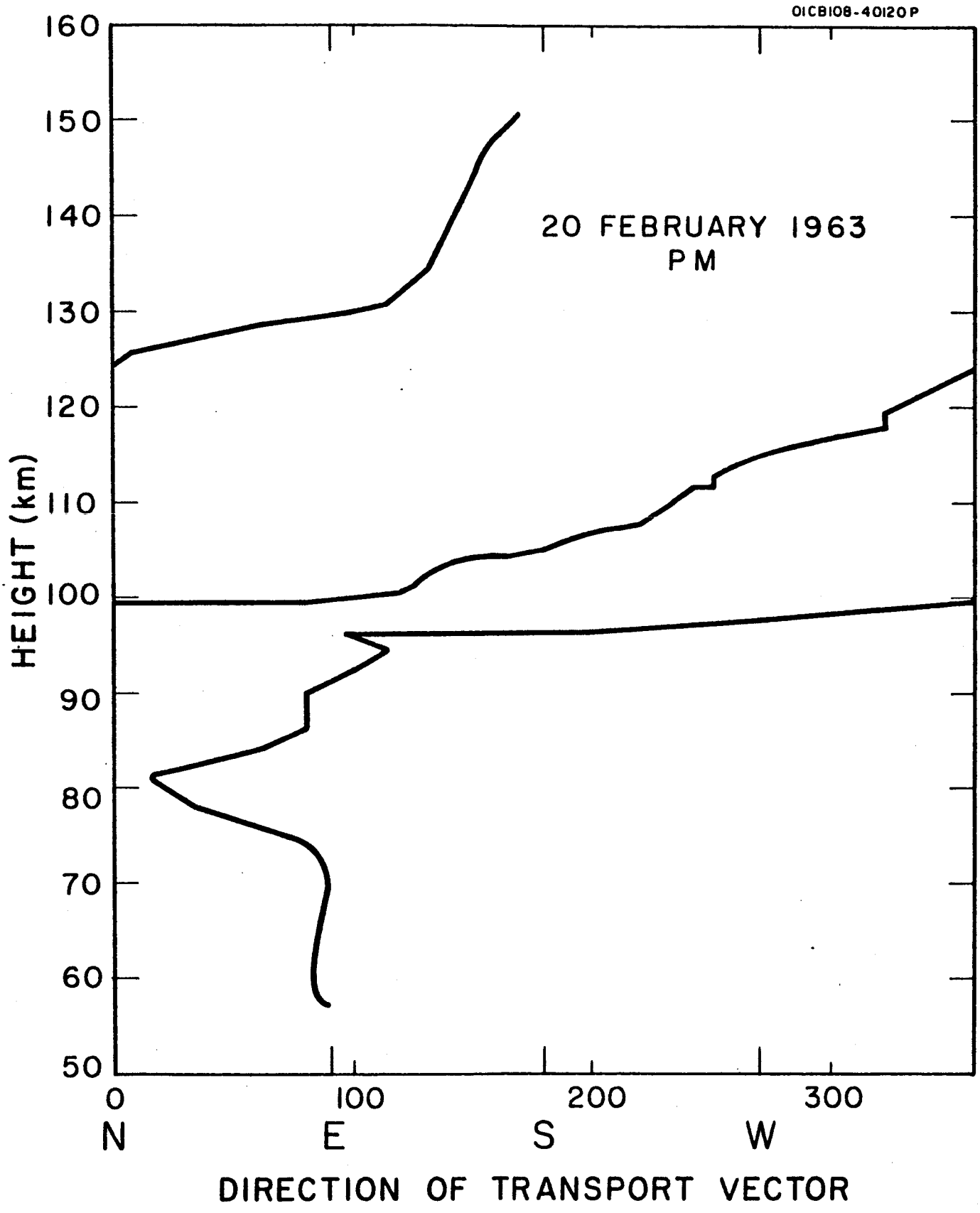

Figure A.21b. Direction of transport vector as a function of height for evening twilight of 20 February 1963.

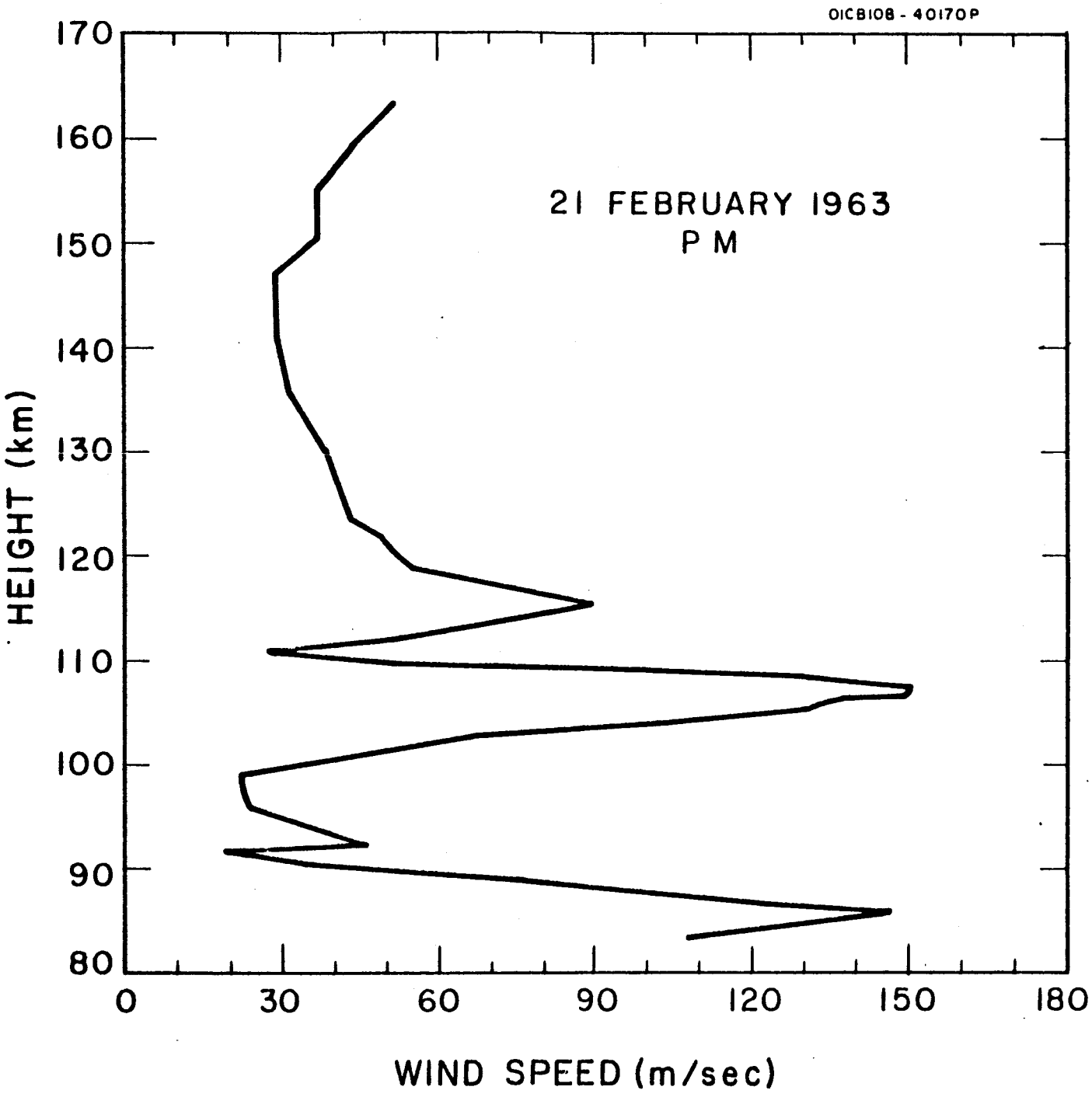

Figure A.22a. Wind speed as a function of height for evening twilight of 21 February 1963.

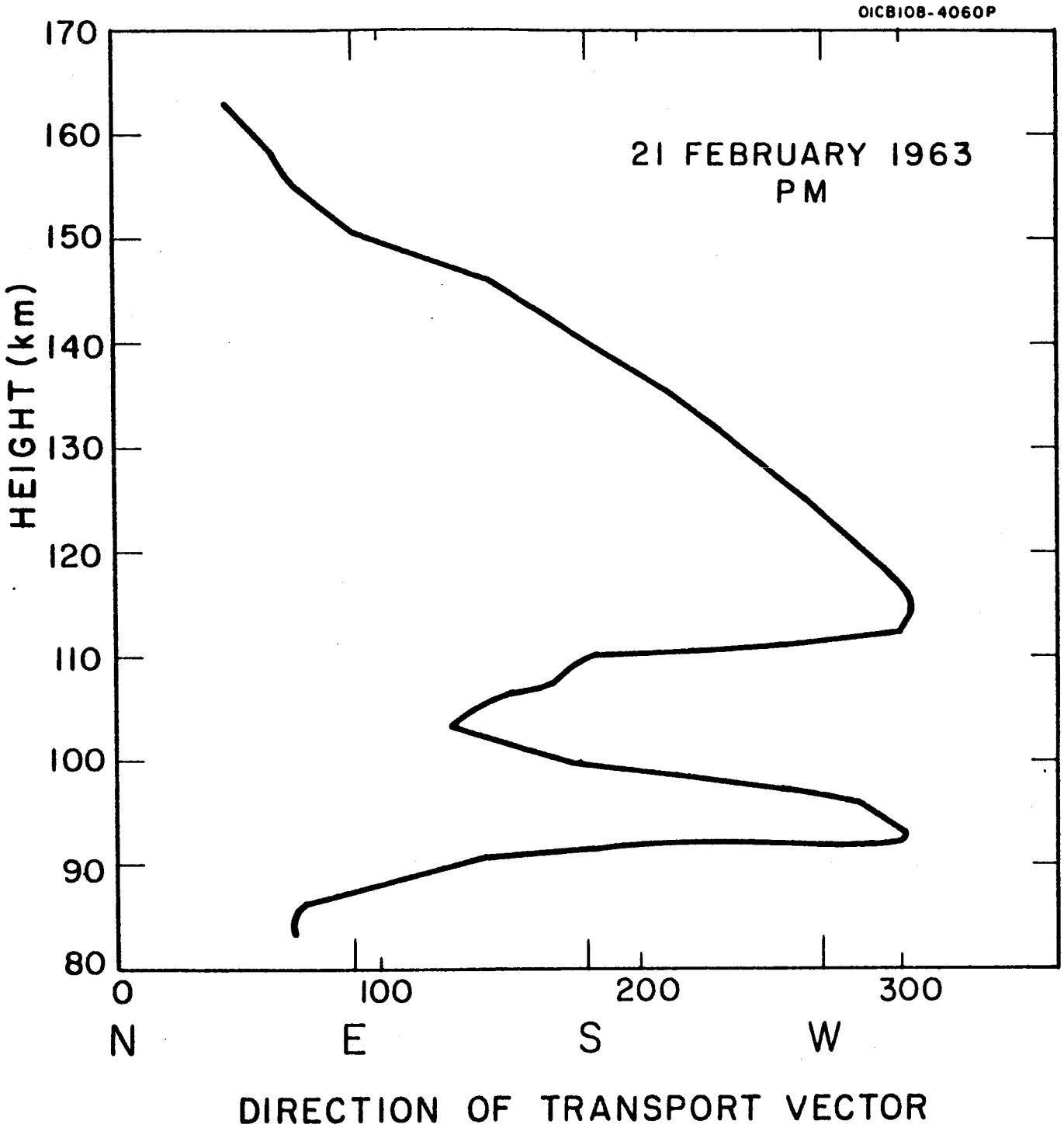

Figure A.22b. Direction of transport vector as a function of height for evening twilight of 21 February 1963.

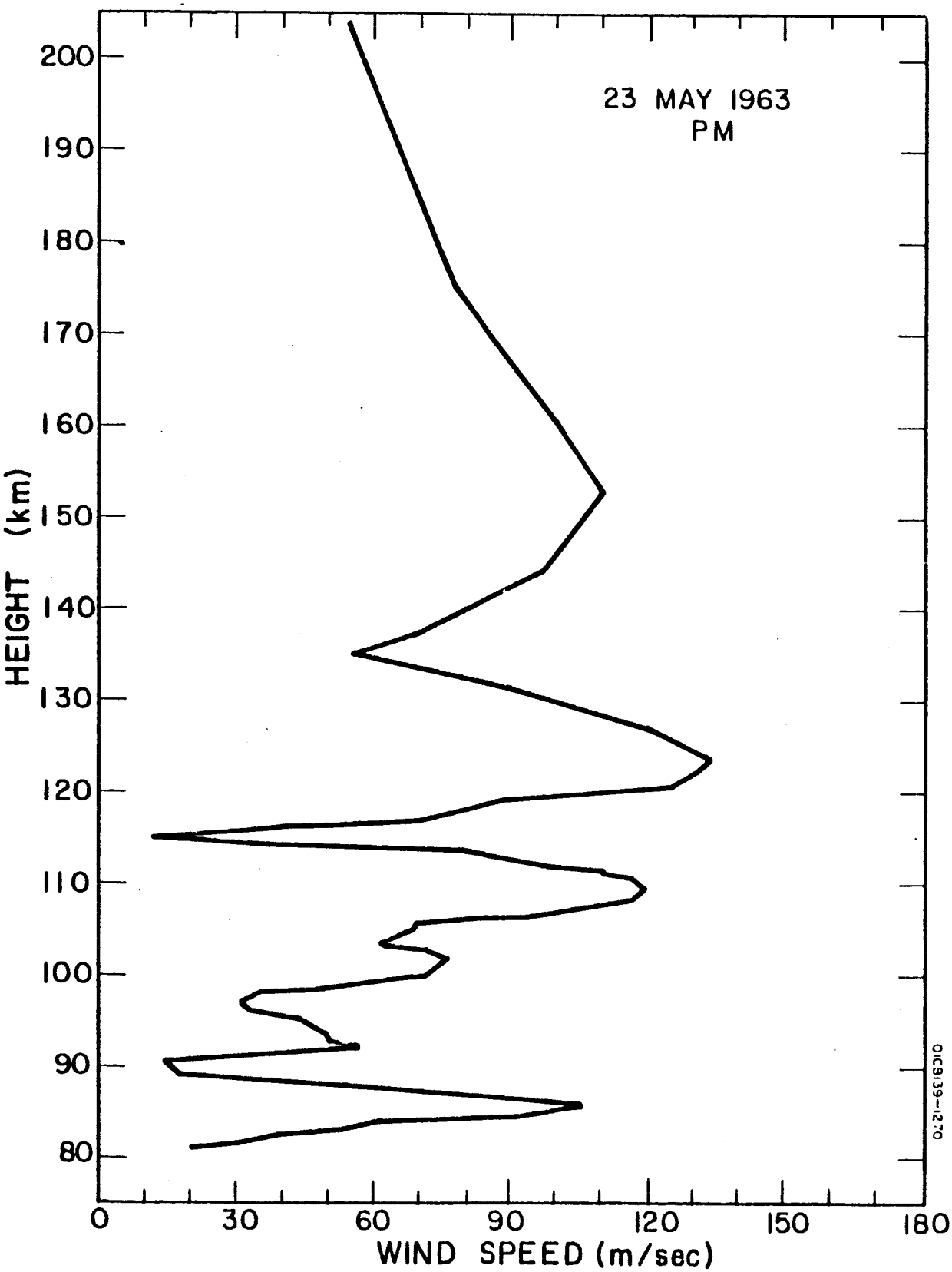

Figure A.23a. Wind speed as a function of height for evening twilight of 23 May 1963.

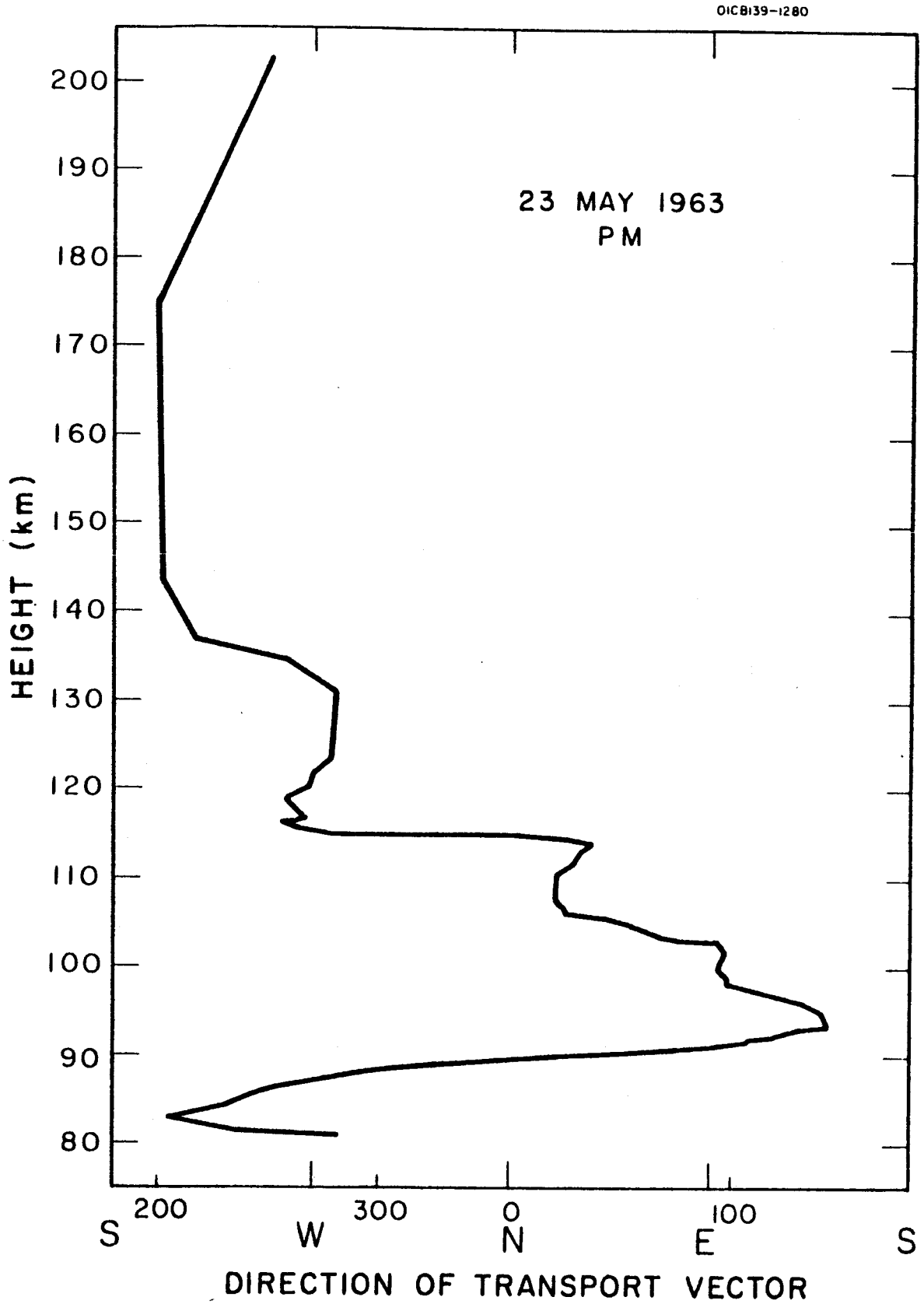

Figure A.23b. Direction of transport vector as a function of height for evening twilight of 23 May 1963.

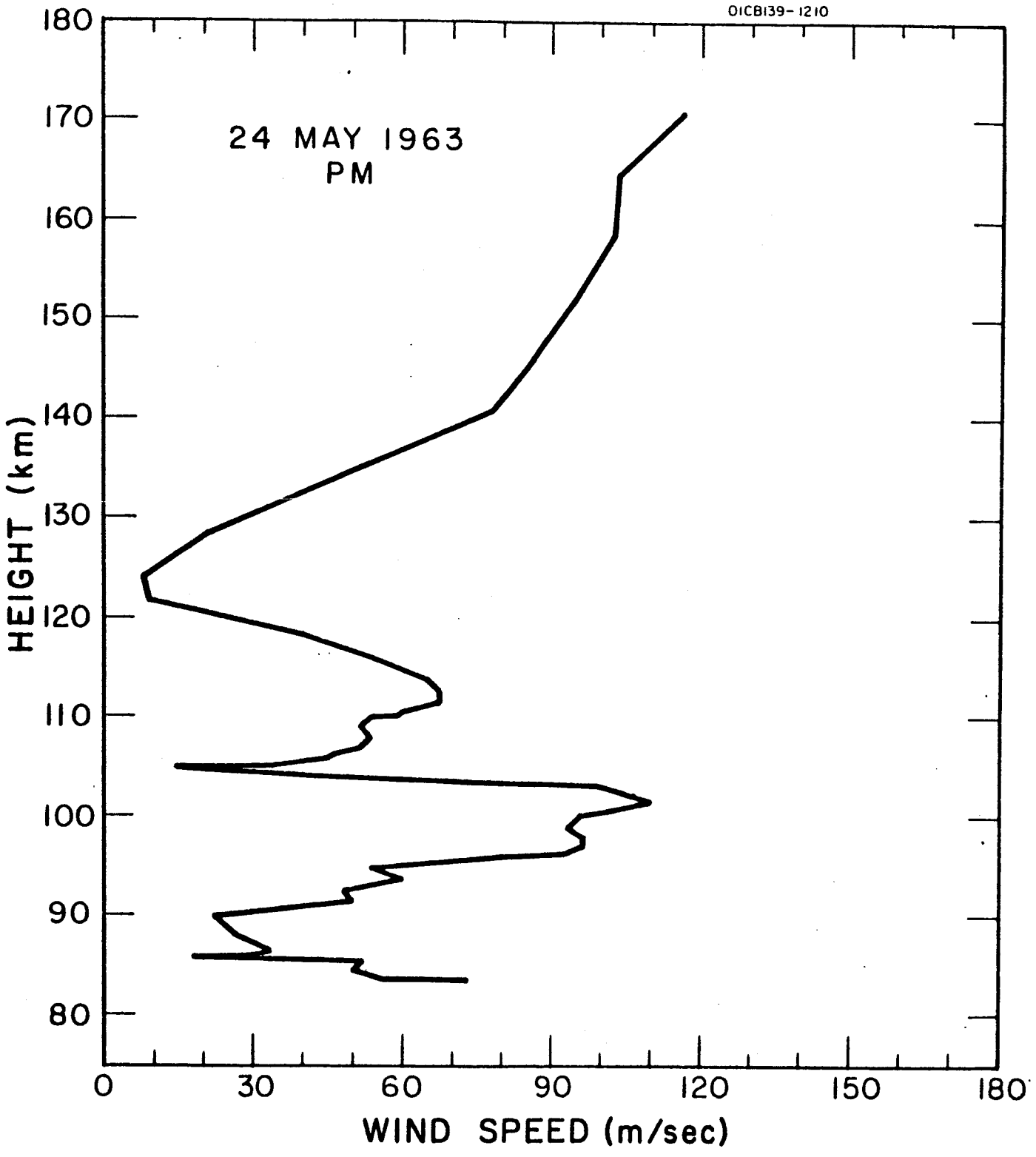

Figure A.24a. Wind speed as a function of height for evening twilight of 24 May 1963.

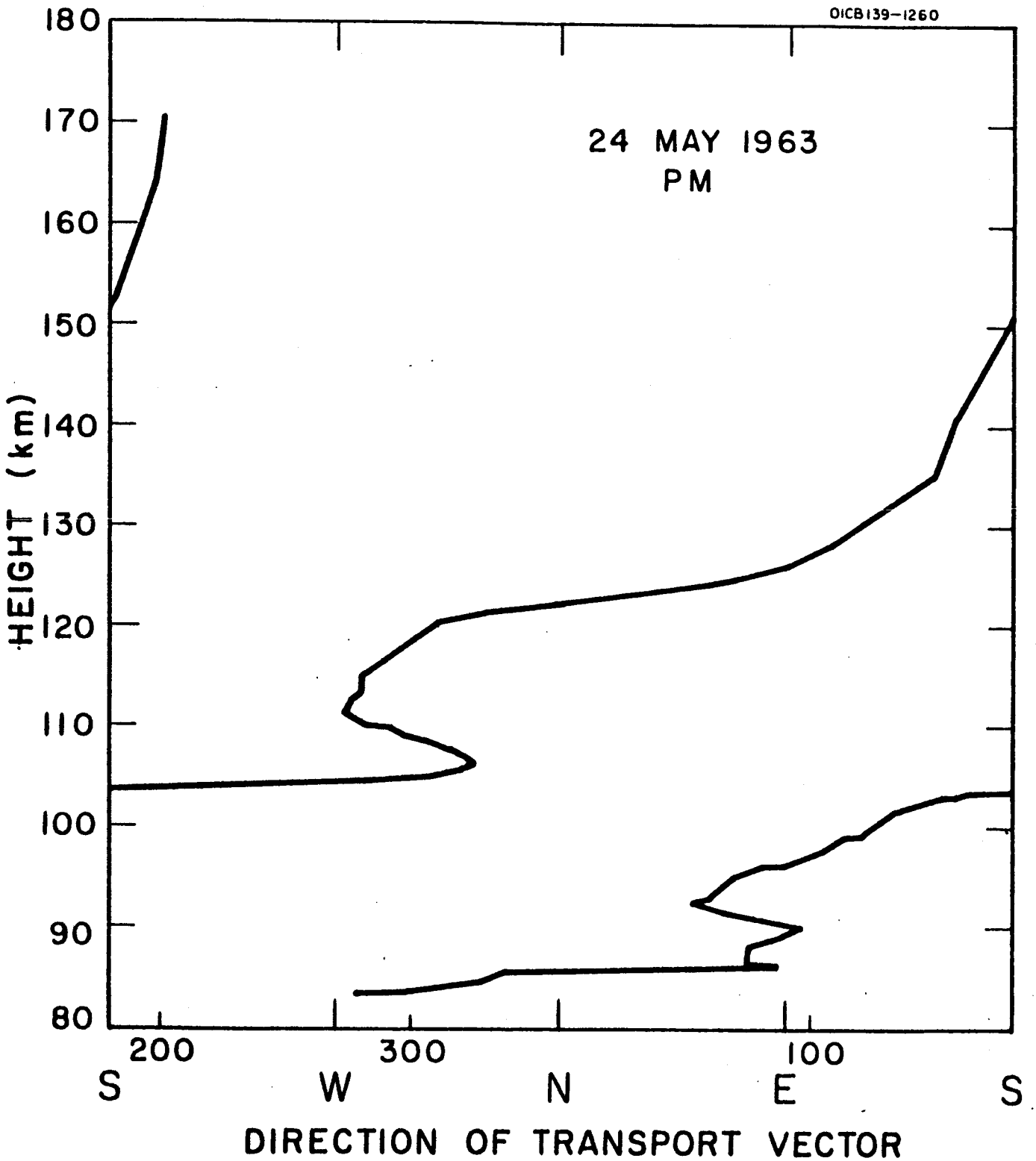

Figure A.24b. Direction of transport vector as a function of height for evening twilight of 24 May 1963.